universität wien

DISSERTATION

Titel der Dissertation

„Production of Titanium Diboride Coatings by Electrolysis of High-Temperature Molten Salts“

Verfasserin

Nataliia Rybakova

angestrebter akademischer Grad

Doktorin der Naturwissenschaften (Dr. rer.nat.)

Wien, 2011

Studienkennzahl lt. Studienblatt:	A 091 419
Dissertationsgebiet lt. Studienblatt:	419 Chemie
Betreuerin / Betreuer:	Univ. - Prof. Dr. Peter Franz Rogl

ACKNOWLEDGEMENTS

I owe my deepest gratitude to Dr. Gerhard Nauer for his support, valuable advices and helpful discussions that I have received during this work.

I would like to thank to Univ.-Prof. Dr. Peter Franz Rogl for the supervision and helpful discussions he provided during the writing of this dissertation.

I wish to thank to Prof. Dr. Christoph Kleber who took the time to read through my thesis and whose comments and advices were highly appreciated.

My sincere thanks belong to Docent, Dipl.Eng., Dr. Olga Babushkina who was anytime willing to share her knowledge and experience in encouraging discussions not only about high temperature molten salts.

I wish to thank to Dr. Olga Linucheva, from NTUU "KPI" in Kiev who provided me with encouragement that resulted to a decision to arrive to Austria.

Furthermore, I am grateful to all colleagues from CEST Centre of Electrochemical Surface Technology (formerly ECHEM Centre of Competence in Applied Electrochemistry, Wiener Neustadt, Austria) who friendly welcomed me. My gratitude is also given to Dr. Yuriy Andriyko, who was initiator to invite students for the practice from Ukraine and who helped me so much in practical things regarding my stay in Austria.

The financial support within the COMET Program sponsored by the Austrian Research Promotion Agency (Österreichische Forschungsförderungsgesellschaft FFG) and the government of Lower Austria is gratefully acknowledged.

Finally I wish to thank to my mother Galina, my father Vladimir, my sister Elena, my niece Svetlana and my husband Dr. Vladimir Nedashkivskyi for all their unconditional love, understanding and encouragement.

Table of Content

Abstract..……..vii
Kurzfassung……..……ix
List of symbols and abbreviations…….. xi
1. Introduction…….. 1
2. Literature overview…….. 4
2.1 Coatings by refractory materials: property and application……...…. 4
2.1.1 Carbide coatings…….. 5
2.1.2 Nitride coatings……... 5
2.1.3 Silicide coatings…….. 6
2.1.4 Oxide coatings……. 6
2.1.5 Aluminide coatings…… 7
2.1.6 Boride coatings…… 7
2.2 Procedures for the preparation of refractory coatings……..... 10
2.2.1 Chemical vapour deposition (CVD)……... 11
2.2.2 Physical vapour deposition (PVD)…….. 12
2.2.3 Thermal spraying……... 13
2.2.4 Electrochemical deposition…….…… 14
2.3 Electrochemical deposition of TiB_2 out of high temperature molten salt……. 16
2.3.1 Electrochemical synthesis of borides…….. 16
2.3.2 State of the art…… 17
2.3.3 Some aspects on molten salts and systems used for electrochemical deposition of TiB_2……..... 22
2.3.4 Systems used for electrochemical deposition of TiB_2…… 25
2.3.5 Basic requirements to the container materials and the design of the cell... 29
2.3.6 Deposition techniques…… 30
2.3.6.1 Electrochemical techniques…… 30
2.3.6.2 Electroplating using pulse current…….. 32
2.3.7 Proposed mechanisms of TiB_2 electrochemical deposition from high-temperature molten salts…… 33
2.3.7.1 Fluoride melt……... 33
2.3.7.2 Chloride-fluoride melt…… 35
2.3.7.3 Fluoride-oxide melt…… 38

3. Experimental part……... 40
3.1 Introduction……... 40
3.2 Deposition experiments……. 40
3.2.1 Samples pre-treatment……. 40
3.2.2 Preparation of the electrolyte…….. 41
3.2.3 Electrochemical deposition experiments…… 43
3.2.4 Cross section preparation of the samples…… 46
3.2.5 Characterization of the coatings …….. 46
3.2.6 Spectroscopic measurements…….. 47
3.2.7 Corrosion characterization of the TiB_2 layers……. 48
3.3 Cyclic voltammetry……... 48
3.3.1 Electrochemical measurements……... 48
3.3.2 Preparation of the melts for cyclic voltammetry..... 49
4. Results and discussion…… 50
4.1 Control of the purity of the melt and electrochemical stability of the electrolyte 50
4.1.1 Introduction……..... 50
4.1.2 FLiNaK electrolyte…… 50
4.1.2.1 Fourier Transform Infrared (FTIR) Spectroscopy…….. 50
4.1.2.2 Cyclic voltammetry measurements……. 52
4.1.3 NaF-KF electrolyte…….. 55
4.1.3.1 Fourier Transform Infrared (FTIR) Spectroscopy…….. 55
4.1.3.2 Cyclic voltammetry measurements……. 56
4.1.4 KF electrolyte…….. 57
4.1.4.1 Fourier Transform Infrared (FTIR) Spectroscopy…….. 57
4.1.4.2 Cyclic voltammetry measurements……. 57
4.2 Electrochemical investigation on the synthesis of TiB_2 out of FLiNaK electrolyte: Electrochemical behaviour of the compounds, KBF_4, K_2TiF_6, K_2TiF_6 - TiF_3 and K_2TiF_6 - Ti wire, KBF_4 - K_2TiF_6…….. 59
4.2.1 Introduction…… 59
4.2.2 Effect of the temperature on the electrochemical reduction of B(III) electrochemical active species……. 60
4.2.2.1 CV at different temperatures…….. 60
4.2.2.2 Characteristics of the electrode reactions in FLiNaK-KBF_4…….. 62

4.2.3 Effect of the temperature on the electrochemical reduction of Ti(IV) species…… 68
4.2.3.1 CV at different temperatures……. 68
4.2.3.2 Characteristics of the electrode reactions in FLiNaK-K_2TiF_6..... 69
4.2.4 Effect of the temperature on the electrochemical reduction of Ti(IV) and Ti(III) species out of FLiNaK electrolyte……..... 75
4.2.4.1 CV at different temperatures……. 75
4.2.4.2 Characteristics of the electrode reactions in FLiNaK-K_2TiF_6-TiF_3 ……..... 77
4.2.5 Effect of the temperature on the electrochemical reduction of Ti(IV) species out of FLiNaK electrolyte in the presence of Ti wire…….. 82
4.2.5.1 CV at different temperatures……. 82
4.2.5.2 Characteristics of the electrode reactions in FLiNaK-K_2TiF_6-Ti wire……... 84
4.2.6 FTIR spectroscopy of Ti (IV) species……... 88
4.2.7 Effect of the temperature on the electrochemical reduction of B(III) and Ti(IV) species……. 89
4.2.8 FTIR spectroscopy of Ti (IV) and B (III) species..……... 91
4.3 Morphology and mechanical properties of TiB_2 layer deposited from chloride-fluoride melt via pulse plating compared with TiB_2 layer deposited via direct current procedure……... 92
4.3.1 Introduction……... 92
4.3.2 Morphology of TiB_2 coating……. 92
4.3.3 Roughness of TiB_2 coating…… 95
4.3.4 Microhardness……... 98
4.3.5 Stress……. 99
4.3.6 Current efficiency……. 101
4.4 Electrochemical deposition of TiB_2 coatings out of FLiNaK electrolyte: influence of additive, pre-treatment of the substrate, temperature and current distribution on the quality of the layer…….. 103
4.4.1 Electrochemical synthesis of TiB_2 layers out of FLiNaK electrolyte in the presence of $TaCl_5$ additive…… 103
4.4.1.1 Cyclic voltammetry……... 103

4.4.1.2 Phase analysis and chemical composition of the coatings…… 107
4.4.1.3 Surface morphology…….. 112
4.4.1.4 Grain size, lattice parameters and thickness of the coatings……. 113
4.4.2 Effect of the substrate pre-treatment on morphology, quality and adhesion of the TiB_2 layer…….. 118
4.4.3 Effect of the temperature on the quality of TiB_2 layer…….. 122
4.4.4 Effect of the current distribution on the thickness of the layer……..... 125
4.5 Stability of electroplated titanium diboride coatings in molten aluminum alloy at high temperature……... 127
4.5.1 Introduction……... 127
4.5.2 Coating process……. 127
4.5.3 Corrosion tests in molten Al alloys……... 129
5. Summary…..……..... 132
Literature index…… 135
CURRICULUM VITAE

Abstract

This work is aimed at a more detailed investigation of the electrochemical reduction process of TiF_6^{2-} and BF_4^- species at the temperature range of 600-700ºC to evaluate the optimal temperature for the electrochemical TiB_2 forming and to contribute to a better understanding on the overall reaction behaviour in FLiNaK electrolyte.

The influence of different factors such as current mode (pulse plating (PP) techniques in forms of periodically reversed (PRC) and periodically interrupted current (PIC), current density, frequency and pulse shape, substrate pre-treatment (chemical or mechanical), additive ($TaCl_5$) in the electrolyte and the temperature of the process on the mechanical properties, morphology and the quality of the TiB_2 coatings deposited out of FLiNaK and chloride-fluoride electrolytes was investigated to determine the optimal conditions for the electrochemical deposition of TiB_2 coatings of high quality. The corrosion behaviour of molybdenum materials, protected by electrochemically plated TiB_2 coatings, in contact with liquid aluminium alloys was studied.

For determining the nature of the complexes in the electrolyte, infrared spectroscopy was used. The analysis of the coatings was conducted using scanning electron microscopy in combination with the energy-dispersive X-ray spectrometry, the X-ray diffraction analysis, optical microscopy, micro-hardness tester and atomic force microscopy.

Correlation between the morphology of the deposits, structural properties and deposition parameters was established. It was found that the morphology and roughness of the deposits depend strongly on the deposition method and conditions. The coatings with the lowest roughness (Ra=102±5 nm) were obtained by PRC pulse plating. The values of microhardness were in the range of 1800-2400 MPa depending on the pulse frequency in PIC electrolysis. The residual stresses are related to the frequency of deposition and vary in the range of -0.7 GPa to -1.3 GPa, being the minimum at pulse frequency of 20 and 100 Hz. Results on the investigation of the influence of $TaCl_5$ additive in FLiNaK electrolyte on the properties of the deposited TiB_2 layers show that a low concentration of $TaCl_5$ in the melt significantly changes the chemical composition and therefore the properties of the coatings. Co-deposition of TaB_2 in TiB_2 layer decreases the grain size and improves the smoothness of the layer. Addition of $TaCl_5$ in the electrolyte permits to obtain TiB_2-TaB_2 layers of high quality and makes the process reproducible. It was established that TiB_2

coatings effectively protect Mo surface against corrosion in molten Al alloys. No visible traces of corrosion were detected on the liquid metal – TiB_2 interface in corrosion tests. The optimization of electrochemical deposition process for the production of homogeneous and dense layers of TiB_2 on various substrates from high temperature molten salts was achieved to make the process reproducible and attractive for industrial application.

The work presented in this thesis was done at CEST Centre of Electrochemical Surface Technology (formerly ECHEM Centre of Competence in Applied Electrochemistry) as part of a joint project with industrial partners.

Kurzfassung

Das Ziel dieser Arbeit ist es, die Elektrochemie von Titan- und Borkomplexen bei Temperaturen von 600 bis 700°C zu untersuchen, um die optimale Temperatur für die elektrochemische TiB_2 Bildung festzustellen. Der Einfluss der verschiedenen Faktoren auf die mechanischen Eigenschaften, Morphologie und die Qualität der TiB_2 Beschichtungen von FLiNaK und Chlorid-Fluorid-Elektrolyte wurde erforscht um die optimalen Bedingungen der TiB_2-Abscheidung von hoher Qualität zu bestimmen.

Folgende Parameter wurden variiert: Strom Modus (Pulsstrom-Verfahren, die in Form von bipolaren und unipolaren (periodischen) Strompulsen - statt der konstanten Gleichstrom, angewendet wird), Stromdichte, Frequenz, Strom-Zeit Profile, Probenvorbereitung (chemisch oder mechanisch), Additive in den Elektrolyten ($TaCl_5$) und die Temperatur des Prozesses. Der Einfluss auf die Korrosion an den TiB_2-Oberflächen wurde in Kontakt mit flüssigen Aluminium-Legierungen ebenfalls untersucht.

Die Struktur der Komplexe in den Elektrolyten wurde mittels FTIR Spektroskopie identifiziert. Die Analyse der Beschichtungen wurde mittels der Rasterelektronenmikroskopie in Kombination mit der Energie-dispersiven X-ray-Spektrometrie, Röntgenbeugung, optische Mikroskopie, Mikro-Härteprüfgerät und Rasterkraftmikroskopie durchgeführt.

Es wurde eine Korrelation zwischen der Morphologie der Schichten, den strukturellen Eigenschaften und Abscheidungsbedingungen beobachtet. Es wurde festgestellt, dass die Morphologie und Rauheit der Schichten stark vom Strom Modus und den Abscheidungsbedingung abhängt. Die Schichten mit der geringsten Rauhigkeit (Ra = 102 ± 5 nm) wurden durch bipolare Strompulse erhalten. Die Werte der Mikrohärte liegen, abhängig von der Pulsfrequenz, zwischen 1800-2400 MPa. Die Eigenspannungen liegen zwischen -0.7 bis -1.3 GPa, wobei das Minimum bei einer Pulsfrequenz von 20 bis 100 Hz ermittelt wurde. Die Ergebnisse der Untersuchung des Einflusses von $TaCl_5$ als Additive auf die Eigenschaften der TiB_2 Schichten zeigen, dass eine niedrige Konzentration von $TaCl_5$ in der Schmelze die Qualität der Überzüge verbessert. Co-Abscheidung von TaB_2 in TiB_2 Schicht verkleinert die Korngröße und vermindert die Rauhigkeit der Abscheidung. Bei Zugabe von $TaCl_5$ erhält man Schichten von hoher Qualität bei gleichzeitig guter Reproduzierbarkeit. TiB_2 Schichten können Mo Substrate gegen Korrosion in flüssigen Al-Legierungen schützen. Es wurden am Interface TiB_2-Metallschmelze keine sichtbaren

Korrosionsspuren festgestellt. Die Optimierung des elektrochemischen Abscheidungsverfahrens zur Herstellung von homogenen und dichten Schichten aus TiB_2 auf verschiedenen Substraten aus Hochtemperatur-Salzschmelzen führte zu einem reproduzierbaren und attraktiven Prozess für den industriellen Gebrauch.

Die vorliegende Arbeit wurde im CEST Kompetenzzentrum für elektrochemische Oberflächentechnologie GmbH (vormals ECHEM Kompetenzzentrum für angewandte Elektrochemie), Wiener Neustadt, als Teil eines gemeinsamen Projekts mit industriellen Partnern durchgeführt.

List of symbols and abbreviations

hBN	hexagonal boron nitride
cBN	cubic boron nitride
pBN	pyrolitic boron nitride
CVD	Chemical Vapor Deposition
PVD	Physical Vapour Deposition
IBAD	Ion Beam Assisted Deposition
HES	High-temperature Electrochemical Synthesis
FLiNaK	ternary eutectic alkaline metal fluoride salt mixture LiF-NaF-KF
MRC	metal-like refractory compounds
CCP	continuous current plating
DC	direct current
PP	pulse plating
PIC	periodically interrupted current
PRC	pulse reverse current
AUX	auxiliary electrode
BSE	back scattered electrons
CV	cyclic voltammetry
ESEM	environmental scanning electron microscope
EDX	energy-dispersive X-ray spectrometer
GC	glassy carbon
SE	secondary electrons
WE	working electrode
RDS	rate-determining step

A	area of the electrode, cm^2
A_f	the frequency factor
c_0	bulk concentration of the electroactive species, $mol \cdot cm^{-3}$
D	diffusion coefficient, $cm^2 \cdot s^{-1}$
E_a	the activation energy, $J \cdot mol^{-1}$
E_p	peak potential, mV
$E_{p/2}$	the half peak potential, mV

F	Faraday constant (charge of one mole electrons), 96485.3 $C \cdot mol^{-1}$
j	flux of the reactants reaching the electrode surface, $mol \cdot cm^{-2} \cdot s^{-1}$
i	current density, $mA \cdot cm^{-2}$
i_p	peak current density, $mA \cdot cm^{-2}$
i_p^c	cathodic peak current density, $mA \cdot cm^{-2}$
i_p^a	anodic peak current density, $mA \cdot cm^{-2}$
k	heterogeneous rate constant for the electron transfer, $cm^3 \cdot mol^{-1} \cdot s^{-1}$
I	current, mA
n	number of electrons
Q	charge passed in electrolysis, $A \cdot s = C$
R	ideal gas constant, 8.31 $J \cdot mol^{-1} \cdot K^{-1}$
T	absolute temperature, °C
T	absolute temperature, K
T_m	melting temperature, K
T_w	working temperature, K
ν	potential scan rate, $mV \cdot s^{-1}$
α	charge transfer coefficient

1. Introduction

Boron forms a wide range of binary compounds with the transition metals of various structures and stoichiometries ranging from Me_5B to MeB_{66}. The diborides (hexagonal system, showing the AlB_2-type) are very important for many industrial applications due to such properties as high hardness, high melting point and high wear and corrosion resistance.

For example, TiB_2 exhibits excellent thermal and chemical stability up to 1700ºC, relatively low density of 4.52 $g \cdot cm^{-3}$ and a high melting point of 3225ºC [1, 2]. Owing to its specific properties TiB_2 is attractive to be used as coatings for high-temperature turbine for aerospace applications, industrial cutting tools and for wear-resistant surfaces. ZrB_2, HfB_2, VB_2, NbB_2, WB_2 and MoB_2 are isotopic with TiB_2, but their production is more expensive.

The most common industrial methods for deposition of refractory coatings are physical vapour deposition (PVD) [3] and thermal spraying [4]. High-temperature electrochemical synthesis from molten salts can be regarded as being one of the most promising methods for the preparation of refractory coatings. It permits to vary thickness of the deposits as well as the process speed and to obtain homogeneous, adherent and dense layers on the metal surfaces of complex configuration [5, 6]. Also, this method seems attractive from the economic point of view, since the temperature of the process is significantly lower and the equipment is quite simple. However, TiB_2 layers are not produced so far in industry due to the difficulties of plating homogeneous coatings with defined properties on large and structured surfaces and lack of the knowledge of the deposition process of TiB_2 out of high temperature molten salts.

As a result, much work is focused on the investigation of the cathodic processes in the electrochemical synthesis of titanium diboride in different molten salt electrolytes and on establishing of the correlations between the plating conditions and the properties of the coating [7-18]. The mechanism of the cathodic process in the electrochemical synthesis of titanium diboride in different molten salts has been studied by Makyta and Utigard [8]. Based on the analysis of the available experimental data, the authors assumed that in all fluoride melts the electrochemical synthesis of TiB_2 can be described via two reactions summarizing several single reaction steps [8]

$$TiF_6^{2-} + e^- \rightarrow TiF_6^{3-}$$

$$TiF_6^{3-} + 2BF_4^- + 9e^- \rightarrow TiB_2 + 14F^-$$

and in fluoride-chloride electrolytes by one overall reaction

$$TiCl_{6-x}F_x^{3-} + 2BF_4^- + 9e^- \rightarrow TiB_2 + (6-x)Cl^- + (8+x)F^- .$$

The effect of current density in DC mode electrolysis on the morphology of TiB_2 coatings on Mo substrate was studied in [12]. Makyta and Utigard [8] established the range of the cathodic current densities, within 0.2-0.5 $A \cdot cm^{-2}$, for deposition uniform, coherent TiB_2 coatings. The PP technique was applied to electrochemical synthesis of TiB_2 from FLiNaK melt by Ett and Pessine [13].This technique was than used in [14] where the effect of substrate (Mo, steel, carbide) was investigated. Lun Li and Bing Li in their investigations [15, 16] compared the electrochemical techniques of DC and PIC. They established that TiB_2 coatings deposited via PIC exhibit uniform thickness and less content of pores and impurities compared with coatings deposited via DC. Analyzing these data, one can conclude that PP technique has some advantages over the DC plating with regard to the quality of TiB_2 coatings, though further studies of the PP process are required for its industrial application.

Despite of all these studies, it seems there is still a lack of theoretical understanding on the electrochemical reduction process in order to describe the mechanisms and the rate determining steps, making the method of TiB_2 electrodeposition mature for a wide technical application.

The main objective of this thesis was to deposit TiB_2 layer out of high temperature molten salts on the large scale, which would protect the substrate material (namely Mo, steel and WC) from corroding in liquid metal.

To this end, three fluoride systems, such as KF, NaF-KF and FLiNaK were examined by means of FTIR spectroscopy as well as cyclic voltammetry measurements to define suitable electrolyte for the investigation of the mechanism of the TiB_2 deposition. FLiNaK electrolyte was chosen as supporting for the K_2TiF_6 and KBF_4 electroactive additives due to the lower melting point and wider electrochemical window in comparison with the other two systems. The individual electrochemical behaviour of the starting compounds, K_2TiF_6, KBF_4, $TaCl_5$ as well as their mixtures was investigated in FLiNaK

electrolyte in the temperature range of 600-700ºC by means of cyclic voltammetry. FTIR spectroscopy was employed prior to the cyclic voltammetry measurements for the estimation of the purity of the melt as well as for establishment and determination the nature of the complexes in the electrolyte.

The influence of the electrolysis conditions such as type of the electrolyte (FLiNaK and chloride-fluoride), mode and density of the applied current, substrate pre-treatment (pickled or sandblasted), and temperature in the range of 600-700ºC on the fundamental properties of the coatings was investigated. Based on some unexpected findings in the course of the improvement of the TiB_2 deposition process, the influence of the addition of $TaCl_5$ to the FLiNaK electrolyte on the electrochemical deposition process of TiB_2 and the properties of the layers deposited was examined. The structure and quality of the deposits were analysed using scanning electron microscopy in combination with the energy-dispersive X-ray spectrometry, the X-ray diffraction analysis, optical microscopy, micro-hardness tester and atomic force microscopy. The corrosion behaviour of molybdenum materials, protected by electrochemically plated TiB_2 coatings, in contact with liquid aluminium alloys was studied.

The data obtained in this work could be used for the electrochemical deposition of TiB_2 coatings in a pilot scale.

All these aspects were treated in the four main parts of the dissertation: chapter 2 is a literature review; the experimental methods used are described in chapter 3; chapter 4 presents the experimental results and discussion; chapter 5 contains the summary of the experimental results.

2. Literature overview

2.1 Coatings by refractory materials: property and application

Compounds with a melting point higher than that of iron (1535ºC) are called refractory. There is however not any lower limit of melting temperature that defines this group. Binary compounds of transition metals (e.g. Sc, Ti, Zr, Hf, Nb, V and Ta) with boron, carbon, silicon, nitrogen, and oxygen with the melting temperatures above 1500-1600ºC belong to such high-melting compounds, and to a certain extent, sulphides, selenides, phosphides, etc. High-melting compounds are extremely hard, chemically inert in corrosive environments, resistant to wear, non volatile at high temperatures and electrically conductive [19, 20]. Owing to this unique combination of properties, they are of great technical importance for several application such as nuclear, fossil and geothermal energy environments, high-temperature turbine coatings for aerospace applications, industrial cutting tools, waste reclamation and water treatment plants, wear-resistant surfaces, high-temperature sensors, systems used in foundry, automotive, heat-treating, incineration and power generation industries. Some properties of protective coatings of high-melting compounds are summarized in Table 2.1.

Table 2.1: Selected properties of hard materials [2]

Compound	**Density ($g \cdot cm^{-3}$)**	**Melting point (K)**	**Micro hardness ($10\ N \cdot mm^{-2}$)**	**Thermal conductivity ($W \cdot K^{-1} \cdot m^{-1}$)**	**Electrical resistivity ($10^{-8}\ \Omega \cdot m$)**
TaC	14.5	4053	1790	22.19	20
WC	15.7	2873	2080	121.42	17
TiC	4.93	3340	3200	20.93	52
SiC	3.2	2473	3500	15.49	10^5
TaN	13.8	3273	3240	8.58	128
TiN	5.21	3223	2450	29.31	25
TaB_2	11.7	3423	2200	21.35	68
TiB_2	4.5	3173	3480	25.96	9
NbB_2	7.2	3273	1300-2600	16.75	12
ZrB_2	6.1	3273	2200	23.03	9.2
HfB_2	11.2	3473	2800	430	10
TiO_2	4.19	2128	700-1100	5	$1.2 \cdot 10^{10}$
ZrO_2	5.6	3023	1200	0.7-2.4	10^{16}

2.1.1 Carbide coatings

Carbides of the IV-VI group transient metals have high melting temperature and hardness, low evaporation rates and vapour pressures at high temperatures, excellent corrosion resistance, and other important properties. All this makes them promising materials for modern engineering. In the carbide group, the most important are WC, TiC, TaC, B_4C, SiC as well as VC, NbC and Mo_2C cemented with cobalt or nickel [21]. Boron carbide has a very high hardness and hence is used as a wear-resistant and abrasive material. Boron-carbide-containing welding rods are used to improve the wear resistance of a surface. Transition metal carbides such as VC are useful wear-resistant materials in tooling and other industrial applications. They possess extreme hardness and chemical inertness [22].

2.1.2 Nitride coatings

Owing to their extreme high-temperature properties, good corrosion resistance and hardness, nitrides coatings such as TiN and BN have been used widely for applications that require withstanding high temperature and corrosive conditions.

Boron nitrides are of three types: hexagonal boron nitride (hBN), cubic boron nitride (cBN) and pyrolitic boron nitride (pBN). Chemical vapour deposited (CVD) pBN crucibles are used for the semiconductor industry. Boron nitride coatings offer excellent protection for metallic and ceramic surfaces against chemical corrosion induced by molten metals like aluminum, magnesium, copper, zinc and their alloys. Titanium nitride coatings are changing both the appearance and performance of high speed steel metal-cutting tools. The life of TiN-coated tools increases by as much as tenfold, metal removal rates can be doubled and more regrinds are possible before a tool is discarded. Another example of a nitride coating is SiN, used as a structural ceramic in gas turbines to give more engine efficiency, fuel savings and less environmental pollution.

Hard coatings based on nitrides of transition metals (e.g. Cr, Hf, Nb, Ta and Ti) may protect the steel surface from erosion and soldering with liquid metals (e.g. aluminum) and improve the resistance against thermal cracking [22].

2.1.3 Silicide coatings

All transition-metal silicides are metallic in character and probably the most important properties in practice are their high melting points, stability and chemical inertness against oxidation and other reactions, maintained up to high temperatures. Because of these properties, silicide coatings are used as protective layers on alloys using in a high-temperature environment. The high thermal conductivities of silicides assist their thermal shock resistance and thus their attraction as high-temperature materials. Chemically, silicides also possess good resistance to the mineral acids and, in the case of titanium and molybdenum silicides, even to hydrofluoric acid and alkalis. The practical field of application of silicides extends not only to protective coatings on gas turbine components, rocket nozzles and re-entry cones in 'space-age' applications (with their very different temperature/time requirements; often short times only at extreme temperatures) but also to covering molybdenum wires or tapes in furnace-heater windings [23]. Molybdenum disilicide ($MoSi_2$) acts as an effective coating in improving the oxidation resistance of furnace components, such as molybdenum electrodes [24]. Use of high-temperature niobium alloys in propulsion systems has been limited primarily by their lack of oxidation resistance. Hence, where oxidizing conditions must be tolerated, niobium alloys are protected with silicide coatings. The typical life expectancy of these coatings ranges from several hundred hours at 1100ºC - 1200ºC to tens of minutes at 1500ºC - 1600ºC. Coatings of Pd–Si, used for space shuttle components, are produced on various substrates such as electrolytic nickel, Armco iron, ferro-nickel (50 wt.% Fe and 50 wt.% Ni), steels and nickel-based super alloys in order to achieve high-temperature oxidation and corrosion resistance [22].

2.1.4 Oxide coatings

The useful lifetime of high-temperature materials depends on the rate at which they oxidize. For some materials oxidation means complete destruction, but for others it means an accumulation of vital and protective oxidation products. The most commonly utilized self-passivating, protective oxides are chromia (Cr_2O_3), silica (SiO_2), alumina (Al_2O_3) and zirconia (ZrO_2). These oxides form a protective barrier between the base metal and the

environment. The level of protection afforded by the oxide is related directly to its morphology and the rate of transport of reactants through the oxide to the substrate. Some of the common oxides that have been deposited are Al_2O_3, SiO_2, CeO_2, the spinel oxides $MgAl_2O_4$ and $NiAl_2O_4$, yttriastabilized zirconia (YSZ) and YBa_3Cu_3Ox (YBCO) [25].

2.1.5 Aluminide coatings

Aluminide coatings forming protective alumina scales fulfil the requirements of high-temperature oxidation and corrosion resistance quite well. Aluminide coatings were the first coatings used to improve the oxidation resistance of vanes and blades in aircraft gas turbines. Aluminide coatings on transition metals such as iron, nickel or cobalt are based on intermetallics such as β-FeAl, β-NiAl or β-CoAl, whereas on refractory metals such as titanium, niobium or tantalum the aluminide coatings are based on $TiAl_3$, $NbAl_3$ or $TaAl_3$. The protective character of these coatings stems from the protective nature of the Al_2O_3 scale formed by oxidation of the intermetallic compound at elevated temperatures. Gamma (TiAl base), alpha (Ti_3Al base) and orthorhombic titanium aluminides can be categorized as having relatively low densities, good oxidation resistance and attractive high-temperature properties [26]. Other high temperature materials such as titanium alloys, titanium aluminides or niobium alloys are looked upon as future potential materials for applications such as space shuttle or subsonic long-distance planes [27].

2.1.6 Boride coatings

Boron forms a wide range of binary compounds with transition metals exhibiting amazing diversity of structures and stoichiometries ranging from Me_5B to MeB_{66}. The most important structural group thereof is the type of MeB_2 (AlB_2 type), which is conveniently described as a sequence of alternating boron and metal layers of hexagonal symmetry [2]. Principal attractions of borides are very high hardness values and high melting points, due to their strong covalent bonding. Metal borides generally have high negative free energies of formation, which gives them excellent stability under varied

conditions, outstanding chemical stability and inertness, implying often good oxidation resistance at high temperatures. The oxidation resistance of refractory borides decreases in the order $HfB_2 > ZrB_2 > TiB_2 > TaB_2$, NbB_2 and MoB_2. A further attraction in this context is their relatively good creep and good thermal shock resistance. Owing to their resistance to oxidation and creep, metal borides have found use in nuclear reactor components, where resistance in both high temperatures and chemical attack becomes important. Molybdenum and zirconium boride coatings are used in corrosion- and abrasion-resisting parts and in cutting tools. ZrB_2 and HfB_2 coatings have been used as coating materials at high temperatures in harsh environments due to their exceptional stability against molten metals, high strength and high temperature resistance to atmospheric oxidation. ZrB_2 coatings bonded within a Ni matrix have found attractive uses due to high oxidation and thermal shock resistance, e.g. in turbine blades and fuel nozzles [23].

The assessed binary phase diagram of Ti and B (Fig. 2.1), being in good agreement with thermodynamic calculations, depict three intermediate phases, orthorhombic TiB (FeB type structure), orthorhombic Ti_3B_4 (Ta_3B_4 structure) and hexagonal TiB_2 (AlB_2 structure) [28].

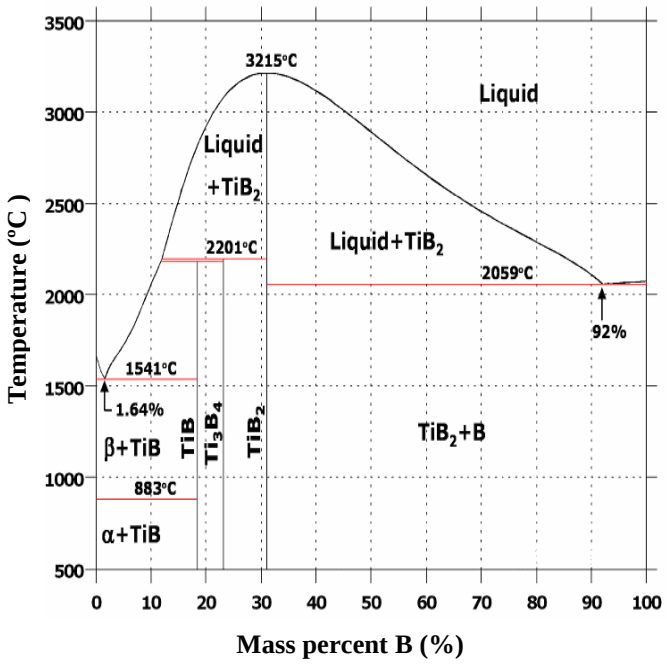

Figure 2.1: Phase diagram of Ti and B [28]

While TiB and Ti_3B_4 decompose peritectically at 2180ºC and 2201ºC respectively, TiB_2 melts congruently at 3215±25ºC [29]. The present work is focused on the electrochemical deposition of TiB_2 coatings.

Single crystal TiB_2 exhibits hexagonal symmetry in the AlB_2-type, with space group P6/mmm [30], where the boron atoms fill trigonal prisms formed by the titanium atoms (Fig. 2.2).

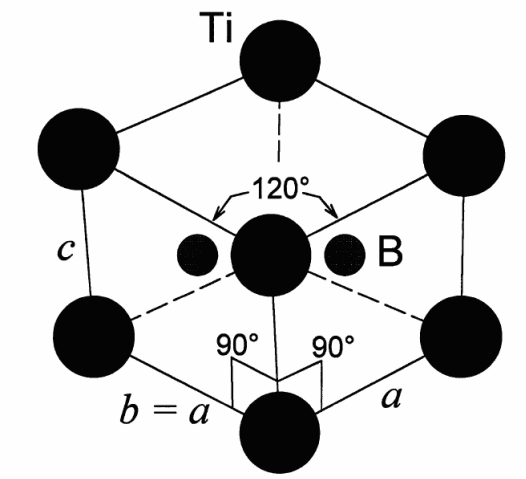

Figure 2.2: The hexagonal unit cell of single crystal TiB_2, a=303.1 pm, c= 322.9 pm, a=b≠c, α=β=90º, γ=120º, 1 formula unit per cell, Ti at (0, 0, 0), B at (1/3, 2/3, 1/2) and (2/3, 1/3, 1/2) [30]

TiB_2 is the technically most important compound of the transition-metal borides. ZrB_2, HfB_2, VB_2, NbB_2, CrB_2, MoB_2, and WB_2 are isotopic with TiB_2 and AlB_2. Titanium diboride has unique properties as extremely high hardness $(3350\ HV)_{0.5N}$, high melting point (2900ºC), excellent wear and corrosion resistance, and electrical conductivity [31-33]. Furthermore, it shows thermal and chemical stability up to 1700ºC, and resists the attack of molten metals and hydrochloric and hydrofluoric acids, but reacts with alkalis, nitric and sulphuric acids. TiB_2 is resistant to oxidation in air up to 1000°C. Due to these properties, TiB_2 is a candidate for a number of applications. The combination of high hardness and moderate strength make it attractive for ballistic armour, but its relatively high density and difficulty in forming shaped components make it less attractive for this purpose than some other ceramics. The chemical inertness, high electric and thermal conductivity as well as wettability by molten aluminium have found an increasing interest of using TiB_2 in the aluminium industry as e.g. coating of stirring tools or replacing/ covering carbon material, overcoming some disadvantages of using carbon in cell lining as cathodes [34, 35]. Carbon is not wetted by molten aluminum, and it is penetrated by the molten electrolyte and can also react with aluminium to form aluminum carbide. These problems shorten the lifespan of a carbon cathode; therefore, it is very essential to replace it by other materials that are suitable to meet the severe conditions in an aluminium

production cell. Ransley [36] proposed the use of TiB_2 – covered carbon as cathode material in aluminium electrowinning cells, since TiB_2 exhibits a good stability and mechanical resistance in cryolite. However, the replacement of the traditional carbon cathode by TiB_2 covered ones is relatively limited because of the high cost associated with its production. Therefore, the development of economical routes for the production of a TiB_2 inert cathode is one of the actual challenges in material sciences. TiB_2 also finds use as a container material for molten beryllium and other metals [37]. The high hardness and good wear resistance make titanium diboride a candidate for use in seals, wear-resistance linings, and bearings, nozzles for sand blasting apparatus and for cutting tools, protective coating on wire rod, tubing strip, pyrometer wells, die blocks, cyclotron, X-ray tube targets [38]. TiB_2 resistance to the attack by molten metals make feasible the use of it as thermocouple protective tubes for measuring elements to determine the temperature of molten metals in metallurgy, porous tube and plate filter assemblies for filtering molten aluminium, and protective coating on Ta or Nb thermocouple tubes used in molten aluminium [39, 40]. In combination with other primarily oxide ceramics, TiB_2 is used to constitute composite materials in which the presence of the material serves to increase strength and fracture toughness of the matrix.

2.2 Procedures for the preparation of refractory coatings

The rapid development of coatings in recent years is due largely to the availability of new coating methods, which can provide materials with properties that were unachievable. The general classification system for the deposition processes presented earlier by Rickerby and Matthews [41] is shown in Fig. 2.3. This classification divides the processes into the following four categories: gaseous state processes, solution state processes, molten and semi-molten state processes and solid state processes.

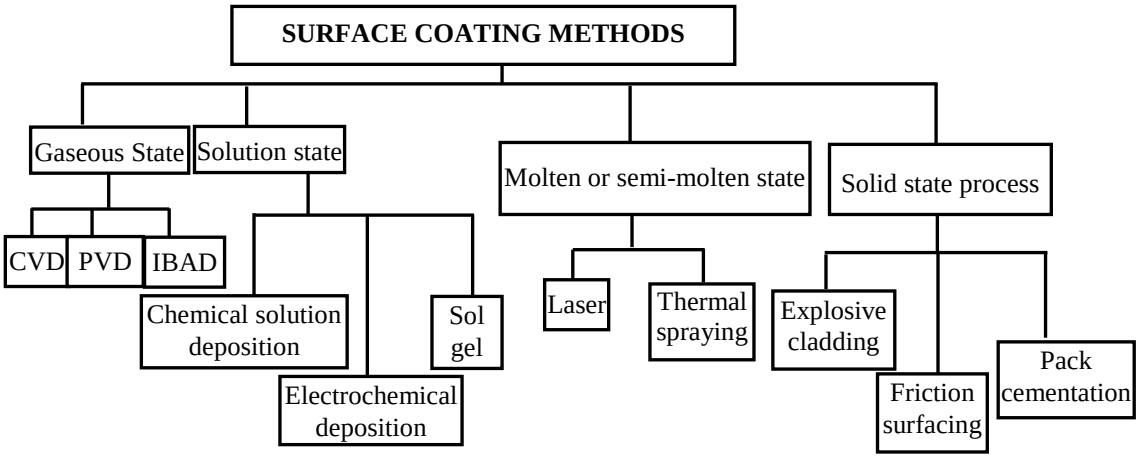

Figure 2.3: General classification of surface engineering techniques [41] (CVD – Chemical Vapour Deposition; PVD – Physical Vapour Deposition; IBAD – Ion Beam Assisted Deposition)

The most used procedures available for the preparation of refractory coatings in industry are chemical vapour deposition, physical vapour deposition, thermal spraying and electrochemical deposition.

2.2.1 Chemical vapour deposition (CVD)

Chemical vapor deposition (CVD) processes are widely used in industry due to their versatility for depositing a very large variety of elements and compounds covering a wide range from amorphous deposits to epitaxial layers having a high degree of perfection and purity. In the basic chemical vapour deposition process, gases containing material to be deposited are introduced into a reaction chamber, and condense on to the substrate to form a coating. The process normally requires deposition temperatures in the range of 800-1200^{o}C. The deposition pressure in CVD can range from atmospheric down to 1 Pa or less. There are various means of assisting the process, such as through the use of laser or electron beams, or by ion bombardment of the growing films [42]. It is possible to deposit films of uniform thickness and low porosity even on substrates of complicated shape via CVD [43]. CVD has various advantages over the other methods (relatively low temperature process allowing the preparation of refractory materials at a small fraction of their melting temperature; high deposition rates; good control over stoichiometry; morphology; crystal structure and orientation; and exceptional high-purity coatings) but

there are also limitations (many of the process and product gases commonly used in CVD are toxic and require special handling due to environmental concerns, thus raising operation costs; and this process is not well suited for multicomponent coatings containing many different constituents). A variety of pure metals or carbides, nitrides, borides, silicides and oxides of metals can be deposited by CVD processes.

2.2.2 Physical vapour deposition (PVD)

Physical vapour deposition (PVD) is a process whereby a material in bulk form is atomistically converted to a vapour phase in a vacuum and condensed on a substrate to form a deposit. There are three physical vapor deposition categories, namely evaporation, ion plating, and sputtering. In the evaporation process, vapors are produced from a material located in a source which is heated by direct resistance, radiation, eddy currents, electron beam, laser beam or an arc discharge. The process is usually carried out in vacuum (typically 10^{-5} to 10^{-6} torr) so that material from a thermal vaporization source reaches the substrate with little or no collision with gas molecules in the space between the source and the substrate. The vacuum environment also provides the ability to reduce gaseous contamination in the deposition system to a low level. The material vaporized from the source has a composition which is in proportion to the relative vapor pressures of the material in the molten source material. Thermal evaporation is generally done using thermally heated sources such as tungsten wire coils or by high energy electron beam heating of the source material itself. Generally the substrates are mounted at an appreciable distance away from the evaporation source to reduce radiant heating of the substrate by the vaporization source. In the ion-plating process, the material is vaporized in a manner similar to that in the evaporation process but passes through a gaseous glow discharge on its way to the substrate, thus ionizing some of the vaporized atoms. The glow discharge is produced by biasing the substrate to a high negative potential (-2 to -5 kV) and admitting a gas, usually argon, at a pressure of 2 to 200 mTorr into the chamber. In this simple mode, which is known as diode ion-plating, the substrate is bombarded by high-energy gas ions which sputter off the material present on the surface. In the sputtering process, positive gas ions (usually argon ions) produced in a glow discharge (gas pressure: 20 to 150 mTorr) bombarded the target material (also called the cathode) dislodging groups of atoms which

then pass into the vapor phase and deposit onto the substrate [44]. Although PVD methods typically require more expensive equipment, more parts preparation, more system maintenance and greater processing times than many alternative processes, PVD is a viable coating process for producing thin refractory and hard coatings. In some instances, PVD is the only method capable of depositing a coating of the desired material. The overall cost of the PVD often can be less than other coating methods when all the factors are taken into account. The primary considerations that must be evaluated before selecting a PVD process include the desired end result, substrate properties, cleaning and preparation, temperature and coating rates. Refractory metals such as Mo, Ta, W and their alloys are well suited for deposition by PVD.

2.2.3 Thermal spraying

Processes of thermal spraying can be grouped into two categories: lower energy processes often referred to as metalizing, which include arc and flame spraying, which are used frequently for spraying metals for corrosion resistance, such as zinc and aluminium; and higher energy processes such as plasma spraying, the detonation gun and high-velocity combustion spraying [22].

The plasma spraying process uses a DC electric arc to generate a stream of high temperature ionised plasma gas, which acts as the spraying heat source. The coating material, in powder form, is carried in an inert gas stream into the plasma jet where it is heated and propelled towards the substrate. The hot material impacts on the substrate surface and rapidly cools forming a coating. Plasma spraying has the advantage that it can spray very high melting point materials such as refractory metals like tungsten and ceramics like zirconia, plasma sprayed coatings are generally much denser, stronger and cleaner in comparison with the other thermal spray processes. Disadvantages of the plasma spray process are relative high cost and complexity of process [45].

2.2.4 Electrochemical deposition

Electrochemical deposition is subdivided into three main processes, namely, electrowinning, electroforming and electroplating. The objective of the electrowinning is to obtain the pure metal via an electrolytic extraction from a compound of the metal dissolved in the molten salt. In practice, it is commonly applied to the formation of the metal in a non-adherent form at the cathode, e.g. as a powder. Electroforming results, when the coating is made so thick that the substrate can be removed, e.g. from a mandrel, or dissolved away to produce a freestanding article of the coating material [46]. Some of the common uses for electroforming are jewellery, mould making and reproduction of parts. Electroplating, the process which was used in this work for the obtaining of TiB_2 layers, results in the formation of a coating on a conductive substrate by a process of electrolysis, whereby, the electroactive species reduce to a metal or alloy. The cathode (negative electrode) is the substrate to be plated. It is immersed in an electrolyte containing the required metal in an oxidised form or as a complex ion. The anode (positive electrode) is usually a bar of the metal being plated. During electrolysis metal is deposited on the substrate (cathode) and metal from the bar (anode) dissolves. Coating thickness is determined by the electrical charge passed through the electrode substrate (current × time), and there is no theoretical upper limit to the thickness which may be achieved. In general, there is a significant interaction between coating and substrate necessary for good adhesion. Industrial electroplating process (so called galvanizing) widely uses aqueous media for common metal electrodeposition (e.g. Zn, Cu, Ni) because of its low cost, non-flammability, high conductivities and high solubility of metal salts. However, despite these advantages, there is a main disadvantage of aqueous electrolytes such as a narrow potential range which makes them unsuitable in using for electrodeposition processes of highly electropositive metals, since applying cathodic potentials to the electrode causes the electrochemical reduction of protons and evaluation of hydrogen.

Another alternatives to aqueous electrolytes are based an organic solvents. Despite their wide potential window, organic media with an appropriate supporting salt have not been studied and are not used for electroplating due to their low electrical conductivity which increases the Ohmic drop between the electrodes and easy decomposition leading to products being found as impurities in the deposits. In addition, these solvents are quite dangerous due to their high vapour pressure, flammability and explosiveness.

By contrast, molten salt based electrolytes are excellent suitable for the electrodeposition of refractory metals and compounds at temperatures of up to 1000ºC. The wide potential window of molten salt electrolytes (ionic liquids) between decomposition at the anode and cathode limits allows the deposition of these highly reactive metals. Various reasons for these possibilities can be mentioned: a wide potential window of fused salts; the high temperature leads to fast electrochemical reaction kinetics, the Faradays efficiencies are close to 100%; the melts exhibits a high electrical conductivity minimizing the Ohmic-drop. Coating adhesion is enhanced by etching the base metal within the molten salt and/or interdiffusion phenomena. The high solubility of electroactive species allows one to work with a high content of the electroactive species. Good wetting of the cathode by the molten electrolyte forms the base for good throwing power [42].

The advantages of electrochemical deposition are relative simplicity of the equipment (Fig. 2.4), the ready accessibility of the initial compounds, the possibility of preparing simple or complex composed coatings of high-melting compounds, the relatively low temperature of the process compared to the melting points of the pure substances, the possibility of controlling the morphology and the composition of the cathodic deposit by varying the electrolysis parameters and producing pure, non-porous and coherent layers of refractory metals on substrates of complex configuration [47].

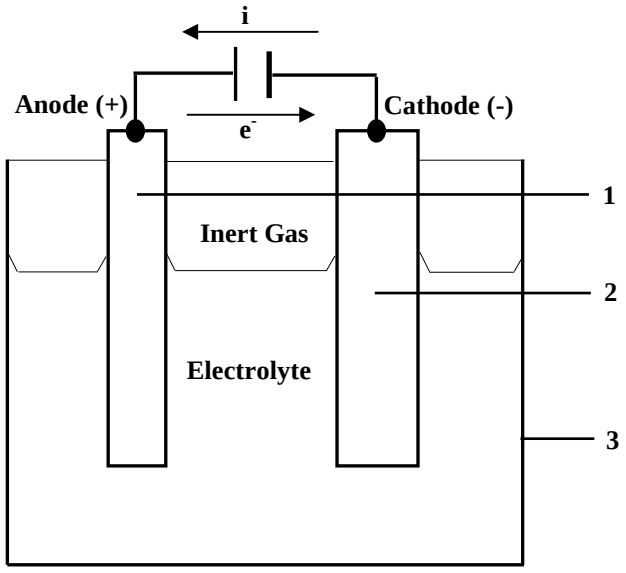

Figure 2.4: Schematic drawing of an electrochemical cell

The basic elements of the electrochemical cell construction as shown in Fig. 2.4 are (1) the electrodes, anode and cathode (metal substrate to be plated), and (2) the cell. The cell

contains the melt and the electrodes. The operation of the cell requires the selection of an appropriate temperature, electrochemical parameters, such as voltage and current density, and atmosphere – generally an inert gas.

For good coating adhesion, it is very important a cleaning process as pre-treatment of the cathode surface to remove surface impurities. This treatment can be mechanically based – grinding and polishing – or chemically based – etching and rinsing by water or organic solvents. Some molten salts, such as fluorides, are themselves good cleaning agents for removing oxide films, but in any case, successful plating requires clean and dry substrates.

2.3 Electrochemical deposition of TiB_2 out of high temperature molten salts

2.3.1 Electrochemical synthesis of borides

There are two principle methods used for obtaining of borides by high-temperature electrochemical synthesis (HES): deposition of boron on metallic substrates and co-deposition of the two components of the desired boride (Fig. 2.5).

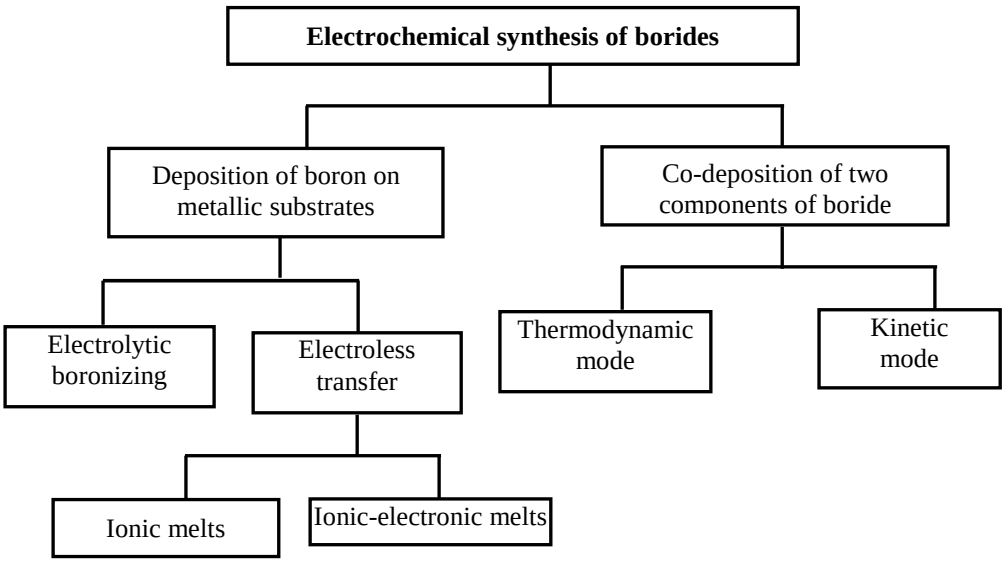

Figure 2.5: Classification of processes of the electrochemical synthesis of borides [48]

In the first approach, a molten electrolyte contains one component, in an ionic form, which is transferred to or discharged on the metal which is the other component (the cathode). The main disadvantages of this method are: a low formation rate of borides, their low thicknesses achievable and formation of compounds of variable composition.

In the second method of synthesis, the electrolyte contains both starting components (the electroactive species), which are reduced simultaneously or successively on the cathode. Afterwards, discharge products interact chemically. This method has some advantages in comparison with the first one. The main one is the possibility to produce borides with stoichiometry and thickness by varying electrolysis parameters, such as electrolyte composition, temperature, current density.

Electrochemical synthesis can be carried out in two modes: thermodynamically and kinetically based. According to Baraboshkin [49], the thermodynamic regime takes place close to the standard potentials of the components. Under these conditions the alloy composition is independent on the current density in a wide range of their values. A difference in deposition potential of metals in this mode does not exceed 0.2 V; otherwise, the kinetic regime takes place. This time, the alloy composition is independent on the difference in standard potential.

On the base of studies in [50, 51] it was established that the electrochemical synthesis of TiB_2 can be performed in the thermodynamic regime, i.e. the MRC (metal-like refractory compounds) is deposited from a melt at a more positive potential than the individual components, due to its high negative Gibbs energy of formation.

2.3.2 State of the art

Andrieux [52] was, apparently, the first who initiated studies on electrochemical synthesis in ionic melts. A large electrochemical school created by him in Grenoble (France) studied electrolysis of molten systems with the aim to obtain many metals, nonmetals, and their compounds.

The first studies concerning TiB_2 electrochemical deposition appeared in 1929 [52, 53], reporting preparation of TiB_2 powder or crystals from two electrolytic mixtures, containing MgO, MgF_2, B_2O_3, TiO_2 and CaO, CaF_2, B_2O_3, TiO_2 at 750ºC on Inconel and graphite substrates without any inert atmosphere. Two mechanisms were proposed for the

formation of titanium diboride out of a bath containing CaO, CaF_2, B_2O_3 and TiO_2. Andrieux [54] concluded that calcium metal was primarily deposited by electrolysis and it reduced chemically titanium dioxide and boric anhydride to titanium diboride. However, Meerson and coworkers [55] established, after an elaborate study with this bath, that titanium and boron were deposited due to discharge of Ti^{4+} and B^{3+} ions. In 1960, Stern et al [56] succeeded in preparing highly pure titanium diboride from titanium carbide and boron carbide at temperature of 720°C in an inert atmosphere using alkali chlorides as the electrolyte. The addition of double fluoride complexes (e.g. K_2TiF_6) had a beneficial effect on the dissolution of titanium carbide and boron carbide and the deposition of titanium diboride on the cathode. The current efficiency was of the order of 80%. Nies et al. [57] found that the addition of double fluorides to a melt containing titanium dioxide, boric anhydride, potassium fluoride and potassium chloride increased the purity of the product and the current efficiency at 800ºC without any inert atmosphere. However, potassium fluoride is hygroscopic and such substances are harmful as they decompose the salts and the double fluorides and increase the oxide content of a bath as given below:

$$2KBF_4 + 3H_2O \rightarrow B_2O_3 + 6HF + 2KF$$

$$K_2TiF_6 + 2H_2O \rightarrow TiO_2 + 4HF + 2KF$$

Over the next few years different oxidic electrolytes were tried. A method for the electrodeposition of TiB_2 at 900ºC out of a mixture of $NaBO_2$-$LiBO_2$-Na_2TiO_3-TiO_2 has been developed by Schlain et al. [58]. Titanium or sintered TiB_2 was used as an anode. The anode made of TiB_2 stabilized the bath. The rate of application of the coatings was 20 to 220 $\mu m \cdot h^{-1}$. The adherence of the TiB_2 deposit varied with the substrate material. Adherence was very good on Mo and 4130 steel, if these substrates were treated with a precoat with Cu and Ni. In 1972, Ganesan and coworkers [59] obtained dendritic TiB_2 deposits out of a TiO_2-B_2O_3-NaCl-NaF electrolyte on steel, copper and graphite substrates at 800ºC. In 1975, Gomes and his group [60] published on TiB_2 deposition out of a $Na_2B_4O_7$-Na_2CO_3-Na_3AlF_6-NaCl-TiO_2 melt, with a working temperature of 1050ºC.

However, since the 1970´s, there was a change concerning the electrolytes using for TiB_2 deposition. Inorganic halogenide salts became more preferred in comparison with oxide melts. The main reason of this was the improvement of the deposit properties, as TiB_2 obtained from oxide melts has higher oxygen content, since titanium is partly

deposited as TiO_2. As a result, the layer has a higher porosity and lower hardness. In addition, the melting point of halide melts is lower than that of oxide-containing melts, which implies that the working temperature also decreases. This facilitates the experimental work, minimizing the damage and corrosion for specific substrates, like stainless steel. Giess [61] in 1972 and Kellner [62] in 1973 patented a preparation of TiB_2 out of the electrolyte constituted by mixtures of LiF-KF-KBF_4-TiF_3 and of LiF-KF-BF_3-TiF_3 at 900ºC. A patent [62] proposes the production of TiB_2 layers by the electrolysis of molten salts with the introduction of BF_4^- ions by dissolving gaseous BF_3 with the use of a soluble anode made of boron. It is necessary that the bath contains fluoride of an alkali metal.

The interest of TiB_2 deposition increased during 1980's and 1990's due to its potential use as an inert cathode material in aluminum electrolytic process. Therefore, Makyta and co-workers focused on the preparation of TiB_2 coatings by electroplating in fluoride and fluoride-chloride containing electrolytes, at temperatures above 750ºC. The results presented involved the fundamental aspects of electrochemical kinetics [7], as well as several tests aimed at the improvement of the preparation process of coatings on some substrates [63]. From the discussion of the experiments [63] it followed that the electrochemical deposition of TiB_2 can be carried out either to form coatings or powders, depending on the composition of the electrolyte (the concentration of electrochemically active components and the B/Ti molar ratio), the employed method (galvanostatic-potentiostatic), operating parameters and temperature. The quality is also time dependent. It was established that electrolysis must be performed in an electrolyte with the molar ratio B/Ti > 4 while a minimum K_2TiF_6 content needs to be above one mol% and the temperature above 750ºC. At galvanostatic conditions, the electrolysis must be carried out at current densities within the range 0.2 to 0.8 $A \cdot cm^{-2}$, while at potentiostatic electrodeposition the potential should not exceed the -0.8 V limit (with respect to a Ni/Ni(II) reference electrode). Nearly at the same time, Wendt et al. [51, 64] in 1989 and 1991 published two papers in which they described the process of TiB_2 electrodeposition in fluoride melts on copper and carbon substrates. It has been shown that well adhering, dense and smooth layers can be obtained if the thickness of the coating is kept below 0.5 mm. In [65] Taranenko et al. examined the possibility of using chloride and chloride-fluoride (with a fluorine content not higher that 10 wt %) melts for high-temperature electrochemical synthesis of titanium diboride. It was shown that the reaction of formation of TiB_2 on the cathode is accompanied by a significant energy effect; the deposition

potential shifts by 0.32 V for TiB_2 at 973 K. The potentials under which synthesis takes place depend on the difference between the reduction potentials of components, i.e. on the shape of electroactive particles. In the systems under study, BCl_3-$TiCl_4$, MBF_4-$MTiF_6$, MBF_4-M_2TiF_6 (against the background of KCl-NaCl melt), the difference between the deposition potentials of titanium and boron does not exceed 0.2 V. Also, the conditions of high-temperature electrochemical synthesis were chosen by varying the cation-anion composition of the electrolyte. By changing the parameters of electrolysis, TiB_2 was obtained in the form of powders with different specific surfaces from 1000 to 50 $m^2 \cdot g^{-1}$ and as dense coatings of thickness up to 20 μm on different substrates.

New results were published in 1992-1996 years [66-68, 8]. All of them are aiming on the optimization of the preparation process of TiB_2 coatings, changing the electrolyte mixture or the experimental technique. In [66] authors investigated the process of electrochemical deposition of TiB_2 out of cryolite based electrolytes at 960ºC and KF-KCl melts at 800ºC using different electroactive species. They established that preparation of coatings from cryolite-based electrolytes containing K_2TiF_6 and KBF_4 was not successful. Coatings prepared from cryolite-based electrolytes containing B_2O_3 and TiO_2 were not coherent. Owing to the relatively high temperature both types of electrolytes undergo thermal decomposition. Electrolysis in potassium fluoride-chloride electrolytes containing KBF_4 and K_2TiF_6 provides coherent coatings with good adhesion to the substrate. In [8] Makyta's group found out the range of the cathodic current density, within 0.2-0.5 $A \cdot cm^{-2}$, for the deposition of uniform, coherent TiB_2 coatings. In 1999, the first research was reported on TiB_2 deposition at 600ºC from FLiNaK electrolyte using pulsed plating techniques [13, 69]. The quality of the TiB_2 coatings obtained on graphite rods were improved by pulse interrupted (PIC) and pulse reversed (PRC) methods. The authors established that the electrodeposition with pulse current plating (PCP) produces coatings with better quality, showing less cracks and better adhesion to the substrate, when compared with those obtained by continuous current plating (CCP). The interval of frequencies more suitable for the application of the current pulses is between 5 and 100 Hz; the best thickness obtained was at 100 Hz, the best ratio of the duration of the pulses t_c/t_{off} is between 5/1 and 3/1. The addition of B ions depolarizes the reduction of the titanium ion and the addition of titanium ions polarizes the reduction of the boron ions resulting in the formation of TiB_2, even at high current densities. No anodic effect was observed, using deposition with current pulse.

Afterwards, different investigations were performed on the influence of the electrolysis conditions (type of the electrolyte, substrate, temperature, mode and density of the applied current) on the fundamental properties of the coatings. Some correlations between the plating conditions and the properties of the coating were described in [70-74, 12, 14-16, 18]. In 1999 the Kaptay's group [70] studied the dependence of the morphology of TiB_2 deposits on different process parameters on the samples obtained from chloride-fluoride molten electrolyte at 700ºC. They stated that by applying PCP technique instead of DC (direct current) technique finer structures can be obtained: at low current densities (100-500 $mA \cdot cm^{-2}$) dense coatings have been observed, while above 500 $mA \cdot cm^{-2}$ - powders. Also the effect of current density in DC mode electrolysis on the morphology of TiB_2 coatings obtained on Mo substrate from NaCl-KCl-NaF-K_2TiF_6-KBF_4 molten system was studied in [12]. The authors marked out three morphology types depending on the current densities. The morphology goes from crystallites not clearly defined in shape at current density up to 50 $mA \cdot cm^{-2}$, to spherolitic in the range of 50-70 $mA \cdot cm^{-2}$, to the development of dendrites as current density increase to values of >70 $mA \cdot cm^{-2}$. PCP technique was used in [14] where the effect of substrate (Mo, steel, carbide) was investigated. Lun Li and Bing Li in their investigations [15, 16] compared the electrochemical techniques of CCP and periodically interrupted current (PIC) at 700ºC for deposition time of 30 min. The solvent used was a eutectic FLiNaK mixture containing K_2TiF_6 and KBF_4 (1:5 molar ratios). The authors established that TiB_2 coatings deposited via PIC exhibit uniform thickness, smaller grain size, less content of pores and impurities compared with coatings deposited via DC. Recently the authors in [18] have applied pulse plating (PP) techniques in forms of periodically reversed (PRC) and PIC instead of traditional DC procedure, which was also used for comparison - for the efficient deposition of the coatings onto molybdenum, stainless steel and tungsten carbide substrates with different geometries and surface areas. The effect of current density, frequency and pulse shape on the coatings properties was studied. It was found that the morphology and roughness of the deposit depend strongly on the deposition method and conditions.

Although fused salt electroplating of TiB_2 coatings had been achieved at the laboratory scale as long ago as the sixties, there has been no major commercial application. The main reasons for this are the following:

- Damage of the substrate material by the high temperature of the process.
- Poor reproducibility of the electrodeposition process due to a lack of theoretical understanding on the electrochemical reduction process.

- Poor adhesion of the deposit to the substrate.
- Low quality of coatings on large surfaces.

2.3.3 Some aspects on molten salts and systems used for electrochemical deposition

Molten salts form a particular class of solvent, usually fully ionized, with cohesion resulting from coulombic forces. Their liquid state properties are similar to those of classical solvents, except for ionic concentration and therefore electrical conductivity, which are both much higher than those of aqueous or organic electrolytes. As an example, in Table 2.2 are compared the main physico-chemical properties of molten sodium chloride at 850ºC (melting point of NaCl is 800ºC) and an aqueous sodium chloride solution (10^{-1} mol.L^{-1}), at 25°C [75].

Table 2.2: Comparison of physico-chemical properties of molten NaCl and an aqueous solution of NaCl [75]

Electrolyte	**Ions concentration (mol·Γ^{1})**	**Density (g·cm^{-3})**	**Electrical conductivity (S·cm^{-1})**	**Viscosity (10^{-3} Pa·s)**
Molten NaCl at 850ºC	26	1.53	3.6	1.2
NaCl at 25ºC	10^{-1}	1.002	1.07×10^{-2}	1.012

Because of the short interionic distances, the melts have tendencies to form ionic or uncharged complexes. Another specific feature of molten salts is the lack of inert molecular medium between the ions.

The temperature range of melting (from -50ºC up to more than 1000ºC) of various molten salts is given in Table 2.3.

Table 2.3: Temperature range of molten salts [75]

Temperature range of melting	Examples of molten salts
-50 to 150ºC	HF-KF, ionic liquids (chlorides of alkylpyridinium, alkylimidazolium, and their mixtures with $AlCl_3$)
150 to 250ºC	Mixtures of alkali halides and $AlCl_3$
250 to 400ºC	Mixtures of alkali nitrates, nitrites, hydroxides
400 to 1000ºC	Alkali halides and their mixtures, alkali sulfates, alkali carbonates, and fluorides (cryolite)
>1000ºC	Silicates, oxides and their mixtures (molten glass, slags)

Fused-salt electrolytes are favored in cases where aqueous solutions cannot be used due to the liberation of hydrogen molecule during electrolysis, narrow electrochemical windows, low thermal stability, and evaporation. These are the reasons why scientists have searched for new non-aqueous melts to electrodeposit metals and compounds. The role of non-aqueous electrolytes especially melts in technology has become more and more important. Facing serious problems concerning the environment and energy, scientists have found out new possibilities in electrochemical applications using non-aqueous electrolytes. Thus, a molten salt electrolyte, almost as a rule, consists essentially of two components, the solvent and the solute. The solvent or the main component, called the supporting electrolyte, consists of a single salt or a combination of salts. The solute or the minor component, called usually as electroactive species, is a complex of the metal to be electrodeposited. On the basis of the electroactive species used they can be divided into two principal groups: (1) system containing halo-complexes of the deposited metals and (2) systems containing oxides or oxy-complexes of the deposited metals. Aside from the used system, it should be appreciably soluble in the melt, generally 5-10%, and be reducible within the electrochemical window of the solvent, i.e. the solute must be reducible in a potential range where the solvent is stable [75].

Usually, a single salt is used as a supporting electrolyte. Sometimes, however, a combination of salts designed to keep the eutectic temperature as low as possible. For example, the melting points of the individual alkali metal fluorides are near 800ºC, but the eutectic temperature of the frequently used eutectic mixture LiF-KF-NaF (FLiNaK) is 456ºC [76] (Fig. 2.6).

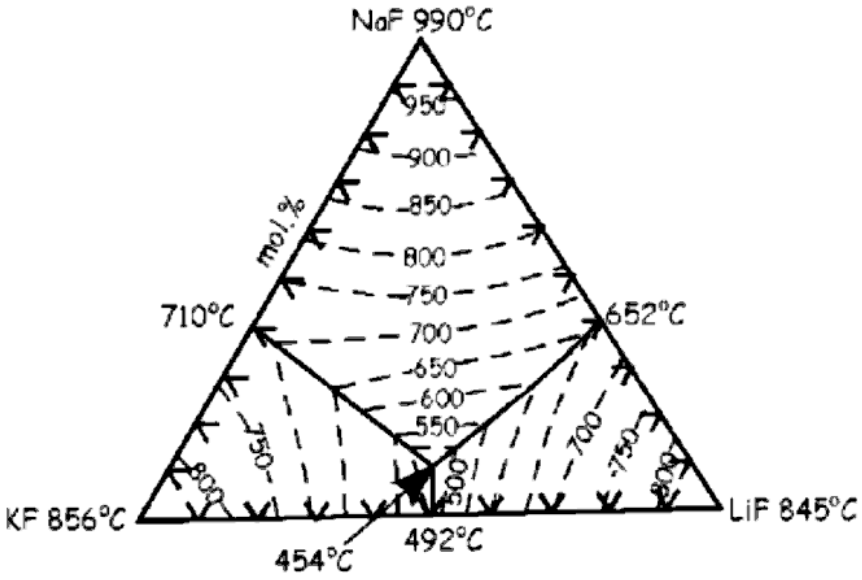

Figure 2.6: Phase diagram of FLiNaK (LiF 46.5 mol%, NaF 11.5 mol%, KF 42.0 mol%) electrolyte [76]

It is very important to keep the plating temperature as low as possible, consistent with good coating properties.

One of the most advantageous features of molten salts is the wide electrochemical window; that is, in many cases the accessible potential range is as wide as between alkali metal deposition (cathodic limit) and halogen gas evolution (anodic limit). The wide electrochemical window offers considerable merits in energy conversion and material synthesis applications. Another outstanding feature is the wide temperature range, for instance, the $AlCl_3$-EMIC system is liquid in the range of 200-450 K and LiF-NaF-KF is liquid between 732-1173 K. The wide temperature range enlarges the opportunity to control electrochemical and chemical reactions by temperature. Also molten salts, characterized by good thermal stability with reasonably low vapour pressure, high thermal conductivities, high specific heats, low viscosities, a very large electrochemical stability and high boiling points, do not suffer radiolysis and are good solvents [77-79]. Moreover, high reaction kinetics (either chemical or electrochemical reactions) is observed in fused salts. The use of fused salts in electroplating allow to avoid hydrogen embrittlement in the

coatings and high efficiency of the electrolysis leading to high rate of electrodeposition due to high throwing power.

In spite of all their advantages, molten salts exhibit some disadvantages ascribed to their chemical reactivity and the high temperature, i.e., specific materials have to be used for containers, vessels, membranes, etc.; due to their chemical interaction with water, molten salts must be carefully isolated from the open atmosphere; the high chemical and electrochemical kinetics entail corrosion problems if gradients are present (temperature, composition, etc.): molten salts may partially dissolve metals, among with alkali metals [75].

For good quality coatings the melt must be free of impurities. Since commercially available chemicals are hardly ever satisfactory, they must be purified before use. The procedure selected depends on the nature of the electrolyte components and the requirements of the particular process, but always includes removal of the water by vacuum baking at gradually increasing temperature (with as much water as possible removed at the lowest temperature to avoid hydrolysis), possibly followed by vacuum melting and bubbling an inert atmosphere through the melt. This procedure removes water but not oxides and hydroxides, which must be removed chemically. Chemical steps include sparging with the appropriate dry hydrogen halide gas (HCl for chlorides, HF for fluorides) followed by an inert gas. In order to remove metallic impurities, such as iron, a pre-electrolysis of the melt may be carried out as a final step. Voltammetric measurements can be used to detect possible interfering impurities in the operating electrochemical window. For solutes, vacuum drying at elevated temperatures is usually sufficient. Obviously, purification should be carried out on solvent and solute, separately, before they are mixed [76].

2.3.4 Systems used for electrochemical deposition of TiB_2

For electrochemical deposition of TiB_2 different salt systems are used. Among them are oxygen-containing and halide systems. Table 2.4 summarizes electrochemical deposition experiments of TiB_2 from different molten salt systems with the production of coatings or powders according to the chosen operating variables: composition of electrolyte, current density and temperature.

Table 2.4 Summary of electrochemical synthesis experiments of TiB_2

Electrolyte	Current density ($A \cdot cm^{-2}$)	T(K)	Structure of deposit	Reference
B_2O_3–TiO_2 – MgO –MgF_2 B_2O_3–TiO_2 – CaO –CaF_2		1223-1273	fines	[53]
TiC–B_4C–K_2TiF_6–KBF_4–NaCl		1273	powders	[56]
TiO_2–B_2O_3–KF–KCl		1073	powders	[57]
$LiBO_2$ – $NaBO_2$ – TiO_2 – $(Li,Na)_2TiO_3$	0.008-2.32	1148-1198	fines	[80-83]
TiO_2–B_2O_3–KF–KCl		1073	dendritic deposits	[59]
KCl-NaCl-NaF-K_2TiF_6-KBF_4		983	powders	[10]
NaCl – KCl – K_2TiF_6 – KBF_4	-	993-1003	fines	[56]
LiF – KF – TiF_3 – BF_3	0.099	810-1033	coating	[62]
LiF – KF – $K_2TiF_6(TiF_3)$ – KBF_4	0.09	973	coating	[61]
Na_3AlF_6 – NaOH – $Na_2B_4O_7$ – TiO_2	0.1-2.5	1173-1373	fines	[84]
Na_3AlF_6 – NaCl – Na_2CO_3 – TiO_2 – $Na_2B_4O_7$	-	1273	fines	[60, 5]
Na_3AlF_6 – Al_2O_3 – TiO_2 – B_2O_3	<0.05	1273	coating	[85]
Na_3AlF_6 – $B_2O_3 \cdot Al_2O_3$ – $CaTiO_3$	<0.02	1273	coating	[86]
NaCl – KCl – $TiCl_3$ - KBF_4	>0.03	973	fines	[11, 87]
$B_2O_3(Na_2B_4O_7, K_2B_4O_7)$ – TiO_2 (M_2TiO_3, $TiCl_3$, M_2TiF_6), M – Li, Na, K	0.01-5.0	1073-1373	coating or fines	[88]
KCl – KF – K_2TiF_6 – KBF_4	0.2-0.8	1073	coating or fines	[8]
LiF – KF – B_2O_3 – TiO_2	0.1-0.8	973-1223	dendrites or fines	[8]
LiF – NaF – KF – K_2TiF_6 – KBF_4	0.2-3.0	873-973	coating or fines	[64]
KCl – KF – K_2TiF_6 – KBF_4	0.2-1.2	873-1073	coating or fines	[64, 66]
Na_3AlF_6 – K_2TiF_6 – KBF_4	>0.25	1233	fines	[66]
Na_3AlF_6 – TiO_2 – B_2O_3 ($Na_2B_4O_7$) – (NaCl)	0.25-1.0	1243	coating or fines	[66]

Table 2.4: (continued)

Electrolyte	Current density ($A \cdot cm^{-2}$)	T(K)	Structure of deposit	Reference
$Na_3AlF_6 – AlF_3 – KF – TiO_2 – B_2O_3$ ($Na_2B_4O_7$) – (Na_2CO_3)	0.3-0.5	1223	coating or fines	[66]
$Na_2B_4O_7 – TiO_2$	0.01-2	1173	coating or fines	[88]
$LiF–NaF–KF–K_2TiF_6–KBF_4$		873	coating	[13, 69]
$NaCl - KCl – NaF – K_2TiF_6 - KBF_4$		973	coating	[18]
$LiF–NaF–KF–K_2TiF_6–KBF_4$		923	coating	[17]

The oxygen-containing electrolytes mainly consist of borates of alkali and alkali-earth metals. With its seeming advantages (it does not require a protective medium, and the reactants are readily available), it also has serious shortcomings - the high temperature of the process (above 1023 K) and the impossibility of obtaining a product that is oxygen-free without its additional purification. The electrolysis of halide melts is done not only with purely fluoride electrolytes - Li, K, Na, Rb, CsF, LiF - KF, Li, K, NaF - Na_3AlF_6 -
but also with chloride-fluoride electrolytes. The sources of titanium and boron are either fluorides of titanium and boron [62] or dissoluble anodes of boron [89], carbides of titanium and boron, and titanium diboride [90].

The basic criteria required for choosing an electrolytic melt are as follows:

- a low vapour pressure,
- a melting point as low as possible,
- a high electrical conductivity,
- a low viscosity,
- a large electrochemical window,
- a low corrosiveness for cell construction materials,
- a readily purified of the deposits and inexpensive.

In spite of the very wide range of molten inorganic solvents, there are very few fulfilling the requirements listed above. As a rule, halide melts satisfy in the best way all these criteria [91]. Amongst the several compounds tested [92] rare earth (e.g. La, Ce), alkaline (e.g. Li, Na, K, Cs) and alkaline-earth (e.g. Be, Mg, Ca, Sr, Ba) [93] metal chlorides and fluorides are the most suitable compounds in comparison with others. They give high stability melt if they are extra dried. It is well known that fluorides and chlorides

are very hygroscopic. With water, the reaction gives highly corrosive hydrogen fluoride or chloride which readily corrodes cell material at high temperatures [94]. With content of oxygen, fluoride anions give oxyfluoride complex anions which react with low-valency cations of the metal and give a protective polymeric film onto the cathode which inhibits a good quality of the deposited material [95]. The advantages of the chlorides as electrolytes are their lower costs compared to the fluorides, they are less corrosive towards the cell materials and substrates, and are more soluble in water, making them easier to analyze and remove from the product. However, most of them are hygroscopic, requiring dehydration and handling in inert atmospheres. Molten alkali fluoride melts are now more preferred for electrodeposition of refractory borides in comparison with chlorides. They have a low melting point especially if they are used in eutectic mixtures and a low vapor pressure even at high temperatures. Also fluoride ions exhibit excellent complexation properties, especially with refractory metal cations. This strong field complexation increases the high valency cation stability in the melt and avoids disproportionation reactions which could occur during the reduction process. The alkali fluoride solutions possess high conductivities which minimize IR losses at the high rates of metal deposition. The wide electrochemical window in these melts provides a versatile electrolyte suitable for the electrodeposition in coherent form of the refractory elements at moderate costs. Fluoride melts have strong etching properties on removal of metallic oxide layer onto the cathode surface [96]. Fluorides reduce the roughness and porosity of the deposit arising from the transport limitation by forming stable fluoride ion complexes in the bath [97]. Herein, molten alkali fluorides are well known from the sixties to provide smooth coatings of refractory metals [98] and surfaces of alloys [99]. So they are widely used as melts for electrochemical deposition coating at higher temperatures. However, the molten fluoride electrolytes possess a number of disadvantages:

- the operation of the electrolyte baths requires temperatures in excess of 600ºC limiting the choice of materials for the construction of the plating cells and the substrates available as cathodes;
- the electrolyte can be modified by atmospheric contamination;
- the plating process is sensitive to impurities such as oxide and chloride ions;
- fluorides and their vapours are toxic.

In practice, only fluoride melts with alkali ions like lithium, sodium, potassium are widely used, in eutectic mixtures, with a ternary (LiF-NaF-KF so called FLiNaK), or binary (e.g.

LiF-NaF, LiF-KF, NaF-KF) composition. In the present work it was important to characterize electrolytes with lower working temperature (< 650ºC) to prevent softening of the pre-hardened steel substrate. The FLiNaK electrolyte has proven to be efficient at these temperatures, presenting a low viscosity, high electrical conductivity and efficient stabilization of the active substances (Table 2.5). Chloride-fluoride electrolytes with a working temperature of 700ºC were used for electrochemical deposition on molybdenum substrates.

Table 2.5: Summary of the properties of FLiNaK electrolyte [100]

Salt composition (mol%)	**Formula weight ($g \cdot mol^{-1}$)**	**Melting point (K)**	**Density ($g \cdot cm^{-3}$)**	**Electrical conductivity ($\Omega^{-1} \cdot cm^{-1}$)**	**Thermal conductivity ($W \cdot K^{-1} \cdot m^{-1}$)**	**Viscosity (10^{-3} Pa·s)**
LiF-NaF-KF (46.5-11.5-42)	41.3	727	2.02	3.8 [101]	0.92	2.9

2.3.5 Basic requirements of the container materials and the design of the cell

As an important requirement concerning the container, the material should not react with the melt. Thus, the selection of the materials depends on the electrolyte and the operating temperature. Glass or quartz can be used only for chloride melts, but cannot be used in fluoride melts for long-term experiments, since small traces of moisture will result in the formation of HF which attacks the containers. For more aggressive electrolytes, such as fluoride melts, metal containers should be selected. Nickel is adequate up to 1000ºC, but some of its alloys, e.g. Inconel, may be attacked. Glassy carbon and platinum are very useful, but the high cost of such materials prohibits their industrial use [75]. Graphite which has been widely used as a crucible material is not suitable for this application. Actually, its surface disintegration leads to graphite flakes in the melt. Moreover when oxygen and moisture are excluded, some pure metals as Cu, Ni and Mo are suitable for handling and storing fluoride melts. Nickel could be selected advantageously. It exhibits good resistance in moisture free fluoride melts, it is easy to machinable and it is a cheap construction material [96]. In any cases, the entire electrochemical system must be protected from atmospheric corrosion. This is accomplished by surrounding it with an oxygen-free inert gas, generally argon. In addition, to prevent impurities from entering into the system, electrodeposition is carried out in an inert atmosphere typically of argon. Since

melts of alkali halides generally have high vapor pressures, the use of a vacuum during electrodeposition rather than an inert gas is not recommended.

For laboratory scale investigations it is possible to use a glove box to avoid the risk of contamination, to facilitate manipulation of additives to the melt and handling of the electrodes. For industrial application a system must be built which accomplishes the same objectives. All designs must provide for:

- Immersion of the electrochemical cell in a furnace to keep the melt at the desired temperature.
- Insertion and removal of electrodes without exposure to oxygen at elevated temperatures; possible additions of solute under the same conditions.
- No electrical shorting between electrodes.
- Insertion of a thermocouple or other temperature-measuring device, preferably into the melt, appropriate protected against corrosion [75].

2.3.6 Electrochemical deposition techniques

2.3.6.1 Electrochemical techniques

In order to deposit a coating a current flow in the melt must be established between the anode and cathode. The type of the current flow applied in the electrochemical deposition of TiB_2 layers significantly influences the basic properties of the layers. The main electrochemical synthesis techniques are based on the continuous current plating (CCP) and the pulse current plating (PCP) modes.

The two most frequency used current profiles at PCP are the periodically interrupted current (PIC) and the periodic reverse current (PRC) (Fig. 2.7).

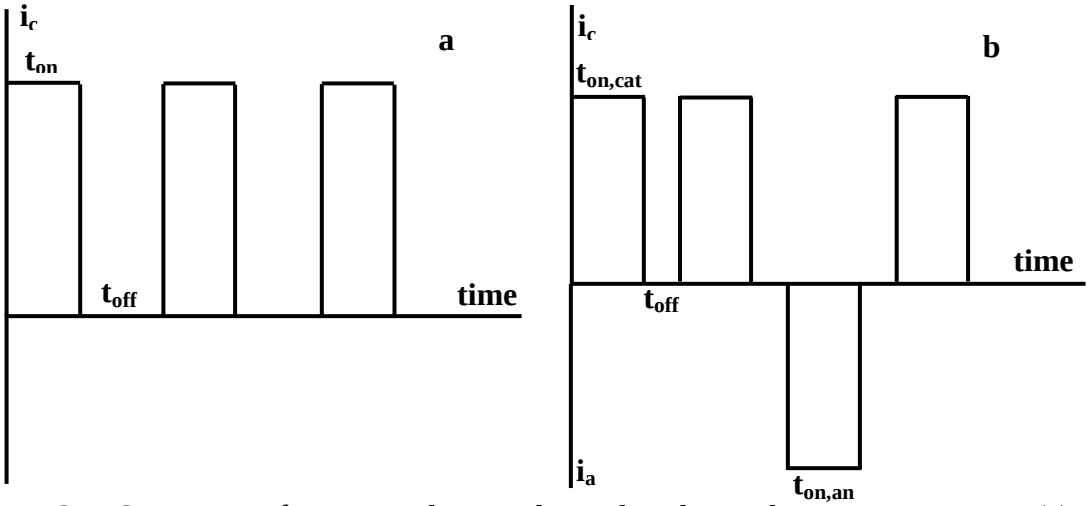

Figure 2.7: Sequences of current pulses used in pulse plating deposition processes (a) PIC mode, (b) PRC mode

Compared with the CCP technique, the PCP technique has more advantages in the deposition of TiB_2:

- uniform and dense deposits, fine grains without pores
- increase of ductility and adherence
- low concentration use of the electrochemical active species
- dendritic growth is less frequent
- increase of current efficiency and limiting current
- high deposition rate
- alteration of the morphology of the coating to surfaces with lower roughness.

The disadvantage of PCP is complex and time consuming optimization process of the parameters due to the number of variables (e.g. t_{on}, t_{off}, i_c and i_a).

Comparing the techniques of CCP and PCP in depositing TiB_2 Ett and Pessine [13, 69] conclude that the last one significantly improve the quality of TiB_2 layers, showing less pores, better adhesion to the substrate, less roughness and also decrease the time of electrolysis.

2.3.6.2 Electroplating using pulse of current

This technique efficiently hinders tertiary distribution of current on the cathode, occurring when the deposition reaction is controlled by mass transport [102]. Since the deposition reaction is controlled by mass transport, tertiary current distribution depends mainly upon the uniformity of the diffusion layer thickness. Geometrical influences and hydrodynamics are therefore involved in tertiary current distribution. As far as geometrical factors are concerned two cases are usually distinguished. Fig.8 recalls the characteristics of a “microprofile” and a “macroprofile” of a cathode surface including crests and holes, simulating a cathode surface where crystals are growing [102].

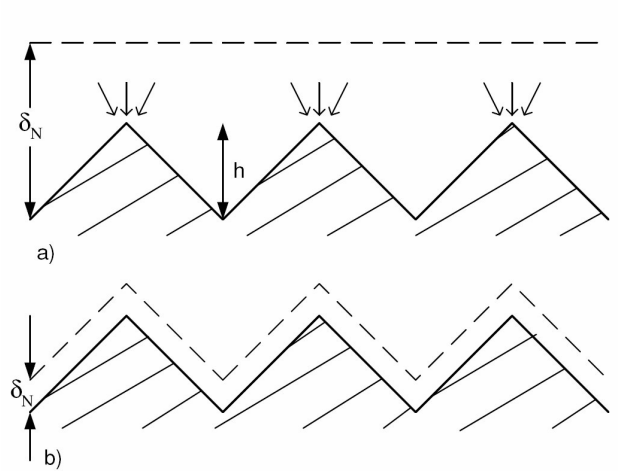

Figure 2.8: Influence of diffusion layer thickness on tertiary current distribution (a) “microprofile”: the crests are privileged from the point of view of diffusion, (b) “macroprofile”: the current density is uniformly distributed [102]

- A surface profile whose characteristic dimension h is smaller than the thickness of the diffusion layer is called a “microprofile” (Fig. 2.8a). The peaks are more accessible to diffusion than the recesses due to a peak effect analogous to that in primary distribution. As a consequence the irregularities of the surface are amplified in the course of the deposition; in other words, the microscopic throwing power under these conditions is bad. This explains the general observation that metal deposits obtained at or near the limiting current are rough or powdery [103]. This effect is of great importance in metal plating because of its influence on the appearance and the properties of the deposits.
- A surface profile with a characteristic length h larger than the diffusion layer thickness is called a “macroprofile” and the corresponding current distribution is

called “secondary” (Fig. 2.8b). In this figure a constant thickness of the diffusion layer is considered; i.e., each point on the surface is equally accessible for diffusion, which is not affected by geometrical factors. The concentration resistance has here an equalizing effect on current distribution.

Obviously, smooth coatings can only be obtained with a secondary current distribution, but the low coating growth rates hinder any industrial applications. The alternative use of pulsed current for electroplating of metals allows smooth coatings to be obtained for high deposition rates. The basic principle of this technique is that the growth of the diffusion layer can be controlled and kept thin during electrolysis. To do so, the duration of the pulses must be short enough to prevent the diffusion layer from growing excessively and off-times must lead to complete relaxation of the diffusion layer [104].

2.3.7 Proposed mechanisms of TiB_2 electrochemical deposition from high-temperature molten salts

2.3.7.1 Fluoride melt

The mechanisms of the electrochemical deposition of TiB_2 in pure fluoride melts (LiF-KF and FLiNaK) were investigated by Makyta and co-workers [8, 105, and 106]. Voltammetric experiments were performed in an electric resistance furnace. The shaft was made of special refractory steel and was protected by an internal nickel anticorrosive lining. It was closed by an air-tight water-cooled head. A Pt crucible was used as the melt’s container and as the auxiliary electrode. Two Pt wires were used as the working and reference electrodes. The experiments were conducted in a dry argon atmosphere at 750ºC. An equimolar LiF-KF mixture was used as the supporting electrolyte (Fig. 2.9) to which potassium hexafluorotitanate (K_2TiF_6) and potassium tetrafluoroborate (KBF_4) were added as the electrochemical active components.

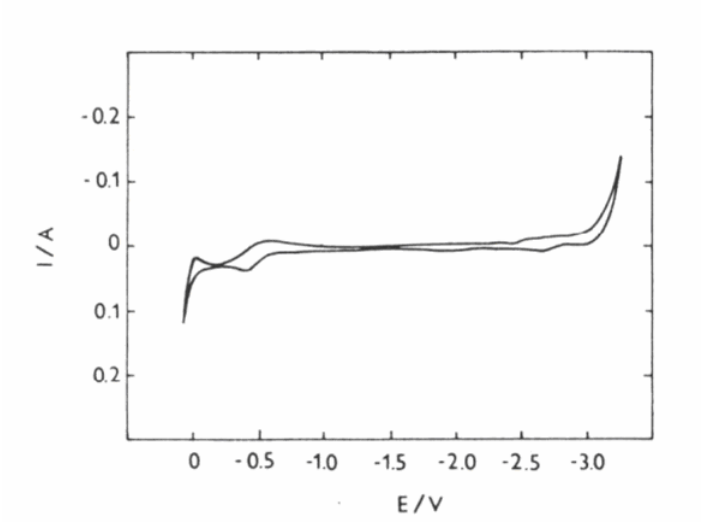

Figure 2.9: Voltammetric curve at a Pt-electrode of the pure supporting electrolyte LiF-KF at 750ºC; scan rate=1 V/, surface of the electrode 0.2 cm^2; Pt – quasi reference electrode [7]

Fig. 2.10 demonstrates the cyclic voltammetric curves recorded in LiF-KF-K_2TiF_6, LiF-KF-KBF_4 and LiF-KF- K_2TiF_6- KBF_4 electrolytes.

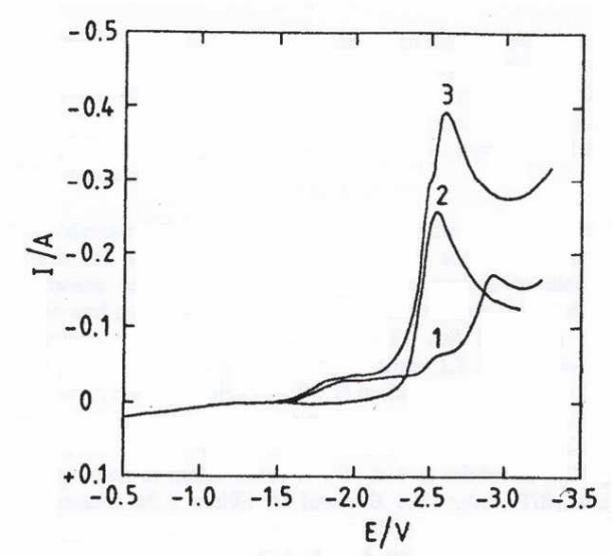

Figure 2.10: Voltammetric curves at a Pt-electrode in different electrolytes at 750ºC; scan rate=1 $V \cdot s^{-1}$; A= 0.2 cm^2; Pt – quasi reference electrode [7]
Curve 1 LiF-KF-K_2TiF_6, c(K_2TiF_6)=0.3 mol%
Curve 2 LiF-KF-KBF_4, c(KBF_4)=0.5 mol%
Curve 3 LiF-KF- K_2TiF_6- KBF_4, c(K_2TiF_6)=0.3 mol%, c(KBF_4)=0.6 mol%.

Based on the analysis of the experimental results the authors established that the reduction of Ti (IV) to metallic titanium in the system LiF-KF-K_2TiF_6 proceeds in two steps:

$$Ti(IV) \rightarrow Ti(III) \rightarrow Ti(0) \qquad (2.1)$$

where the first reduction step occurs at -1.7 V and the second step at -2.7 V, respectively (all the potential values are referred in this case to the potential of a platinum quasi reference electrode).

The voltammetric curves recorded in the system LiF-KF-KBF_4 (Fig. 2.10-curve 2) exhibits a single maximum at about -2.3 V, demonstrating that the reduction of B (III) to B (0) can be described by a simple 3-electron reaction:

$$BF_4^- + 3e^- \rightarrow B + 4F^- \qquad (2.2)$$

Hence, it was concluded that the electrochemical synthesis of TiB_2 in the system LiF-KF-K_2TiF_6-KBF_4 can be described by the following electrochemical reaction step:

$$TiF_6^{2-} + e^- \rightarrow TiF_6^{3-} \qquad \text{E = -1.7 V} \qquad (2.3)$$

$$TiF_6^{3-} + 2BF_4^- + 9e^- \rightarrow TiB_2 + 14F^- \qquad \text{E = -2.4 V} \qquad (2.4)$$

The electrochemical synthesis of TiB_2 by reaction (4) is facilitated by depolarization owing to the high negative value of the Gibbs energy for the formation of TiB_2 ($\Delta G^0_{(1000K)}$=-264 kJ/mol).

2.3.7.2 Chloride-fluoride melt

The mechanism of the electrochemical deposition of TiB_2 in chloride-fluoride melts was studied by Taranenko and co-workers [11]. Electrochemical measurements were performed in a three electrode cell, inserted in a quartz tube. The cell was thoroughly flushed with dry purified argon before each experiments and a slight overpressure of argon was kept in the cell throughout the experiments. Tungsten wires and glassy carbon rods (the active surface area of the electrode A = 0.2-0.5 cm^2) were used as working electrodes, and as a reference, an Ag/AgCl-KCl electrode constructed of a quartz tube sealed with a

fine quartz fritted disk. An eutectic mixture of NaCl-KCl-NaF was used as supporting electrolyte. $TiCl_3$ and $NaBF_4$ were added as electrochemical active components. Fig. 2.11 shows the voltammetric curves recorded in three different systems.

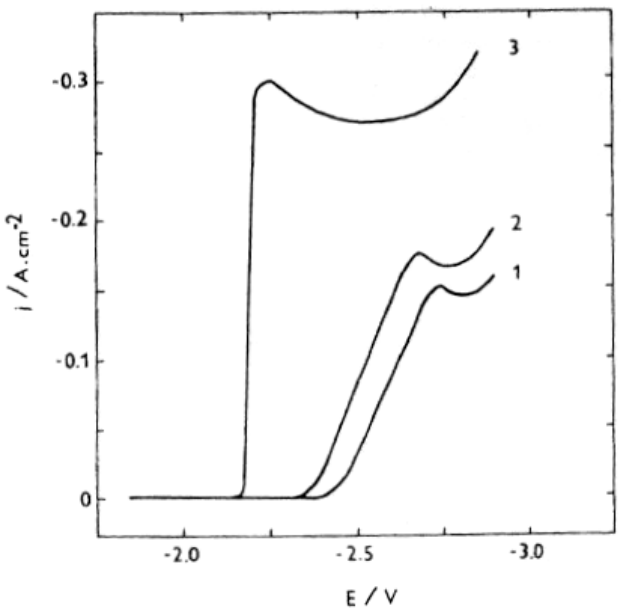

Figure 2.11: Voltammetric curves in different electrolytes at 700ºC; scan rate=1 $V \cdot s^{-1}$ [11]
Curve 1: NaCl-KCl-NaF-$NaBF_4$, c($NaBF_4$)=0.35 mol%
Curve 2: NaCl-KCl-NaF-$TiCl_3$, c($TiCl_3$)=0.4 mol%
Curve 3: NaCl-KCl-NaF-$NaBF_4$-$TiCl_3$, c($NaBF_4$)=0.4 mol%, c($TiCl_3$)=0.2 mol%.

Curve 1 represents the reduction of B(III) to elementary boron. Curve 2 represents the reduction of Ti(III) to titanium metal in the electrolyte NaCl-KCl-NaF-$TiCl_3$. According to Volkov and Yatsimirsii [107], titanium is present as a $TiCl_6^{3-}$ complex in this melt. The stability of this complex can be increased by a partial substitution of the large chloride ions by the smaller fluoride ones. It was found that the formation of the chloro-fluoride complexes of the type $TiCl_{6-x}F_x^{3-}$ is causing a change in the disproportionate reaction as well as in the mechanism of the Ti (III) reduction. Thus, the complex anion $TiCl_4F_2^{3-}$ at a molar ratio of Ti/F = 1/2 is reduced in a single $3e^-$ step

$$TiCl_4F_2^{3-} + 3e^- \rightarrow Ti + 4Cl^- + 2F^- \qquad (2.5)$$

The reduction potentials of the boron complexes are 0.05 V more negative than the reduction potentials of the titanium complexes (curves 1, 2 in Fig. 2.11).

When the melt NaCl-KCl-NaF contains both $TiCl_3$ and $NaBF_4$, there is a sharp increase in current, and the wave which is formed rises more steeply than in the reduction of titanium and boron containing complexes (curve 3 in Fig. 2.11). The voltammetric curve 3 exhibits a distinct reduction peak at -2.17 V, i.e. at a potential by 0.20 V more positive than the deposition potential of Ti and by 0.25 V more positive compared with the B reduction recorded at comparable conditions in the systems NaCl-KCl-NaF-$TiCl_3$ and NaCl-KCl-NaF-$NaBF_4$, respectively.

Based on the analysis of the available experimental data, the authors assumed that the synthesis of TiB_2 proceeds in two subsequent electrochemical reactions:

$$TiCl_{6-x}F_x^{3-} + 3e^- \rightarrow Ti + (6-x)Cl^- + xF^- \qquad (2.6)$$

$$BF_4^- + 3e^- \rightarrow B + 4F^- \qquad (2.7)$$

accompanied by the chemical reaction

$$Ti + 2B \rightarrow TiB_2 \qquad (2.8)$$

Thus, the process of the electrochemical synthesis of TiB_2 can be described by the overall reaction

$$TiCl_{6-x}F_x^{3-} + 2BF_4^- + 9e^- \rightarrow TiB_2 + (6-x)Cl^- + (8+x)F^- \qquad (8)$$

The observed shift of the potential corresponding to the synthesis of titanium diboride, is ascribed to the high negative value of the Gibbs energy of TiB_2 formation ($\Delta G^0_{(973K)}$ = - 264 kJ·mol^{-1}) [11]. Owing to it, the synthesis is facilitated by depolarization.

2.3.7.3 Fluoride-oxide melt

The mechanism of the electrochemical deposition of TiB_2 in fluoride-oxide melts was studied by Makyta and co-workers [105]. The cell and electrodes were the same as in the experiments in fluoride electrolytes (see 2.3.7.1). The experiments were performed in a dry argon atmosphere at 860ºC. An equimolar LiF-KF mixture was used as the supporting electrolyte to which B_2O_3 and TiO_2 were added as the electrochemical active components. Fig. 2.12 shows the voltammetric curves recorded in three different systems.

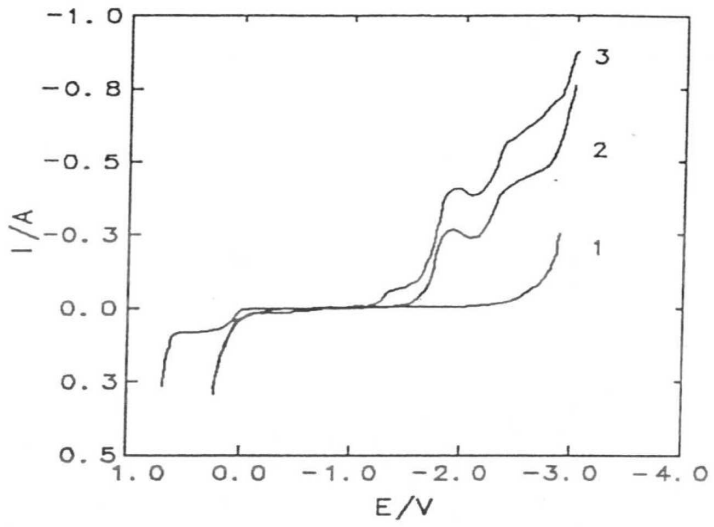

Figure 2.12: Voltammetric curves at a Pt electrode in different electrolytes at 850ºC; scan rate = 1 $V \cdot s^{-1}$, A=0.2 cm^2; Pt – quasi reference electrode [105]
Curve 1: LiF-KF-Li_2O, c(Li_2O)=0.5 mol%
Curve 2: LiF-KF –B_2O_3, c(B_2O_3)=5 mol%
Curve 3: LiF-KF –B_2O_3-TiO_2, c(B_2O_3)=5 mol%, c(TiO_2)=2 mol%.

Curve 1 is a voltammetric curve recorded in a LiF-KF electrolyte containing Li_2O which was added to the melt as Li_2CO_3. It is evident from the shape of the curve that the platinum electrode is well polarized in the alkali fluoride melt. The current flow at -2.9 V and 0.7 V correspond to the reduction of alkali metal cations and platinum oxidation, respectively. The wave at 0 V denotes oxidation of oxide ions. Curve 2 is a characteristic voltammetric curve recorded in a melt containing B_2O_3. In agreement with [106], the peak at -1.8 V is associated with the electrodeposition of boron from fluoroborate and oxoborate anions.
Curve 3 represents a voltammetric curve recorded in molten LiF-KF- B_2O_3- TiO_2. There are visible changes in the shape of voltametric curves brought about by addition of TiO_2 to

the LiF-KF–B_2O_3 electrolyte. A new wave appears on the cathodic part of the voltammetric curve starting at -1.3 V, attributed to the reduction of titanium and boron species with the formation of TiB_2. The position of the peaks compared to curve 2 remains in principal unaffected but the current value increases with the addition of TiO_2. The following mechanism of the synthesis of TiB_2 in fluoride-oxide melt was suggested by the authors [105]:

- During the dissolution of TiO_2 in a LiF-KF – B_2O_3 melt, complex ion(s) containing Ti and B are created. These ions were simultaneously cathodically reduced. The cathodic process is accompanied by the chemical reaction between titanium and boron creating TiB_2. The electrode process observed in the potential range from -1.3 V to -1.7 V is attributed to the reduction of complex ions containing titanium and boron with the chemical creation of TiB_2.
- The reduction of BF_4^- to elementary boron starts at -1.7 V. This process is accompanied by the reduction of Ti(IV) from complex compounds to titanium metal with the simultaneous formation of TiB_2.
- The electrochemical process starting at -2.2 V is ascribed to the reduction of B(III) from metaborate and tetraborate anions. The electrodeposition of boron is accompanied by the reduction of species containing titanium under the creation of TiB_2.
- At potentials more negative than -2.9 V, the processes discussed above are accompanied by the reduction of cations of alkali metals. The deposited alkali metal reacts in the melt with species containing boron and titanium leading to the formation of titanium diboride (electro-metallothermal mechanism).

3. Experimental part

3.1 Introduction

This chapter describes the materials and the experimental set up used in this work. The procedure of the pre-treatment of the substrates, preparation of the electrolyte and electrochemical deposition experiments is represented in detail. Electrochemical measurement techniques and microstructural analysis techniques such as X-ray diffraction (XRD), scanning electron microscopy (SEM), energy-dispersive X-ray spectrometry (EDX) and Bruker FTIR-spectrometer are also discussed.

3.2 Deposition experiments

3.2.1 Samples pre-treatment

Substrates (Mo, WC, steel) of different shapes were used as cathodes for the electrochemical deposition experiments (Fig. 3.1).

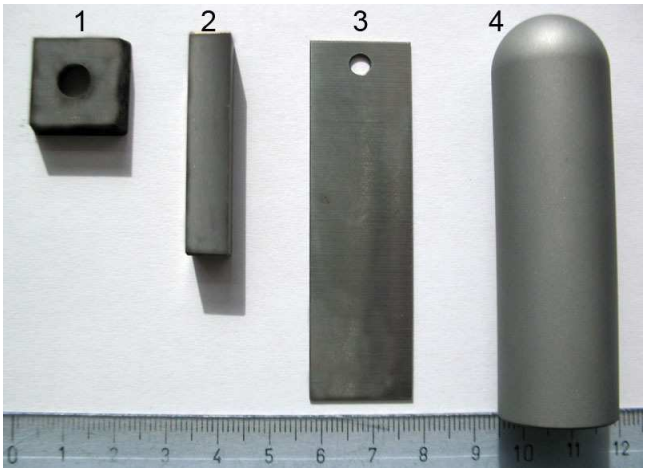

Figure 3.1: Geometries of the samples (1) tungsten carbide sample (area 13 cm^2), (2) stainless steel (area 17 cm^2) plate, (3) molybdenum plate (area 17 cm^2) and (4) molybdenum cylinder (diameter 30 mm, area 50 cm^2)

Chemical and mechanical methods were used to clean the surface of the sample. The steel substrates were pre-treated by the most common procedure used in the steel industry called as pickling/etch-cleaning to remove thick oxide scales. The steel substrates were pickled in 10% H_2SO_4 solution for 5 min. The mechanism of pickling involves the penetration of acids through the cracks into the oxide layer. Acid reacts with the innermost layer of the scale and forms hydrogen according to the reaction [108]:

$$Fe + H_2SO_4 \rightarrow FeSO_4 + H_2 \uparrow$$

As the hydrogen gas pressure increases, the scale is broken and gets detached from the metal surface.

The molybdenum and tungsten carbide samples were degreased in a solution of 30% NaOH and etched in a solution of 10% HNO_3 or sand blasted with Al_2O_3 300 mesh at 2.5 bar (Fig. 3.2).

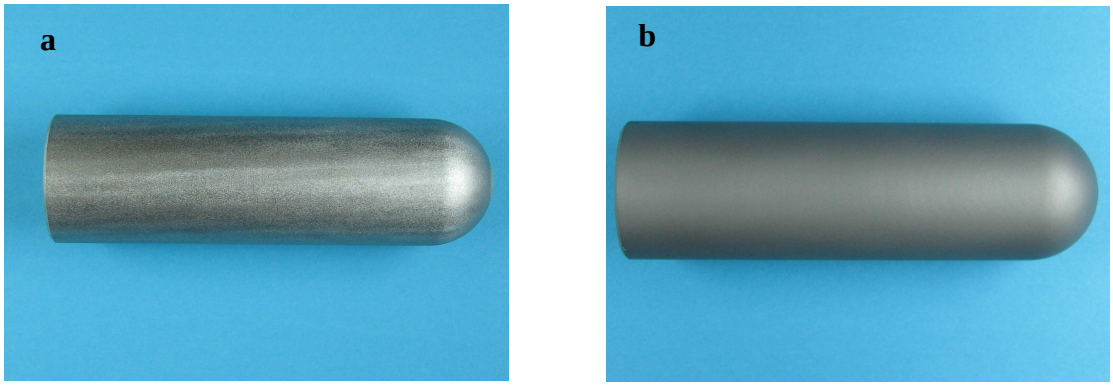

Figure 3.2: Optical pictures of the pre-treated samples (a) pickled Mo substrate (Ra=600 nm ± 20) and (b) sandblasted Mo substrate (Ra=2500 nm ± 20)

3.2.2 Preparation of the electrolyte

For the electrochemical deposition experiments two molten salt systems were used: FLiNaK (the molten eutectic mixture of 46.5 mol% LiF, 11.5 mol% NaF, 42.0 mol% KF, m.p. 454ºC) and a chloride-fluoride (43.3 mol% KCl, 43.3 mol% NaCl, 13.4 mol% NaF, m.p. 612ºC) mixture. Active components, K_2TiF_6, KBF_4 were taken at molar ratios 1:5 for the electrochemical deposition to get an excess of the volatile compound KBF_4.

The chemicals purchased from Aldrich and Fluka Chemical Companies (99.95%) were used as received without further purification. Only a drying procedure was applied before the electrochemical experiments since impurities such as H^+, OH^-, H_2O and O^{2-} in the electrolytes are undesirable. They decrease the mechanical properties of TiB_2 coatings, promote corrosion of the apparatus and allow some undesirable electrochemical reactions. For drying the solvent the following procedure was carried out:

1. Drying the individual components in an oven under vacuum (ca. 0.01 mbar) at 180ºC at least 48 hours
2. Mixing the electrolyte, placing it in a glassy carbon crucible and pre-drying it in the vacuum oven at 180°C for 24 hours
3. Introducing it in the electrolysis cell
4. Heating the eutectic salt mixture under vacuum (ca. 0.01 mbar) with a step height of 100ºC up to 400ºC (ca. 50°C below the melting point) for dehydration. Then melting it at 650ºC (m.p. 454ºC) under pure argon atmosphere
5. Cooling and crushing the electrolyte
6. Adding dried (in the vacuum oven at 100°C for 48 hours) active substances (K_2TiF_6, KBF_4, $TaCl_5$) to the fused solvent after cooling
7. Repeating procedure №4
8. Eliminating of the metallic impurities in the melt by the pre-electrolysis for 2 hours at 650ºC at 0.2 $A \cdot cm^{-2}$ using a Mo cathode.

3.2.3 Electrochemical deposition experiments

The electrochemical deposition experiments were performed on various (Mo, steel, WC) substrates at different temperatures under argon atmosphere in the electrochemical cell (Fig. 3.3) using a glassy carbon crucible as the melt's container and as the anode (Fig. 3.4).

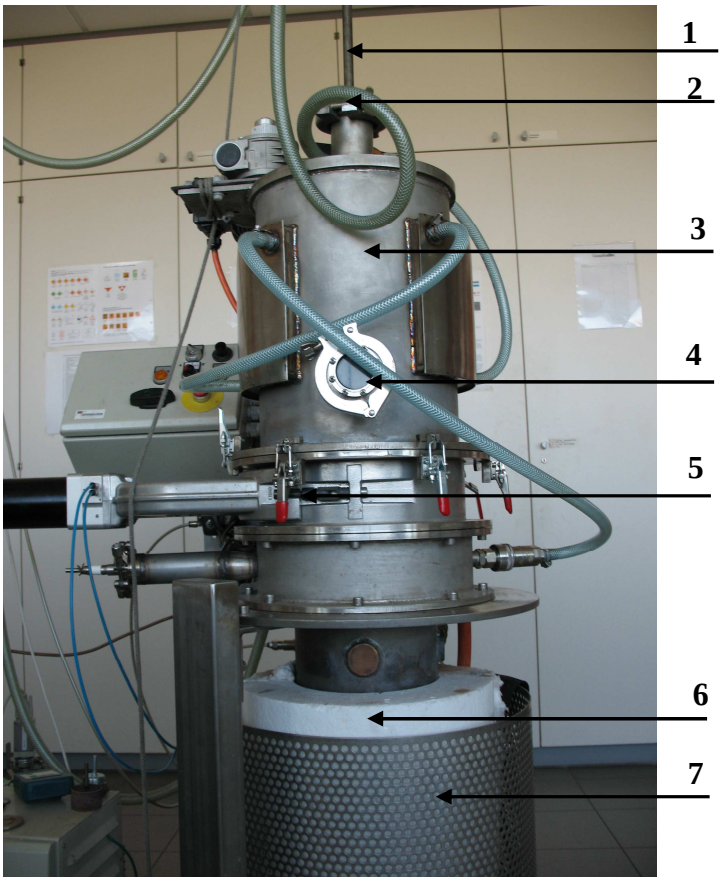

Figure 3.3: High temperature electrochemical cell (1) sample holder, (2) CaF_2 window, (3) evacuation chamber, (4) CaF_2 window, (5) sliding pressurized door, (6) thermal isolator, (7) the oven

Figure 3.4: Anode - glassy carbon crucible with a total volume of 3L

The cell is consisted of two main parts, the oven and evacuation chamber, which is separated from each other by a sliding pressurised door. The oven heating system is comprised of the electric heating coils attached to a stainless steel chamber, which is covered with a thermal isolator. The bottom is lined with stones for isolating the crucible and preventing the distribution of current out of the system. The upper part of the cell is used as the receiver for the deposits. It is equipped with a water cooled receiver-lock where the cathode deposit is held for cooling in argon atmosphere before removal from the cell. Two CaF_2 windows (positions 2 and 4 in Fig. 3.3) are used enabling a view to the melt and the sample.

Prior to each experiment the cell was evacuated and filled with argon 2-3 times. Before the deposition experiments a pre-treatment of the electrolyte was performed to reduce the concentration of contaminating compounds to a level below that which would interfere with the deposition process.

A power supply (Plating Electronic PE 86-20-5-25, D) was used for the pulse plating. Typical pulse sequences and parameters for pulse plating depositions are shown in Fig. 3.5.

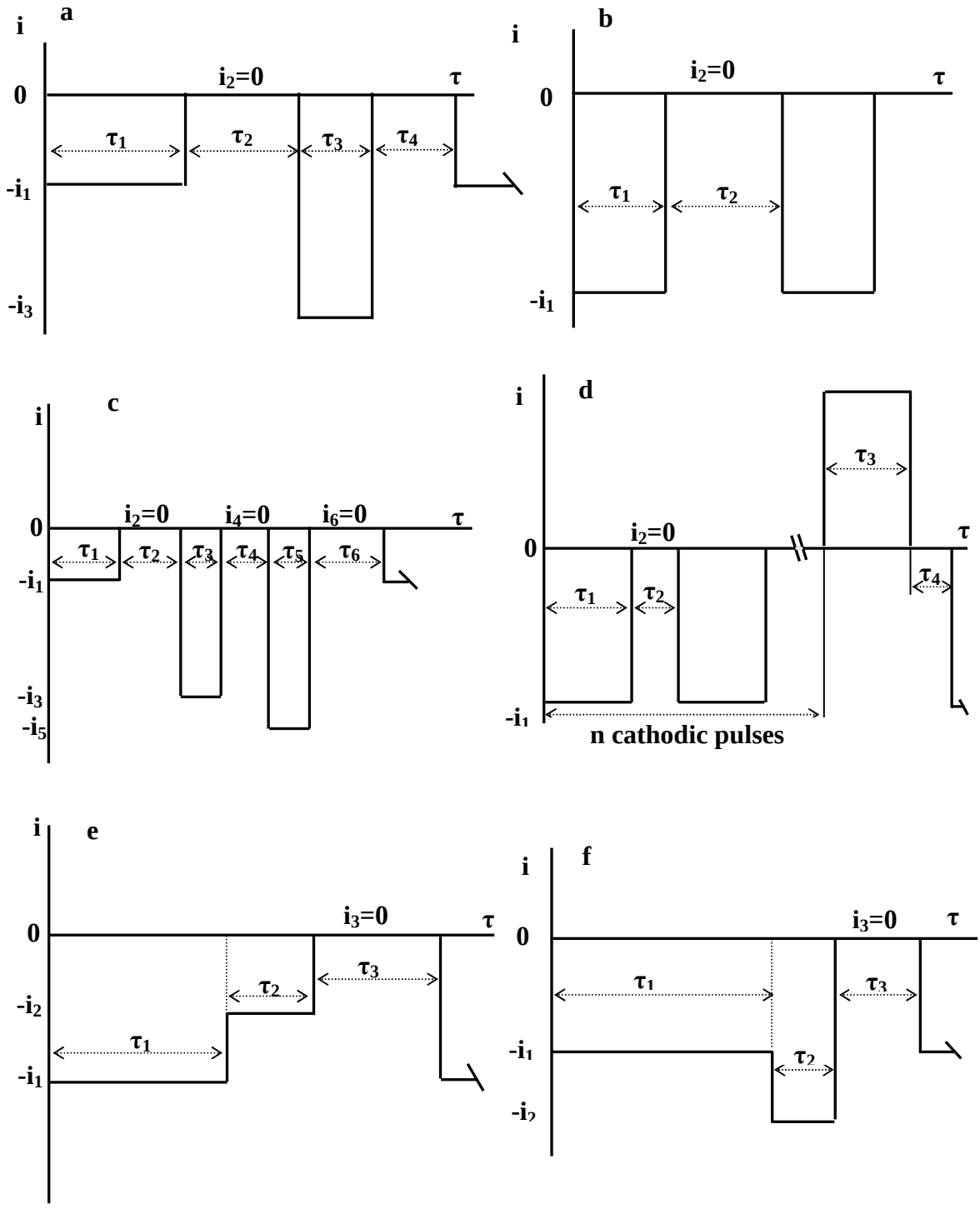

Figure 3.5: Shapes of current used in pulse plating deposition of TiB_2 and TiB_2/TaB_2. In PIC mode (a) $-i_1$= 0.01-0.03 A·cm^{-2}, $-i_3$= 0.1-0.5 A·cm^{-2}, $\tau_1=\tau_2=\tau_4$=0.1-10 ms, τ_3=1-4 ms; (b) $-i_1$=0.1-0.9 A·cm^{-2}, τ_1=0.8-8 ms, τ_2=0.2-20 ms; (c) $-i_1$=0.1-0.25 A·cm^{-2}, $-i_3$=0.4-0.5 A·cm^{-2}, $-i_5$=0.5-0.7 A·cm^{-2}, $\tau_1=\tau_2$= 5 ms, $\tau_3=\tau_4$=3-5 ms, τ_5=3 ms, τ_6=5 ms. In PRC mode (d) one anodic pulse follows by 5 cathodic ones, $-i_1=i_3$=0.3-0.75 A·cm^{-2}, $\tau_1=\tau_3$= 0.8-8 ms, $\tau_2=\tau_4$=0.2-2 ms. In pre-pulse plating (e and f) $-i_1$=0.07-0.6 A·cm^{-2}, $-i_2$=0.07-0.6 A·cm^{-2}, τ_1=1-20 ms, τ_2=1-10 ms, τ_3=1-20 ms.

Layers with a thickness of 10-30 µm were deposited within a polarization time of 15-30 min. After the experiments and cooling down the samples, residual salts were dissolved in hot water and the samples were further rinsed in 0.1% HCl solution for 10 minutes.

3.2.4 Cross section preparation of the coated samples

Cross section preparation of the coated samples consists of the following steps:

1. Cutting the samples on a diamond cut-off wheel
2. Mounting the samples in epoxy resin, which should be conductive and present low porosity
3. Polishing with SiC grinding papers (grit 120, 180, 500, 1200 and 2400) around 1 min with each one
4. Final polishing with 0.05 µm alumina
5. In addition, cross sections were ion etched (Precision Etching Coating System (PECS^{TM}) – Model 682 Gatan, USA) with 6.5 kV Ar-ions, during 4 min, using an angle between sample surface and ion beam of 65º
6. Making the samples electric conductive by coating with a thin layer (10 nm) of chromium.

3.2.5 Characterization of the coatings

The structure and quality of the layers were characterized by scanning electron microscopy (Philips XL-30 ESEM-FEG, NL) in combination with an energy-dispersive X-ray spectrometry (EDAX Phoenix system, USA), by X-ray diffractometry Bragg-Brentano mode (Philips diffractometer XR MPD, NL) with CuKα radiation (40 kV/30 mA) and optical microscopy (Olympus GX51, J). Rietveld refinement of the lattice parameters was performed using the TOPAS software package (Bruker AXS, D).

The 3D reconstruction of the specimen surface was done using the MeX software (Alicona (Al). The microhardness was measured using a microhardness tester (MHT-10, Anton Paar, AT) with a load of 1 N for 10 seconds. Atomic Force Microscopy (ATOS

Explorer, D) and a perthometer S2 (MarSurf XR 20, D) were used for characterization of the surfaces and the determination of the roughness values. Also surface roughness values of the coatings were calculated from stereoscopic images obtained by tilting the sample in the ESEM at the eucentric point at an angle of 5º. Compositions of the layers were measured via GDOES (glow discharge optical emission spectroscopy, GD-Profiler 2, Horiba Jobin Yvon, F). Residual stress was measured by X-ray method using CuK_α radiation and an automatic texture cradle (PW3068/00 ATC3, Philips, NL). The measurements were performed using the χ-mode, i.e. the angle of sample rotation was perpendicular to the ω- and to the 2θ-axes. The sample tilt angles ψ were selected in a way to achieve an equidistant sequence of $\sin^2\psi$ values [109]. The residual stress values in TiB_2 coatings were calculated using as a value of 5.4×10^{11}Pa Young´s modulus and 0.110 as Poisson´s number.

3.2.6 Spectroscopic measurements

FTIR-internal reflection spectra of the quenched samples of the melts were recorded using a Bruker FTIR-spectrometer Equinox 55 (MKII Golden Gate Single Reflection ATR System with Diamond Top Plate and KRS-5 lenses) with a MCT-nitrogen cooled detector in the range of 4000-350 cm^{-1} at room temperature (64 scans min^{-1}).

3.2.7 Corrosion characterization of the TiB_2 layers

The chemical resistance of the TiB_2 coatings on Mo cylinders was characterized by immersion tests in molten aluminium alloy in a furnace at air atmosphere under static conditions. These tests were carried out in the Österreichischen Gießerei Institut.
Static corrosion tests were performed in molten alloy, AlSi7Mg. The samples were half immersed into the melts under the atmosphere of ambient air at 720ºC. Durations of the tests were 24 and 168 hours.

The corrosion changes of the samples were first monitored visually with optical microscopy. Then the samples were studied by SEM, and elemental analysis by EDX on the respective cross-sections was performed.

3.3 Cyclic voltammetry

3.3.1 Electrochemical measurements

The electrochemical data were obtained using a potentiostat Voltalab 40 model PGZ 301 (Radiometer Analytical, France). A special miniature cell (Fig. 3.6) was constructed to carry out the experiments. It allows measure the cyclic voltammograms in the glassy carbon crucible (volume 3 ml) in inert atmosphere of argon up to 900°C with the reagents of high purity and controlling the influence of different parameters on the electrochemical behaviour.

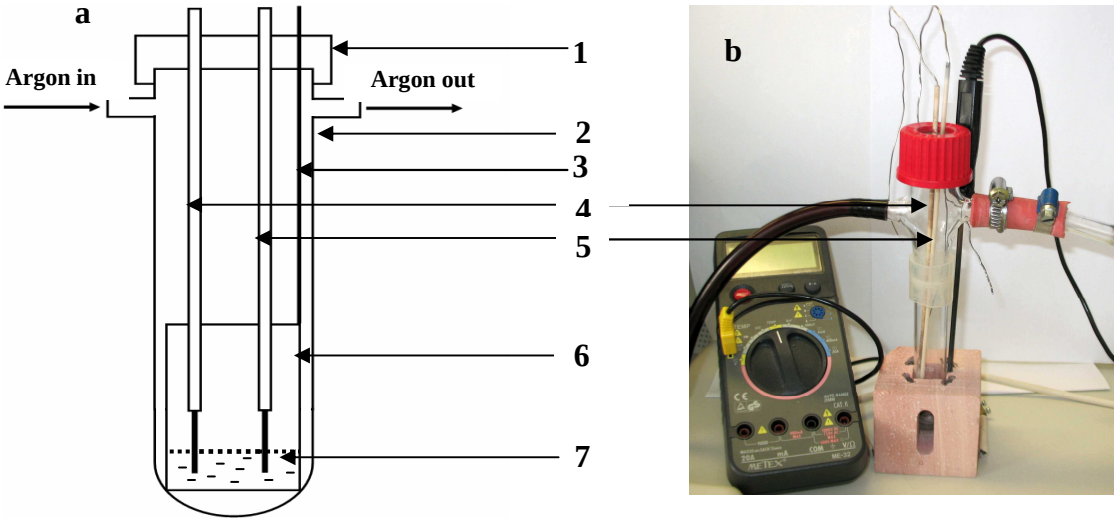

Figure 3.6: Electrochemical cell (a) schematic drawing (1) silicone rubber stopper, (2) quartz tube, (3) contact of the glassy carbon crucible, (4) working electrode, (5) reference electrode, (6) glassy carbon crucible as a counter electrode, (7) molten salt electrolyte and (b) optical picture

The glassy carbon crucible with the electrolyte was placed in a tightly closed three-electrode quartz cell in the glove box. Pt wires were used as the working (area of 0.16 cm^2) and reference electrodes and the glassy carbon crucible acts as the counter electrode. Before the measurements, the Pt-electrodes were carefully cleaned using silicon carbide

grinding paper (#4000), washed thoroughly with water, rinsed with distilled water and dried at 80ºC. The experiments were performed in the temperature range of 570 - 700ºC in an inert atmosphere of argon (99.999%) flow.

3.3.2 Preparation of the melts for cyclic voltammetry

FLiNaK, the eutectic mixture LiF-NaF-KF at a ratio of the components equal to 46.5-11.5-42.0 mol %, (m.p. 454°C) was used as the melt. LiF (m.p. 870°C) of analytical quality 99.99% was purchased from Merck, NaF (m.p. 993°C) and KF (m.p. 860°C) of analytical quality 99.99% were purchased from Sigma-Aldrich Chemical Company. K_2TiF_6 (m.p. 780°C) of analytical quality 98 % was purchased from Fluka and KBF_4 (m.p. 530°C) of analytical quality 97% was purchased from Riedel-de Haen. $TaCl_5$ (m.p. 211°C) purchased from Aldrich Chemical Company (99.999%, ampoule packed) was used as received.

Prior to use, alkali metal fluorides, K_2TiF_6, and KBF_4 were dried under high vacuum (~ 0.01 mbar) at 200°C for 48 hours in the glassy carbon crucibles placed in a quartz envelope. After drying, the chemicals were stored in a glove box (MBraun Star, O_2 and H_2O content below 1 ppm). The eutectic salt mixture was prepared in the glove box by mixing of the corresponding amounts of alkali fluorides and placed in the glassy carbon crucible. The FLiNaK mixture was stepwise heated under vacuum in the quartz envelope placed in the oven with a step height of 100°C up to 400°C (~ 50°C below the melting point of FLiNaK). Then the quartz envelope was refilled with Ar (99.999%) and the eutectic mixture was melted at 650°C for 20 min. After cooling down, the melt (FLiNaK) was crushed, grinded in the glove box and mixed with the individual precursors K_2TiF_6 (3 mol%), KBF_4 (6 mol%) and $TaCl_5$ (0.2 mol%). The mixtures with the individual active components were melted again in the glassy carbon crucible at 650°C for 20 minutes and were used for further electrochemical measurements.

In addition, a mixture with the compounds K_2TiF_6, KBF_4 and $TaCl_5$ at molar ratio of 1:2:0.06 was prepared in the same way.

The experiments characterizing the stability and purity of the electrolyte will be discussed later.

4. Results and discussion

4.1 Control of the purity of the melt and electrochemical stability of the electrolyte

4.1.1 Introduction

The use of molten salt electrolytes is not complete without discussing the importance of their purity. It is well known that fluorides are very hygroscopic and can adsorb significant amount of water from atmosphere leading to changes in the physical and chemical properties of the electrolyte and to initiation some undesirable electrochemical reactions. The purity of supporting electrolyte is of a great importance to obtain reproducible results, as well as to get the precise information of the electrochemical window of the melt (i.e. the range of potential where the melt being investigated is stable). Therefore, prior to the experiments, FTIR spectroscopy – detecting impurities in the melt and cyclic voltammetry of the FLiNaK, NaF-KF and KF electrolytes in defining the electrochemical stability have been performed.

4.1.2 FLiNaK electrolyte

4.1.2.1 Fourier Transform Infrared (FTIR) Spectroscopy

Before adding active substances to the electrolyte, the quality of the pure melt was checked by FTIR spectroscopy. The spectra of FLiNaK electrolyte before and after drying of the initial components are depicted in Fig. 4.1.1.

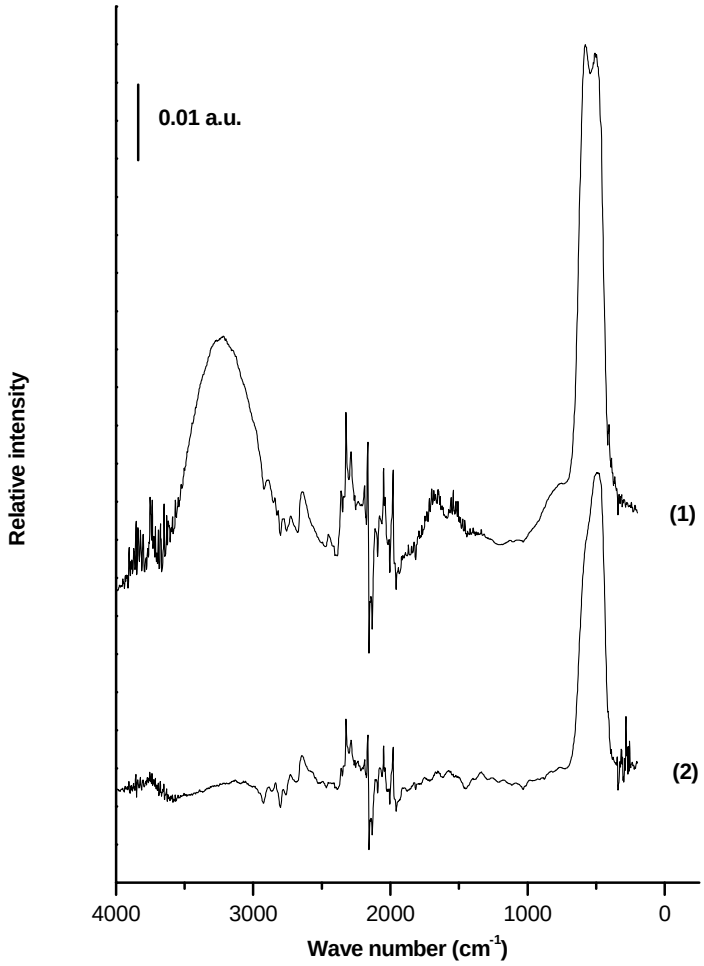

Figure 4.1.1: FTIR absorption spectra of FLiNaK electrolyte (1) before and (2) after drying of the components

The spectrum of FLiNaK electrolyte – before drying of the components (Fig. 4.1.1, curve-1) indicates an unsatisfactory quality of the salt mixture. As one can see, it exhibits additional bands resulting from different impurities: at 3200 cm^{-1} and 1687 cm^{-1} (vibrations of -OH), at 870 cm^{-1} oxyfluoride impurities [110]. After drying, the moisture content in FLiNaK melt was negligible (Fig. 4.1.1, curve-2).

Fig. 4.1.2 demonstrates the spectra of the FLiNaK electrolyte with the different qualities of the initial substances (99 and 99.99%).

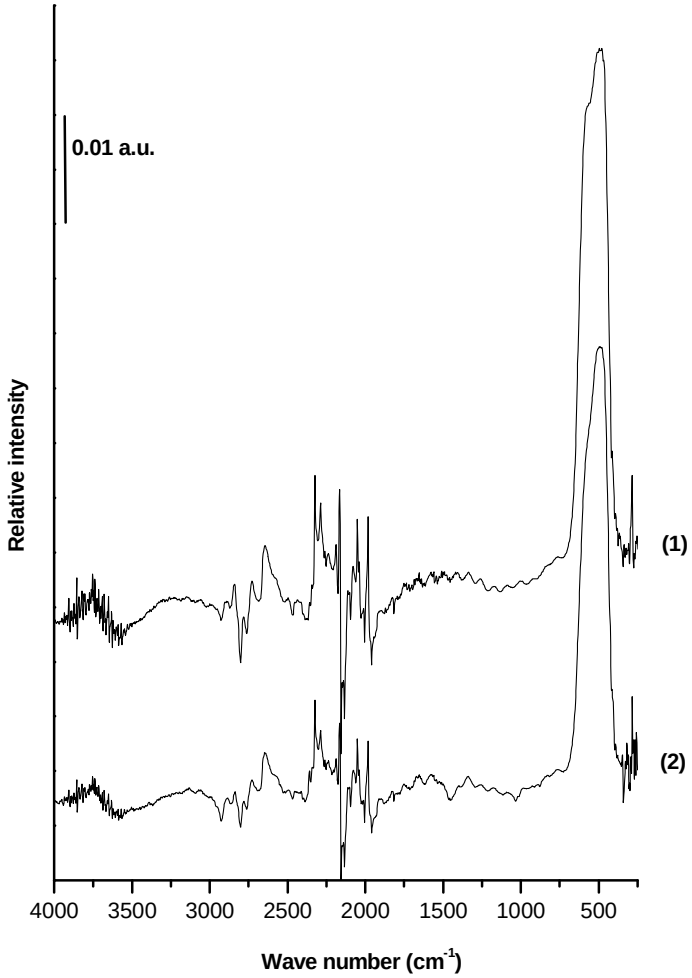

Figure 4.1.2: FTIR absorption spectra of the FLiNaK electrolyte after drying (a) the initial substances of 99.0% quality and (b) the initial substances of analytical quality 99.99%

The spectra demonstrate a good quality in both cases. Therefore, the chemicals with 99.0% quality were used in the further studies.

4.1.2.2 Cyclic voltammetry measurements

As a prerequisite in the investigation of the mechanism of the cathodic processes in the electrolytic deposition of TiB_2 and TiB_2-TaB_2 layers, the stability of the melt (supporting electrolyte) must be characterised. The electrode potential was scanned from 0 V (vs. Pt quasi reference electrode) in the negative direction at a scan rate 100 $mV \cdot sec^{-1}$ (Fig.4.1.3).

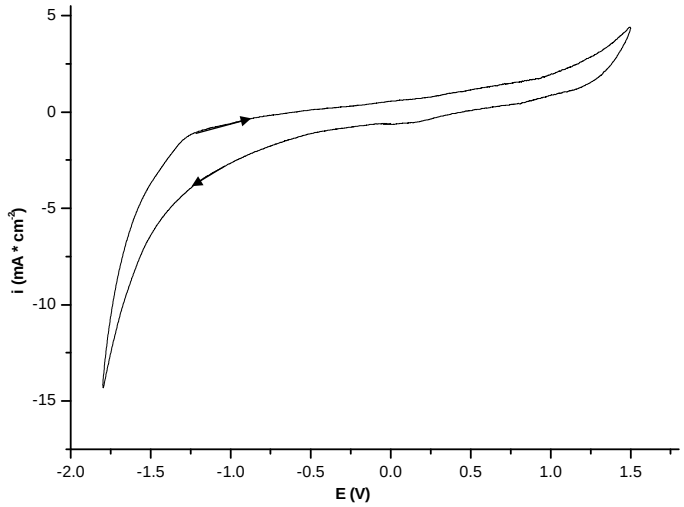

Figure 4.1.3: Cyclic voltammetry of the pure FLiNaK electrolyte; scan rate 100 $mV \cdot s^{-1}$, T= 600ºC, WE - Pt wire, A=0.16 cm^2; Pt – quasi reference electrode, GC – counter electrode

The pure FLiNaK electrolyte is stable in the range of -1.5 V to 1.5 V vs. Pt wire quasi reference electrode. The cathodic limit for the pure FLiNaK electrolyte is defined by the reduction of alkali metal cation (K^+) to metallic potassium. The potentials of KF, NaF and LiF dissociation in the corresponding pure alkali metal and fluorine, calculated from thermodynamic data are 4.86, 4.87 and 5.41, respectively [111]. Thus K^+ ions should be reduced first. In the anodic direction, the oxidation of F^- anion with F_2 formation is limiting the electrochemical window of the pure FLiNaK electrolyte. As one can see, neither peaks of oxidation nor peaks of reduction are observed in the potential range of -1.5 V to 1.5 V vs. Pt wire quasi reference electrode, indicating that the purity of the supporting electrolyte is satisfactory.

Besides, the curves were recorded in the pure FLiNaK electrolyte at different temperatures, varied from 570ºC to 700ºC at a scan rate 100 $mV \cdot sec^{-1}$ (Fig.4.1.4).

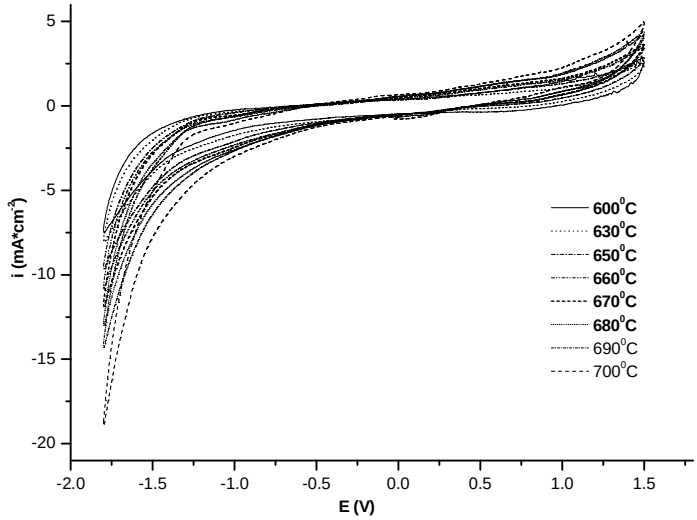

Figure 4.1.4: Cyclic voltammograms of the pure FLiNaK electrolyte recorded at the different temperatures; scan rate 100 mV·s^{-1}, T= 600-700ºC, WE - Pt wire, A=0.16 cm^2, Pt – quasi reference electrode, GC – counter electrode

The change in the temperature range of 600-700ºC has almost no effect on the shape of the voltammograms and the stability of the electrolyte. At 700°C the current flow at -1.5 V responsible for the reduction reaction K^+/K^0 is enhanced by a factor of 3.

The effect of water on the electrochemical window of the supporting electrolyte is shown in Fig. 4.1.5.

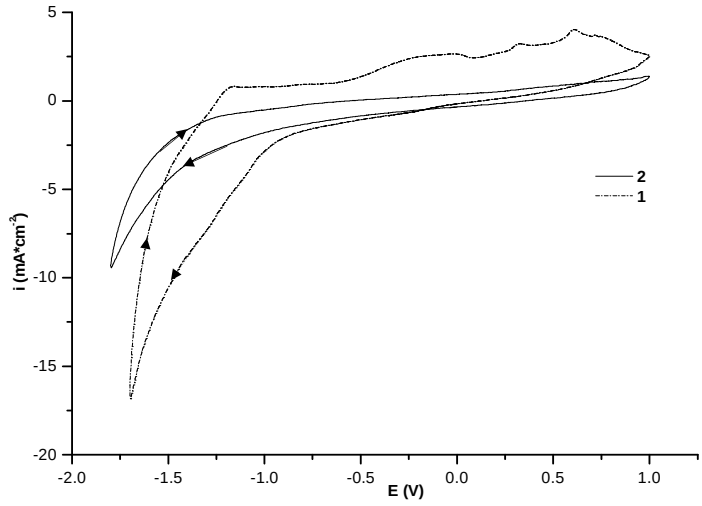

Figure 4.1.5: Cyclic voltammograms of FLiNaK electrolytes (1) before and (2) after drying of the components, scan rate 100 mV·s^{-1}, T= 650ºC, WE - Pt wire, A=0.16 cm^2, Pt – quasi reference electrode, GC – counter electrode

The potential window of the FLiNaK electrolyte consisted of the initial compounds which were not dried is shifted in the anodic direction by ~0.5 V. In addition, some anodic peaks can be observed (Fig. 4.1.5, curve 2), resulting in forming some undesirable oxyfluoride complexes.

4.1.3 NaF-KF electrolyte

4.1.3.1 Fourier Transform Infrared (FTIR) Spectroscopy

The IR-spectrum of NaF-KF electrolyte measured at room temperature after pre-melting, cooling down and grinding are depicted in Fig.4.1.6.

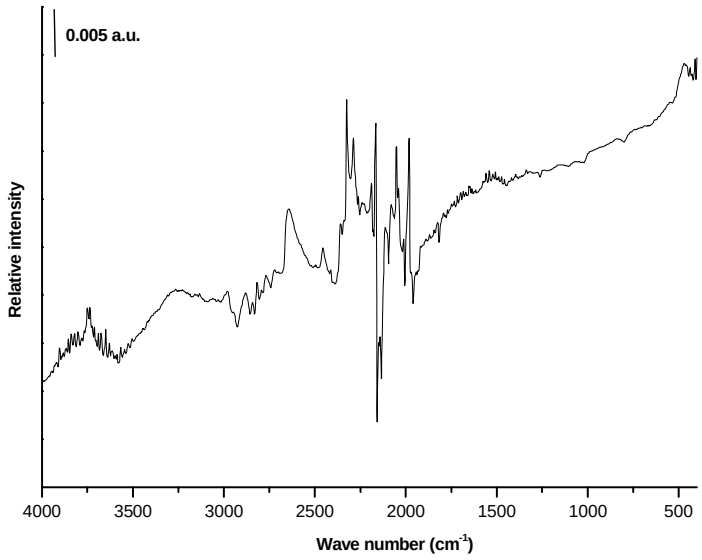

Figure 4.1.6: FTIR absorption spectrum of NaF-KF electrolyte after drying of the components

According to the spectrum in Fig. 4.1.6, the NaF-KF electrolyte (consisted of dried initial compounds) has unsatisfactory quality because of the extremely high moisture content (vibrational band at 3200 cm^{-1}) [110].

4.1.3.2 Cyclic voltammetry measurements

It was found that the pure NaF-KF electrolyte is stable in the range of -0.8 V to 0.5 V vs. Pt wire quasi reference electrode (Fig. 4.1.7).

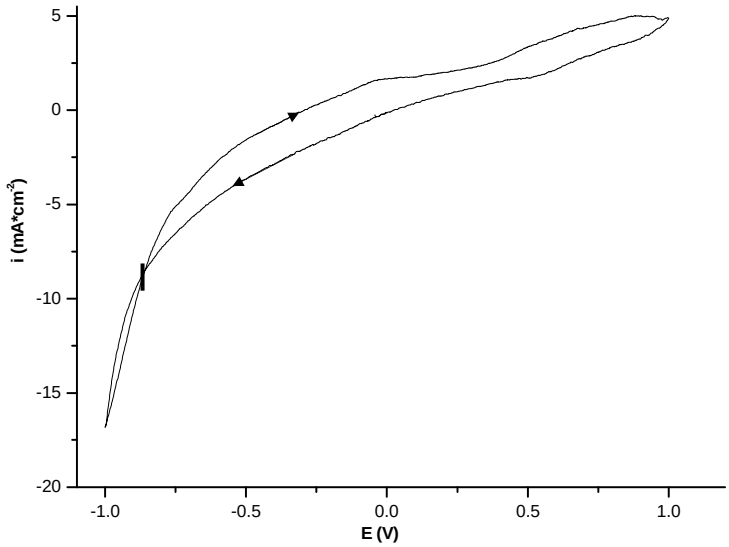

Figure 4.1.7: Cyclic voltammetry of the pure NaF-KF electrolyte; scan rate 100 $mV \cdot s^{-1}$, T= 720ºC, WE - Pt wire, A=0.16 cm^2, Pt – quasi reference electrode, GC – counter electrode (Inflection point at -0.85 V indicates the K^+ reduction reaction)

As in the case of FLiNaK electrolyte, the stability in the cathodic direction for the pure NaF-KF electrolyte is limited by the reduction of alkali metal cation (K^+). In the anodic direction, oxidation of F^- anion with F_2 formation (at potentials > 1.0 V vs. Pt – quasi reference electrode), limits the electrochemical window of the pure melt. Inflection point at -0.85 V indicates the K^+ reduction reaction.

4.1.4 KF electrolyte

4.1.4.1 Fourier Transform Infrared (FTIR) Spectroscopy

The IR-spectrum of the KF electrolyte after drying is depicted in Fig. 4.1.8.

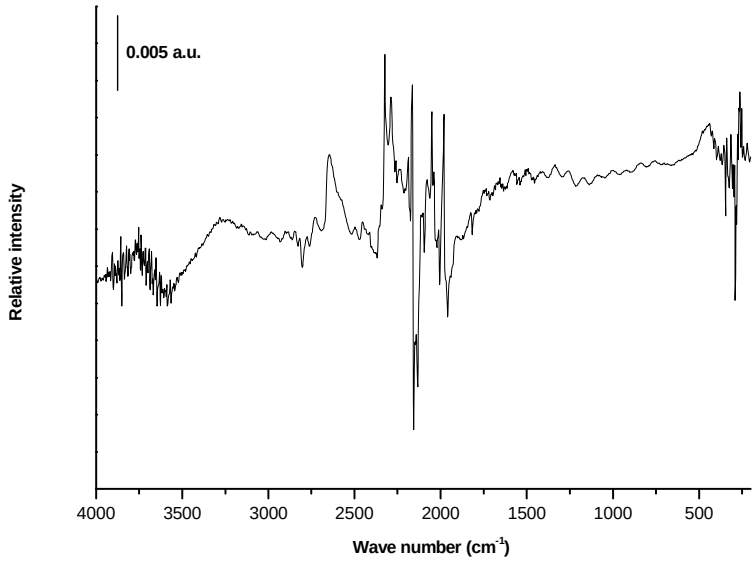

Figure 4.1.8: FTIR absorption spectra of KF electrolyte after drying of the KF

As in the case of the NaF-KF electrolyte, the spectrum in Fig.4.8 exhibits vibrational bands due to the water content (typical band at 3250 cm^{-1}) [110] indicating an unsatisfactory quality of the melt.

4.1.4.2 Cyclic voltammetry measurements

The pure KF electrolyte is stable in the range of -0.4 V to 0.4 V vs. Pt wire reference electrode (Fig. 4.1.9).

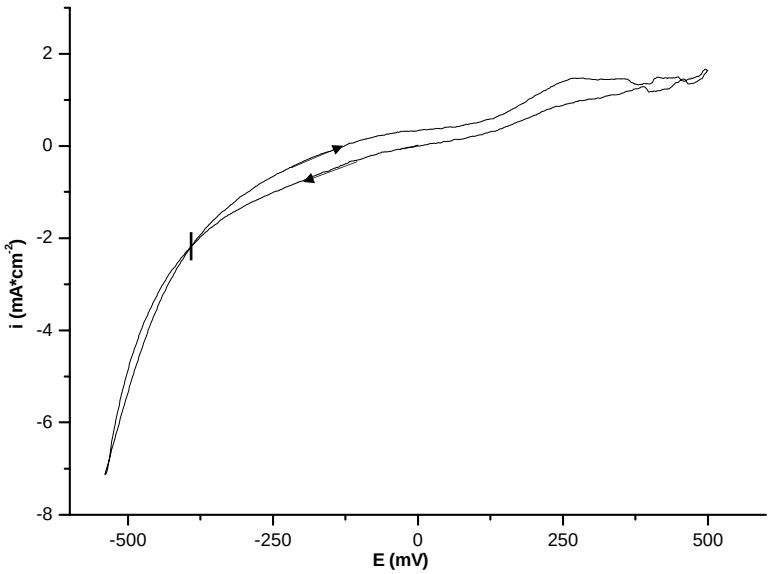

Figure 4.1.9: Cyclic voltammetry of the pure KF electrolyte; scan rate 100 $mV \cdot s^{-1}$, T=900ºC, WE- Pt wire, A=0.16 cm^2, Pt – quasi reference electrode, GC – counter electrode (Inflection point at -0.4 V indicates the K^+ reduction reaction)

The cathodic limit for the pure KF electrolyte is caused by the reduction of alkali metal cation (K^+) indicated by the inflection point at -0.4 V. The shift in the anodic direction compared to the NaF-KF electrolyte is also caused by the higher temperature of the melt. In the anodic direction, oxidation of F^- anion with F_2 formation, is limiting the electrochemical window of the pure melt.

Table 4.1.1 summarizes the electrochemical stability for the high temperature molten salts.

Table 4.1.1: The electrochemical stability of the melts; sweep rate 100 $mV \cdot s^{-1}$, WE-Pt wire, A=0.16 cm^2, Pt – quasi reference electrode, GC – counter electrode

Electrolyte	**Electrochemical stability (V)**		**T_m (K)**	**T_w (K)**
	cathodic	anodic		
FLiNaK	-1.5	1.5	727 [92]	873-923
NaF-KF	-0.8	1.0	993 [112]	1013
KF	-0.4	0.4	1131 [113]	1173

4.2 Electrochemical investigation of the synthesis of TiB_2 out of FLiNaK electrolyte: Electrochemical behaviour of the compounds and mixtures, KBF_4, K_2TiF_6, K_2TiF_6 - TiF_3 and K_2TiF_6 - Ti wire, KBF_4 - K_2TiF_6

4.2.1 Introduction

There are a lot of work focused on the investigation of the cathodic processes in the electrochemical synthesis of titanium diboride in different molten salt electrolytes and on establishing of the correlations between the plating conditions and the properties of the coating [7-11]. The mechanism of the cathodic process in the electrochemical synthesis of titanium diboride in different molten salts has been studied by Makyta and Utigard [8]. Based on the analysis of the available experimental data, the authors assumed that in all fluoride melts the electrochemical synthesis of TiB_2 can be described via two reactions summarizing several single reaction steps [8]

$$TiF_6^{2-} + e^- \rightarrow TiF_6^{3-}$$

$$TiF_6^{3-} + 2BF_4^- + 9e^- \rightarrow TiB_2 + 14F^-$$

and in fluoride-chloride electrolytes by one overall reaction [8]

$$TiCl_{6-x}F_x^{3-} + 2BF_4^- + 9e^- \rightarrow TiB_2 + (6-x)Cl^- + (8+x)F^- .$$

In both cases, a reaction path involving the consumption of nine-electrons is assumed. The RDS is not clarified. Despite of all these studies, it seems there is still a lack of theoretical understanding on the electrochemical reduction process in order to describe the mechanisms and the rate determining steps, making the method of TiB_2 electrodeposition mature for a wide technical application.

This chapter is aimed at a more detailed investigation on the electrochemical reduction process of TiF_6^{2-} and BF_4^- species at different temperatures to evaluate the temperature range where the electrochemical TiB_2 forming is possible and to get more knowledge on the overall reaction behaviour in a FLiNaK electrolyte.

4.2.2 Effect of the temperature on the electrochemical reduction of B (III) electrochemical active species

4.2.2.1 Cyclic voltammograms at different temperatures

The description of the pure FLiNaK electrolyte cyclic voltammetry is given in chapter 4.1.

The influence of the temperature on the reduction mechanism of BF_4^- electroactive species was investigated by recording cyclic voltammograms in a FLiNaK-KBF_4 (6 mol%) electrolyte in the temperature range of 600-700ºC (Fig. 4.2.1).

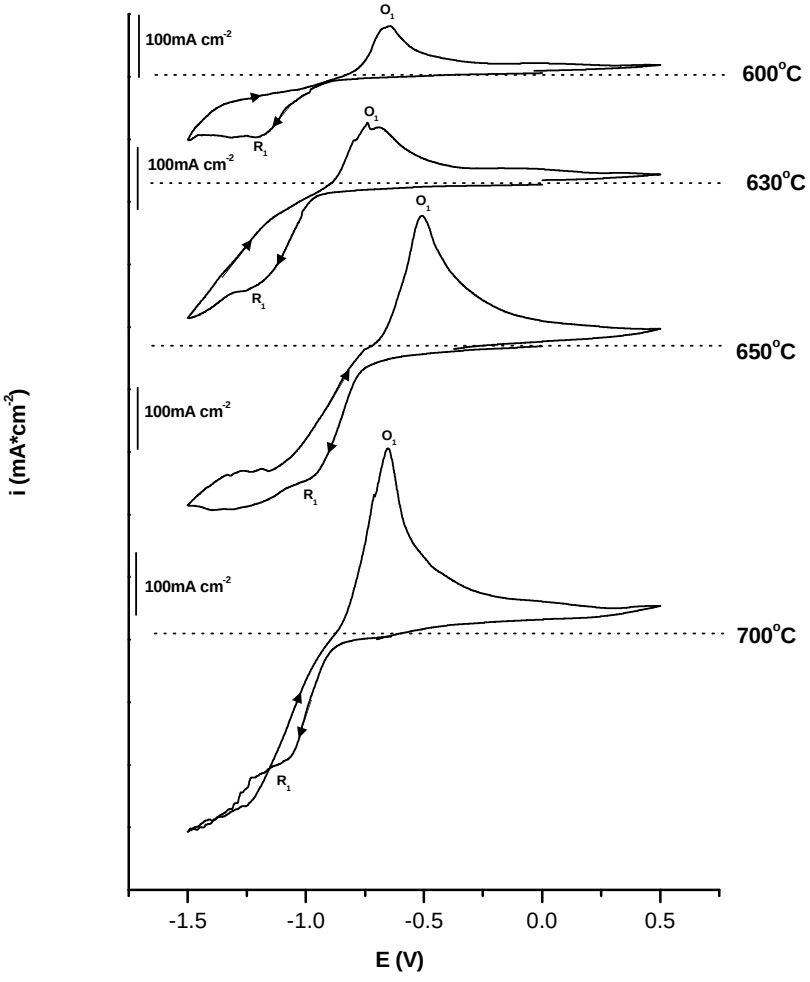

Figure 4.2.1: Cyclic voltammograms (3rd cycle) in FLiNaK-KBF_4 (6 mol%) molten salt system at different temperatures (WE-Pt wire, A=0.16 cm^2; quasi RE - Pt wire, scan rate 100 $mV \cdot s^{-1}$)

One can see in Fig. 4.2.1, over this temperature range, no noticeable changes in the shape of the voltammograms were detected. An increase of the peak current was observed

with increase of the temperature, indicating the increase of the diffusion coefficient of the electroactive species due to the decrease of the viscosity of FLiNaK electrolyte (Fig. 4.2.2).

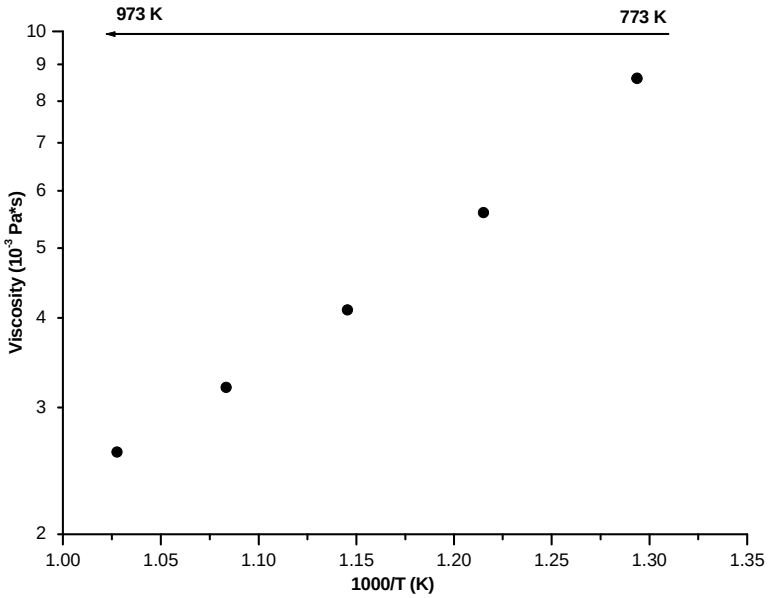

Figure 4.2.2: Effect of temperature on the viscosity of the FLiNaK electrolyte [114]

The reduction reaction of the BF_4^- electrochemical active species around -1.2 V is observed in the cyclic voltammogram at the temperature of 600°C. In the temperature range between 630°C and 650°C this peak is shifted significantly toward lower overvoltage by ~300 mV. It implies that the reduction processes become more favourable with increasing of the temperature. The effect of the reduced viscosity can attribute only to a part of the increased temperature, the change in the complex composition or the change in the reaction kinetics can also contribute to the change in the reduction potentials. During the reverse sweep, a steeper anodic peak O_1 is obtained, which corresponds to oxidation process of boron.

At the temperature of 700ºC a typical cross-over of the direct (in cathodic direction) and the reverse scanning (in the anodic direction) curve is observed, indicating the formation of B.

4.2.2.2 Characteristics of the electrode reactions in FLiNaK-KBF_4

Cyclic voltammetry was used to test the reversibility of B^{3+}/B reduction process. Scan rate in the range of 600-200 $mV \cdot sec^{-1}$ was chosen. Fig. 4.2.3 illustrates the cyclic voltammograms in FLiNaK-KBF_4 system at different scan rates at the temperatures of 600ºC, 650ºC and 700ºC.

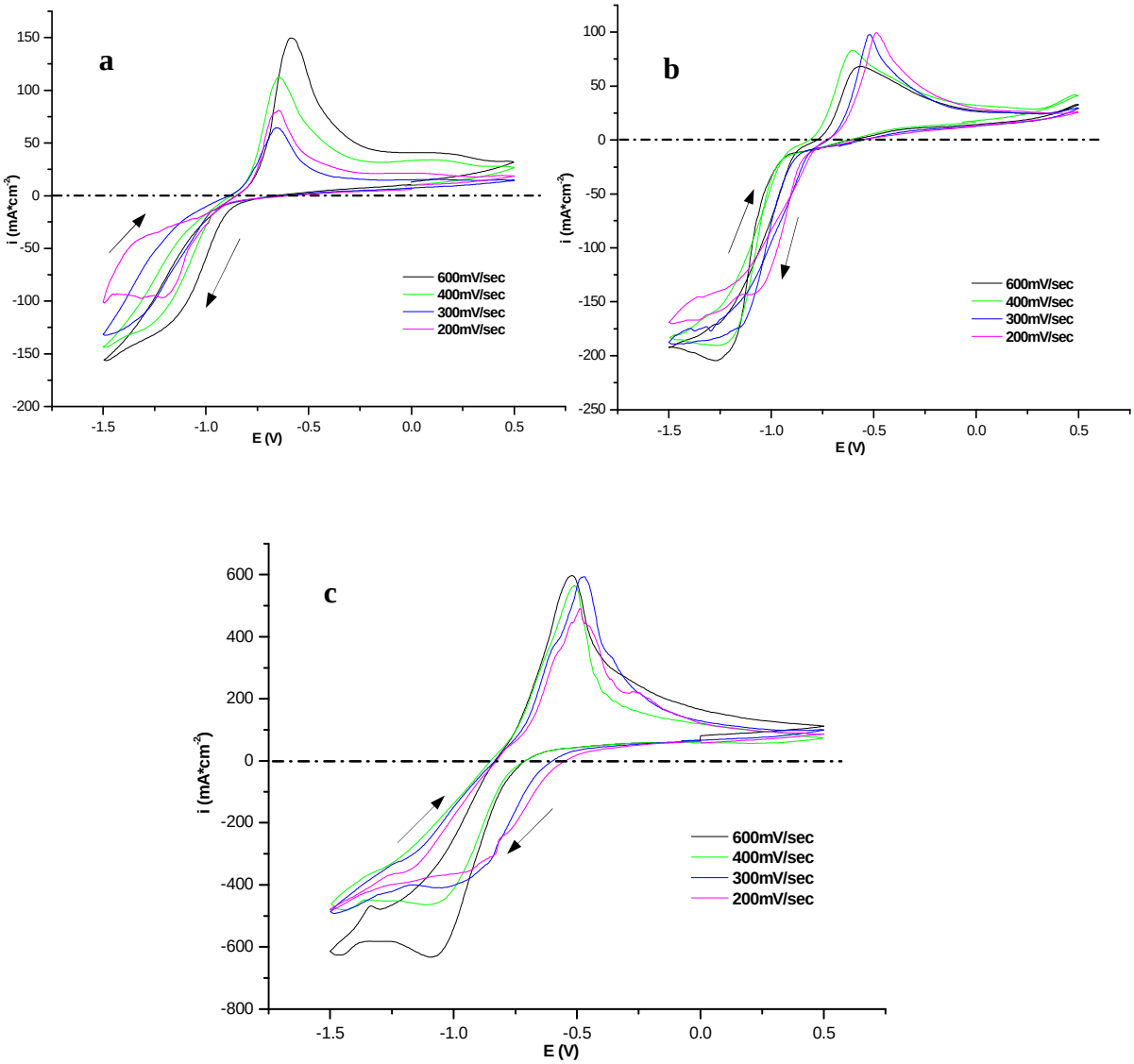

Figure 4.2.3: Cyclic voltammograms (3rd cycle) in FLiNaK-KBF_4 (6 mol%) at different scan rates (WE - Pt wire, A=0.16 cm^2; quasi RE - Pt wire): (a) T=600ºC, (b) T=650ºC and (c) T=700ºC

One can observe that at the temperatures 650ºC and 700ºC the cathodic peak potential (E_p^c) depends on the polarization rate (Fig. 4.2.4 a), i.e., an increase in the sweep rate shifts the E_p^c in the cathodic direction.

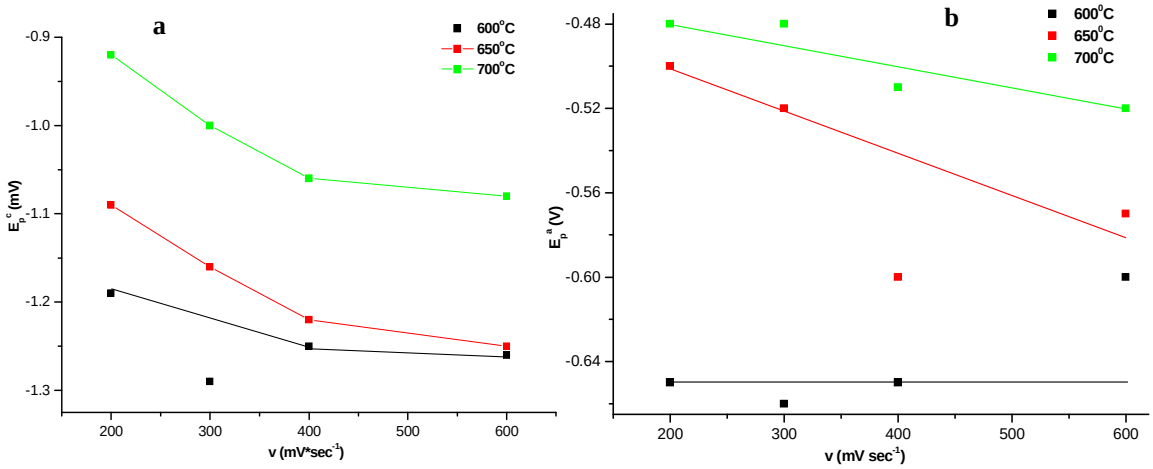

Figure 4.2.4: Potential (a) of the cathodic peak (E_p^c) and (b) of the anodic peak (E_p^a) as a function of the scan rates in FLiNaK-KBF_4 (6 mol%) melt at the temperatures of 600ºC, 650ºC and 700ºC (3rd cycle)

Fig. 4.2.5 demonstrates that the dependence of the cathodic peak current i_p^c is not proportional to the square root of the scan rate, as expected for a reversible reaction, showing weak adsorption of the reactant.

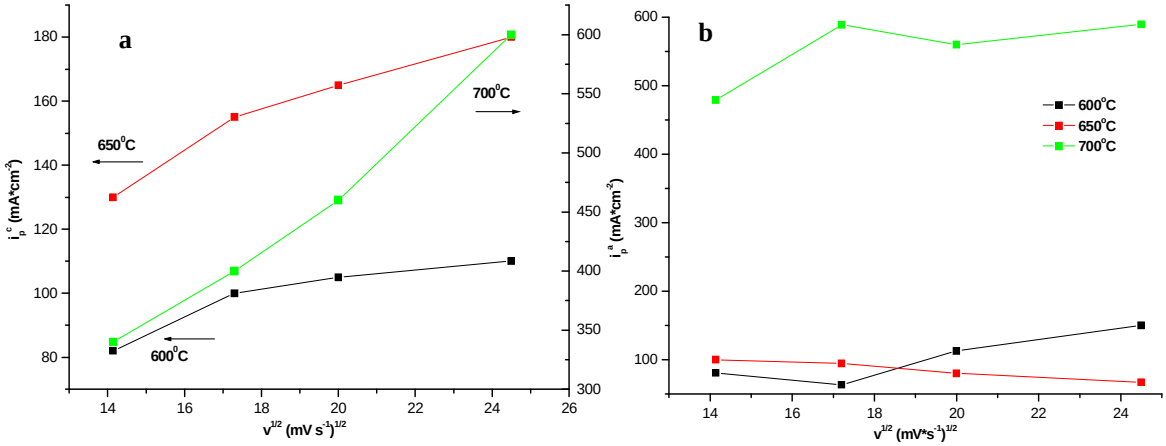

Figure 4.2.5: Current (a) of the cathodic peak (i_p^c) and (b) of the anodic peak (i_p^a) as a function of the square root of the scan rates in FLiNaK- KBF_4 (6 mol%) melt at the temperatures of 600ºC, 650ºC and 700ºC (3rd cycle)

In addition, cathodically consumed charge to the anodically consumed one (at all temperatures $Q_c/Q_a>1$) increase linearly with an increase of the temperature (Fig. 4.2.6), being a sign that the reduction process of B(III) species to B^0 in FLiNaK electrolyte in the

investigated temperature range is not only controlled by diffusion but also by the charge transfer kinetics.

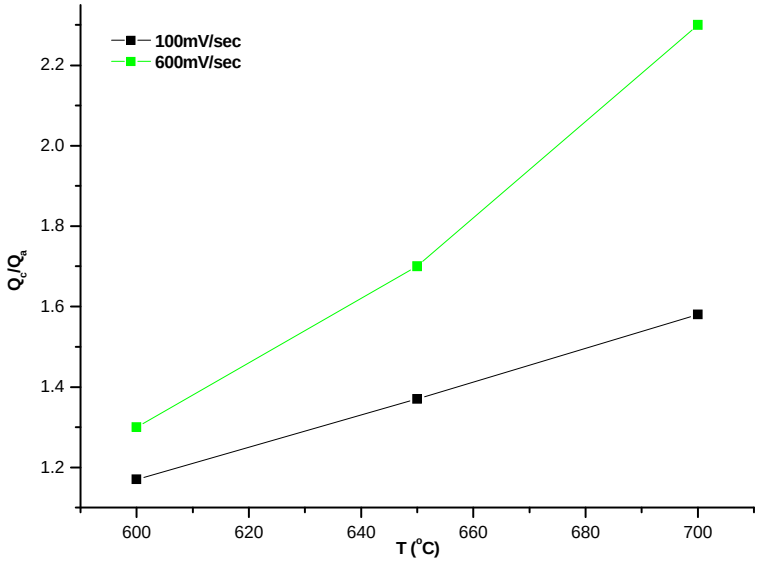

Figure 4.2.6: Ratio of the cathodic/anodic charge vs. temperature for the peaks of cathodic and anodic reaction (black line - scan rate 100 $mV \cdot s^{-1}$ and green line - scan rate 600 $mV \cdot s^{-1}$)

Based on the diagnostic criteria of the reversibility of the process, one can conclude that the reduction process of BF_4^- species is quasi-reversible at low scan rates and temperatures < 650°C and irreversible at high scan rates ≥ 600 $mV \cdot s^{-1}$ and temperatures ≥ 650°C. The body of mathematics for processing voltammograms on case of quasi-reversible processes is very complicated [115]. Therefore, to determine the kinetic parameters, all the equations relevant an irreversible process were used, considering that at the scan rate ≥ 600 $mV \cdot s^{-1}$ the BF_4^- complex irreversibly reduce at the temperature of 700°C. The value of charge transfer coefficient (α, $0.1 \leq \alpha \leq 0.9$), which is a measure of a symmetry barrier in a non-reversible (quasi- and irreversible) electrode process, was determined from the peak and half-peak potential difference according to equation (4.2.1) [115]

$$E_{p/2} - E_p = \frac{1.857RT}{\alpha nF} \qquad (4.2.1)$$

The values αn for the temperatures 600ºC, 650ºC and 700ºC are summarized in Table 4.2.1.

Table 4.2.1: Kinetic parameters of electrochemically active species (BF_4^-) in FLiNaK electrolyte (WE – Pt wire, A_{cath}=0.16 cm^2)

T (K)	ν ($V \cdot s^{-1}$)	i_p^c ($A \cdot cm^{-2}$)	$-E_p^c$ (V)	$-E^c_{p/2}$ (V)	αn
873	0.2	0.082	1.19	1.1	0.74
923	0.2	0.13	1.09	0.9	0.81
973	0.2	0.34	0.92	0.75	0.9
873	0.3	0.1	1.29	1.11	0.74
923	0.3	0.155	1.16	0.98	0.82
973	0.3	0.4	1.0	0.82	0.86
873	0.4	0.105	1.25	1.06	0.75
923	0.4	0.165	1.22	1.1	0.83
973	0.4	0.46	1.06	0.88	0.86
873	0.6	0.11	1.26	1.08	0.78
923	0.6	0.18	1.25	1.07	0.82
973	0.6	0.6	1.08	0.91	0.89

The diffusion coefficient of BF_4^- species has been calculated using the Delahey equation for the case of an irreversible electrode reaction with the formation of an insoluble product [115].

$$i_p^c = 0.496nFcA\sqrt{D}\sqrt{\frac{\alpha nF\nu}{RT}} \qquad (4.2.2)$$

where i_p^c – cathodic peak current in $A \cdot cm^{-2}$, C - concentration of electrochemically active species in $mol \cdot cm^{-3}$, A - cathode area in cm^2, D - diffusion coefficient in $cm^2 \cdot s^{-1}$, F - the Faraday constant, n – the number of exchanged electrons, v – the potential sweep rate in $V \cdot s^{-1}$, α - the charge transfer coefficient and T is the absolute temperature in K.

Using equation (4.2.3) the values of the charge transfer rate constant [115] have been calculated.

$$E_p^c = -1.14\frac{RT}{\alpha nF} + \frac{RT}{\alpha nF}\ln\frac{K_{fh}^0}{\sqrt{D}} - \frac{RT}{2\alpha nF}\ln\alpha n\nu \qquad (4.2.3)$$

where E_p^c - cathodic peak potential, K^0_{fh} – constant of charge transfer rate.

The diffusion coefficient and the charge transfer rate constant for (BF_4^-) species, calculated from cyclic voltammograms recorded at the scan rate of 600 $mV \cdot s^{-1}$ in FLiNaK electrolyte at 700ºC, are $4.2 \cdot 10^{-7}$ $cm^2 \cdot s^{-1}$ and $1.22 \cdot 10^{-8}$ $cm \cdot s^{-1}$, correspondently.
The temperature dependence of the peak current is qualitatively indicative of the diffusion coefficient which is related to the mass transport. The value of the current is written as [116]:

$$I = AFj \qquad (4.2.4)$$

where A is the area of the electrode in cm^2, F is the Faraday constant and j the flux of the reactants reaching the electrode surface in $mol \cdot cm^{-2} \cdot s^{-1}$.

$$j = kc \qquad (4.2.5)$$

where k is the heterogeneous rate constant for the electron transfer and c the concentration of the reactants at the electrode surface in $mol \cdot cm^{-3}$.

$$k = A_f \exp\frac{-E_a}{RT} \qquad (4.2.6)$$

where A_f the frequency factor, E_a is the activation energy of diffusion of the electroactive species in $J \cdot mol^{-1}$, R the molar gas constant in $J \cdot K \cdot mol^{-1}$ and T the temperature in K.

Combining equations (4.2.4) – (4.2.6) for the reduction peak, a logarithmic expression for the energy of activation can be obtained in a logarithmic form as:

$$\ln I = \ln(AA_f Fc) - \frac{E_a}{RT} \qquad (4.2.7)$$

from which it follows that a plot of ln *I versus 1000/T* (Fig. 4.2.7) should be a straight line having a slope of - E_a/R.

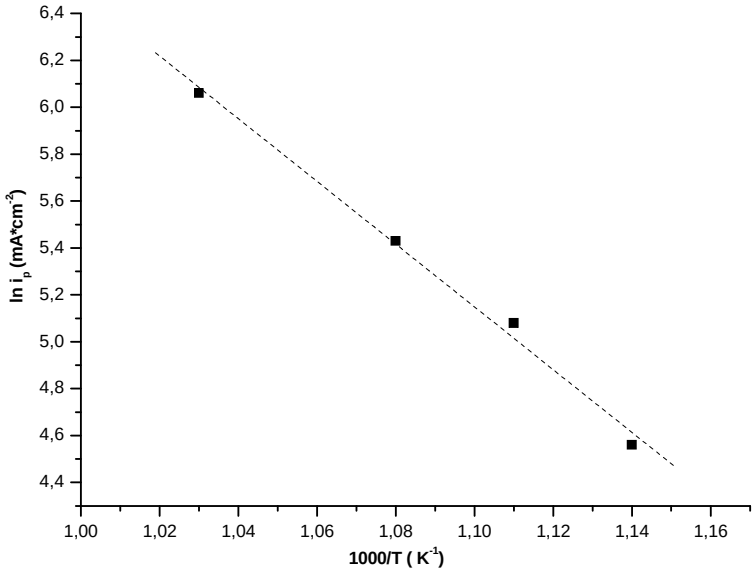

Figure 4.2.7: Arrhenius plot of peak currents for the cathodic peak (scan rate 100 mV·s^{-1})

The activation energy of the overall reduction reaction, calculated from the data in Fig. 4.2.7 is equal to 112 kJ·mol^{-1}.

Based on the results of voltammetric studies, it could be assumed that in the temperature range of 600-700°C the change in the mechanism of the reduction of BF_4^- complexes in FLiNaK electrolyte takes place. The reduction process of BF_4^- species is quasi-reversible at low scan rates and temperatures < 650°C and irreversible at high scan rates ≥ 600 mV·s^{-1} and temperatures ≥ 650°C, i.e. it is controlled by the rate of charge transfer. In the studied temperature range the electrochemical reduction process of the B (III) species occurs via a single $3e^-$ consumed step according to literature data [16]:

$$BF_4^- + 3e^- \rightarrow B + 4F^-$$

4.2.3 Effect of the temperature on the electrochemical reduction of Ti(IV) species

4.2.3.1 Cyclic voltammograms at different temperatures

The influence of the temperature on the reduction reaction of the TiF_6^{2-} electrochemical active species was investigated by recording cyclic voltammograms in FLiNaK electrolyte in the temperature range of 600-700ºC. A representative selection of voltammograms is depicted in Fig. 4.2.8. The voltammograms are initially scanned in the cathodic direction, starting at 0 V vs. a Pt quasi reference electrode.

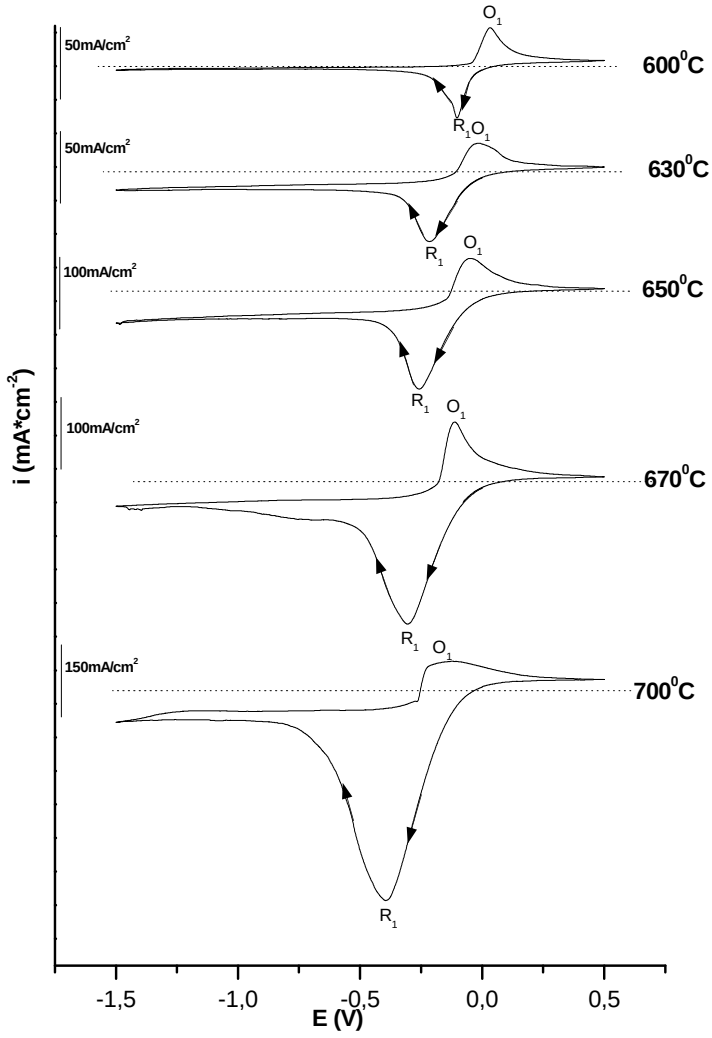

Figure 4.2.8: Cyclic voltammograms (3rd cycle) in FLiNaK-K_2TiF_6 (3 mol%) molten salt system at different temperatures (WE - Pt wire, A=0.16 cm^2; quasi RE - Pt wire, scan rate 100 $mV \cdot s^{-1}$)

As expected, increasing the temperature causes an enhancement of the current density of the peaks, especially at temperatures > 650ºC. This means that the decrease in the apparent viscosity connected with an increase in conductivity of the electrolyte provide the higher mobility of the assumed electrochemical active species, TiF_6^{2-}. At the temperature ≥ 600ºC a shift of the potential values of the reduction peaks toward higher potential values can be observed due to the change in complex composition or the change in the reaction kinetics. As one can see in Fig. 4.2.8, at 600ºC only one cathodic peak (at -100 mV) and its corresponding anodic peak (at 35 mV) are observed. The cathodic peak can be attributed to a reduction reaction of Ti^{4+} to Ti^{3+} species and the anodic peak to its reverse. At 670ºC the shape of the current peaks change, one small additional reduction peak (at -780 mV) appears, which can be assigned to the further reduction of Ti^{3+} to $Ti^{(3+ - x+)}$ ($x \leq 3$) species. With increasing the temperature up to 700ºC, the cathodic peak (at -300 mV) increases in height and additionally a significant current flow at higher cathodic potentials was found. Increasing the temperature up to 700ºC did not generate an additional anodic peak.

4.2.3.2 Characteristics of the electrode reactions in FLiNaK-K_2TiF_6

The influence of the scan rate was examined in order to get some information about the mechanism of the reaction of the first peak (R_1) in Fig. 4.2.8. Linear sweep voltammetry experiments were performed in the FLiNaK electrolyte, containing 3 mol% K_2TiF_6, at temperatures of 600ºC, 650ºC and 700ºC at different scan rates (Fig. 4.2.9).

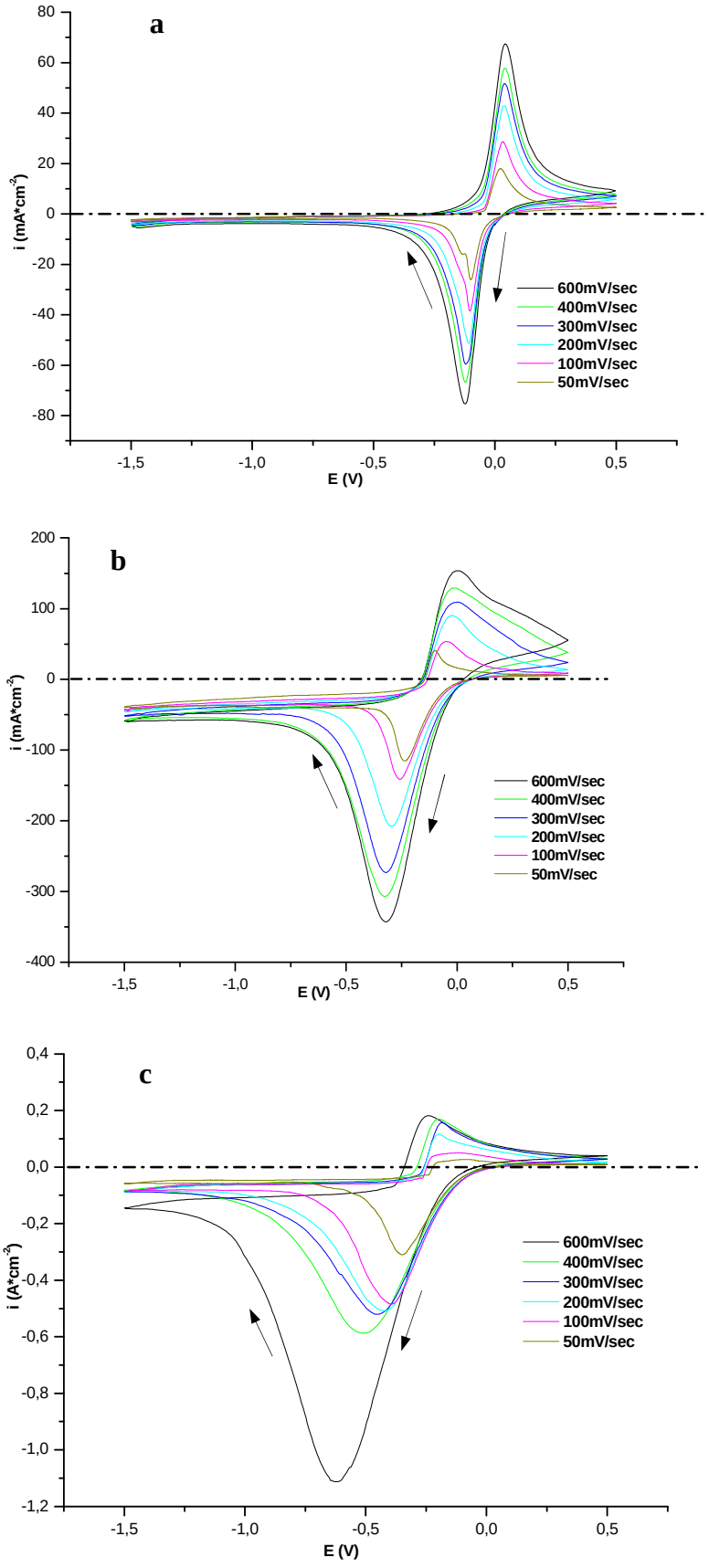

Figure 4.2.9: Cyclic voltammograms (3rd cycle) in FLiNaK-K_2TiF_6 (3 mol%) at different scan rates (WE - Pt wire A=0.16 cm^2; quasi RE - Pt wire;) (a) T=600ºC, (b) T= 650ºC and (c) T=700ºC

To check whether a plot of peak current (i_p) is linearly proportional to the square root of the sweep rate (ν) and E_p is independent of sweep rate is useful as the primary test of reversibility of the process (Fig. 4.2.10 - 4.2.11).

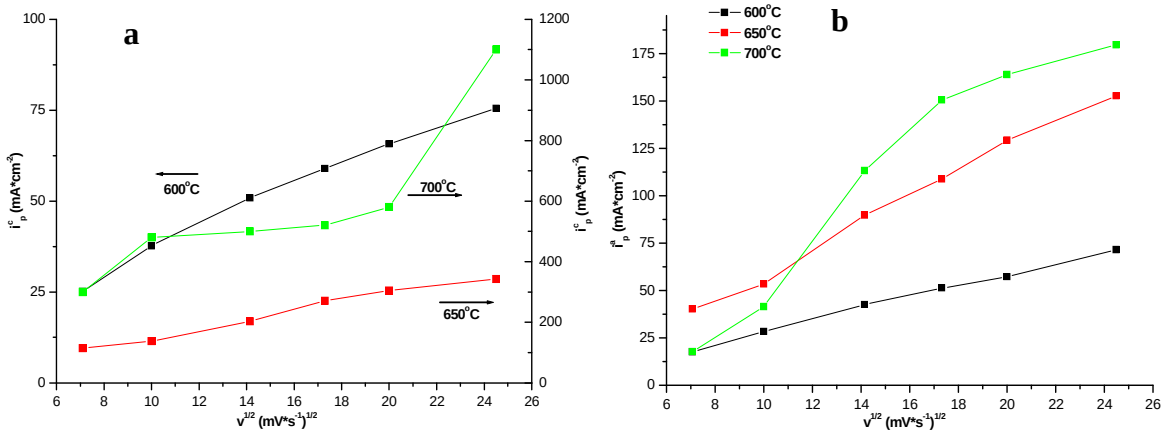

Figure 4.2.10: Current (a) of the cathodic peak (i_p^c) and (b) of the anodic peak (i_p^a) as a function of the square root of the scan rates in FLiNaK-K_2TiF_6 (3 mol%) melts at the temperatures of 600ºC, 650ºC and 700ºC (3rd cycle)

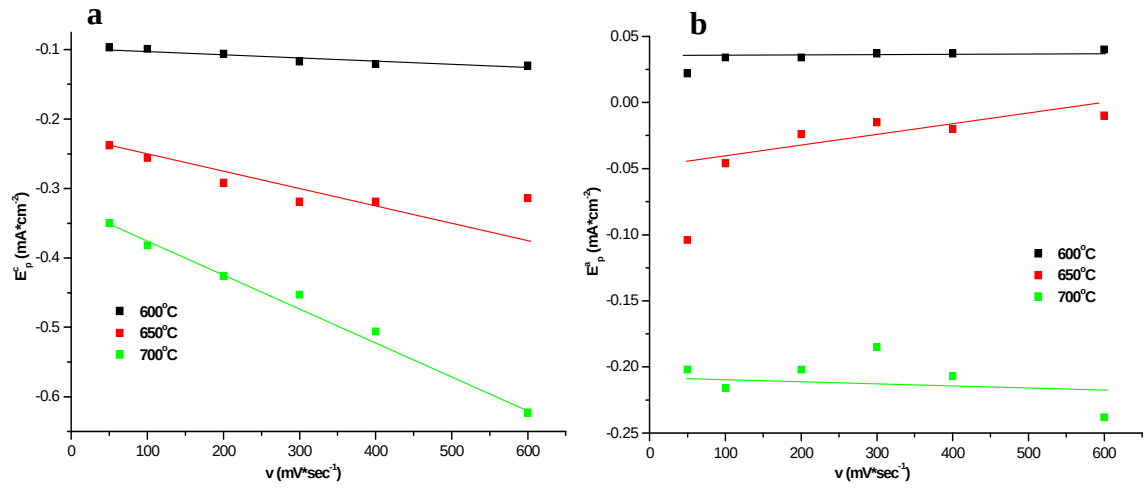

Figure 4.2.11: Potential (a) of the cathodic peak (E_p^c) and (b) of the anodic peak (E_p^a) as a function of scan rates in FLiNaK-K_2TiF_6 (3 mol%) melt at the temperatures of 600ºC, 650ºC and 700ºC (3rd cycle)

To determine the electrode reaction reversibility also the ratio of $|i_p^a/i_p^c|$ which should be equal to 1 (unity) was calculated (Table 4.2.2).

Table 4.2.2: Diagnostic criterion for cyclic voltammograms of a reversible process: absolute values of current ratio of anodic and cathodic peaks

v (mV·s^{-1})	**i_p^a/i_p^c**		
	600ºC	650ºC	700ºC
50	0.68	0.35	0.05
100	0.74	0.38	0.08
200	0.84	0.43	0.22
300	0.86	0.40	0.29
400	0.88	0.42	0.29
600	0.96	0.45	0.30

A ratio of one is expected for a simple reversible electron transfer [117]. For voltammetric curve recorded at the scan rate of 600 mV·sec^{-1} at 600°C the ratio of $|i_{pa}|/|i_{pc}|$ is equalled 0.96. This value is approximately 1, demonstrating that the process was a reversible one. This ratio decreases with decreasing scan rate and at higher temperatures, indicating that the product of reduction enters into a subsequent chemical reaction and thereby it brings an increase of the cathodic density with a corresponding decrease of the anodic current density.

Plotting the ratio of cathodically consumed charge vs. the anodically one, as a function of temperature, (Fig. 4.2.12) one can see that the charge ratio linearly increases with increase of the temperature indicating a higher degree in irreversibility.

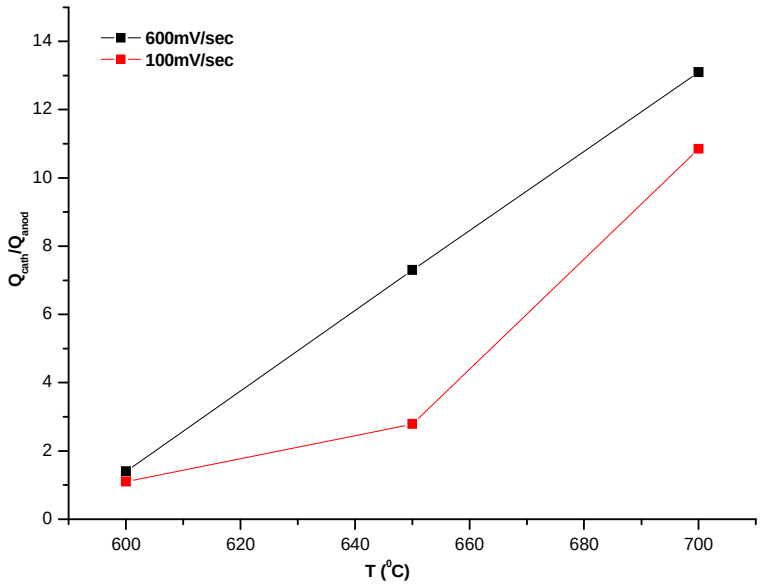

Figure 4.2.12: Ratio of the cathodic/anodic charge vs. temperature for the peaks of cathodic and anodic reaction (red line - scan rate 100 mV·s^{-1} and black line - scan rate 600 mV·s^{-1})

As one can see in the cyclic voltammograms recorded at 600°C (Fig. 4.2.9-a), changes of the sweep rate in the range of 0.05-0.6 $V \cdot s^{-1}$ have no effect on the shape of the voltammetric curves, whereas the peak current is directly proportional to the square root of the sweep rate ($v^{1/2}$) (Fig. 4.2.10) and the peak potential does not depend on the sweep rate (Fig. 4.2.11). The anodic to cathodic ratio was close to 1 (unity) at sweep rate 0.6 $V \cdot s^{-1}$ (Table 4.2.2). Respecting with the theory of linear voltammetry [115], the analysis of these dependences demonstrates that the process of the electrochemical reduction of Ti(IV) from fluoride complexes to Ti(III) at 600ºC at rates ranging from 0.05 to 400 $mV \cdot sec^{-1}$ is quasi-reversible. At higher sweep rates $\geq$ 600 $mV \cdot sec^{-1}$, the first reduction process of Ti(IV) species to Ti(III) is not accompanied by any side reaction and its only controlled by diffusion. In the temperature range of 650-700ºC the peak current (i_p^c and i_p^a) was not linearly proportional to the square root of the scan rate ($v^{1/2}$) (Fig. 4.2.10) and the peak potential depends on the polarisation rate, i.e. an increase in the polarisation rate shifts the cathodic peaks (E_p^c) towards more negative potential values and the peak potential of the anodic peak (E_p^a) shifts to more positive potential values, indicating that coupled chemical reaction takes place (Fig. 4.2.11). As one can observe in the cyclic voltammograms recorded 700ºC (Fig. 4.2.9-c), with decrease the sweep rates the anodic peak is decreased indicating, according to diagnostic tests, that at 700ºC an irreversible chemical reaction with the Ti^{3+} species following charge transfer takes place.

This electroanalysis for the range of the sweep rate 50-600 $mV \cdot sec^{-1}$ at 600-700°C allowed us to indicate that the process of the electrochemical reduction of Ti(IV) fluoride complexes to Ti(III) in a FLiNaK electrolyte changes from a quasi-reversible behaviour at 600ºC (at the scan rates of < 600 $mV \cdot sec^{-1}$) to the irreversible process at 700ºC.

The number of electrons exchanged during the reversible reduction process of TiF_6^{2-} species at 600ºC (for the scan rate 600 $mV \cdot sec^{-1}$) was evaluated applying the equations [118].

$$E_p^a - E_p^c = \ln 10 \frac{RT}{nF} \qquad (4.2.8)$$

where E_p^a and E_p^c are, respectively, the anodic and the cathodic peak potential.

From the data $E_p^a = 0.042\ V$ and $E_p^c = -0.129$ at 600 mV·sec^{-1}, the calculated number of electrons *n* was equal to be 0.99. The diffusion coefficient of Ti(IV) species at 600ºC (scan rate 600 mV·sec^{-1}) has been calculated using the Randles-Ševčik equation [115]:

$$i_p = 0.4463nF\sqrt{\frac{nFD}{RT}}Ac_0\sqrt{\nu} \qquad (4.2.9)$$

where i_p is the peak current, *n* is the number of electrons, *F* is the Faraday constant in $C{\cdot}mol^{-1}$, *T* is the temperature in *K*, *R* the molar gas constant in $J{\cdot}K{\cdot}mol^{-1}$, *A* the surface area of the working electrode in cm^2, *D* is the diffusion coefficient of the electroactive species in $cm^2{\cdot}s^{-1}$, c_0 is the bulk concentration of the electroactive species in $mol{\cdot}cm^{-3}$ and ν is the scan rate of voltammograms in $V{\cdot}sec^{-1}$.

The value of the diffusion coefficient for TiF_6^{2-} at 600°C was found to be 2.2 ·10^{-7} cm^2·s^{-1}. The value of the diffusion coefficient for TiF_6^{2-} at 700°C were calculated applying equation (4.2.2) and (4.2.3) and summarized in Table 4.2.3.

Table 4.2.3: Kinetic parameters of electrochemically active species (TiF_6^{2-}) in FLiNaK electrolyte (WE-Pt wire, A_{cath}=0.16 cm^2, T=700°C)

ν (V·s^{-1})	**i_p^c (A·cm^{-2})**	**$-E_p^c$ (V)**	**$-E_{p/2}^c$ (V)**	**αn**	**D (cm^2·s^{-1})**
0.1	0.48	0.38	0.25	0.93	5.69·10^{-6}
0.2	0.5	0.43	0.27	0.69	4.16·10^{-6}
0.3	0.52	0.45	0.27	0.58	3.77·10^{-6}
0.4	0.58	0.51	0.29	0.52	3.71·10^{-6}

The activation energy of the overall reaction in the temperature range of 600-700ºC, calculated from the data in Fig. 4.2.13 and Eq.(4.2.7) is equal to 254 kJ·mol^{-1}.

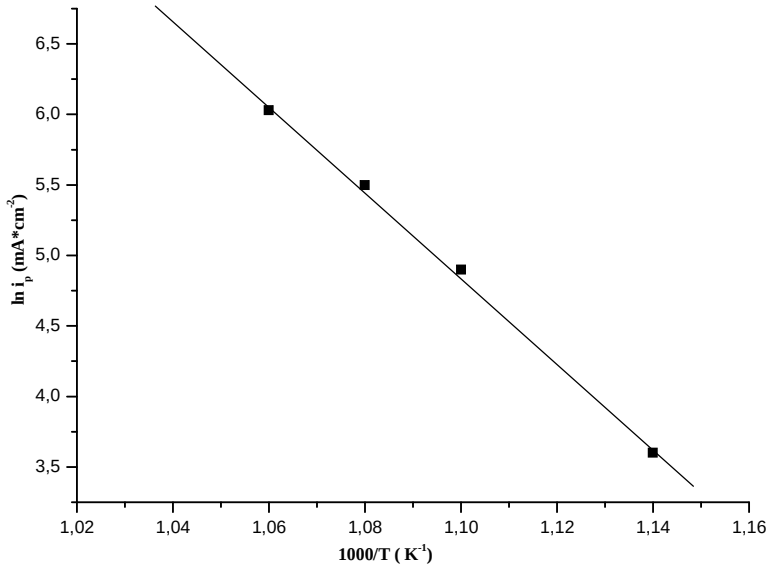

Figure 4.2.13: Arrhenius plot of peak currents for the reduction of the Ti (IV) species (scan rate 100 $mV \cdot s^{-1}$)

4.2.4 Effect of the temperature on the electrochemical reduction of Ti(IV) and Ti(III) species in FLiNaK electrolyte

4.2.4.1 Cyclic voltammograms at different temperatures

The influence of the temperature on the reduction mechanism of Ti(IV) and Ti(III) species was investigated by recording cyclic voltammograms in FLiNaK electrolyte at the temperature range of 600-700ºC, containing 3 mol% K_2TiF_6 and 1.5 mol% TiF_3. A representative selection of voltammograms is illustrated in Fig. 4.2.14. The voltammograms are initially scanned in the cathodic direction, starting at 0 V vs. Pt quasi reference electrode.

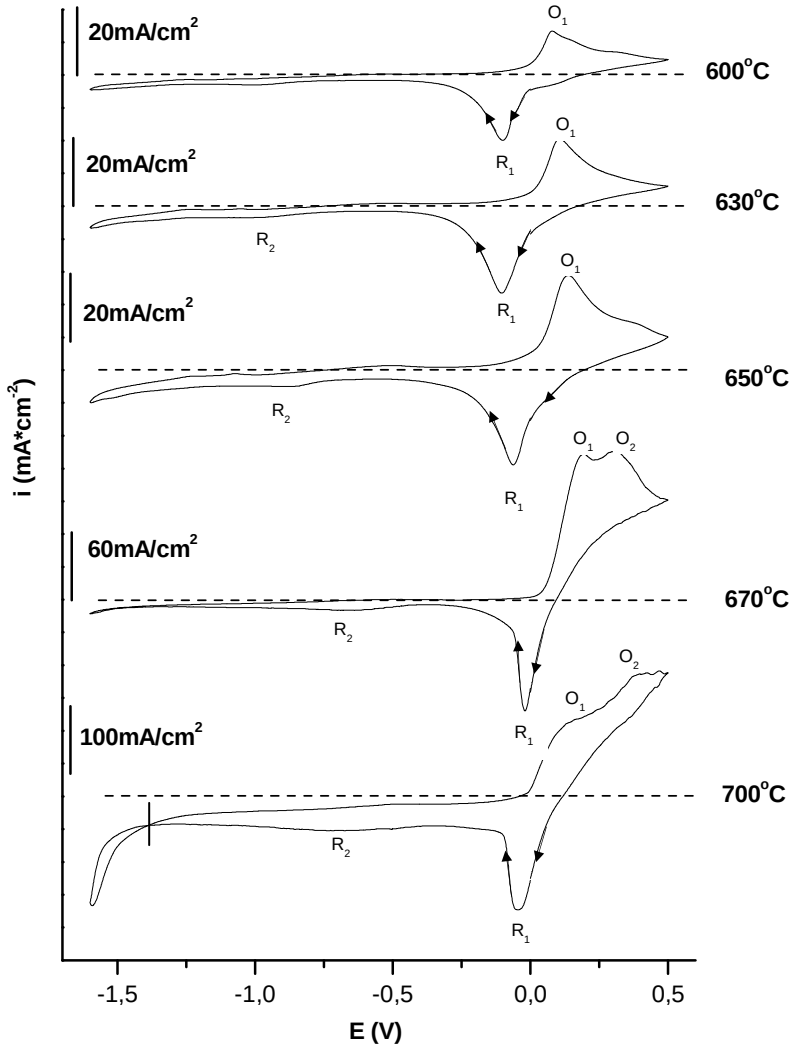

Figure 4.2.14: Cyclic voltammograms (3rd cycle) in the FLiNaK-K_2TiF_6 (3 mol%)-TiF_3 (1.5 mol%) molten salt system at different temperatures (WE-Pt wire, A=0.16 cm^2; quasi RE-Pt wire, scan rate 100 $mV \cdot s^{-1}$)

As in the case of FLiNaK-K_2TiF_6 system, increasing the temperature causes an enhancement of the current density. At increased temperatures, due to the higher mobility of the ions, the concentration of the electrochemically active species on the cathode is higher, resulting in higher current density. At the temperature ≥ 630ºC there is a slight shift of the potential values of the reduction peaks toward lower value. At higher temperatures the diffusion of the electrochemically active species toward the cathode occurs faster, therefore, their reduction occurs at more anodic potentials.

One cathodic peak (at -0.1 V) and its corresponding anodic peak (at 0.1 V) are observed at 600ºC, assigned to the one electron reversible charge transfer process involving the reduction of Ti(IV) to Ti(III) species. At the temperatures ≥ 630°C one more additional cathodic peak R_2 is recorded, attributed to the reduction process of Ti^{3+} to Ti^{3+-x+} complex.

This peak is shifted in the anodic direction with higher temperature. At 700ºC besides the reduction of Ti (IV) to Ti (III) and Ti^{3+} to Ti^{3+-x+} complex, an inflection point at 1.4 V can be observed, indicating the formation titanium metal. The second oxidation peak appeared at temperatures 670 and 700°C (~0.35 V) may be tentatively ascribed to the dissolution of Pt-Ti alloy, which is formed at the high temperatures. Such compounds as $TiPt_3$, TiPt and Ti_3Pt have been obtained in the investigation into the phase equilibrium in the Pt-Ti system [119].

Thus, the preliminary study of FLiNaK-K_2TiF_6-TiF_3 system by cyclic voltammetry revealed at least two temperatures range where the electrochemical behaviour of Ti(IV) and Ti(III) species is essentially different: 600-630ºC and 630-700ºC. Based on the cyclic voltammograms it can be assumed that at the temperature range of 600-630ºC the reduction of Ti(IV) to Ti(III) takes place and further enhancement of the temperature up to 700ºC enables a further reduction process, namely the reduction of Ti^{3+-x+} species to metallic Ti.

4.2.4.2 Characteristics of the electrode reactions in FLiNaK-K_2TiF_6-TiF_3

In order to investigate the first reduction process (reduction of Ti(IV) to Ti(III) species), cyclic voltammetry in FLiNaK electrolyte was performed over a wide range of sweep rates at 600, 650 and 700ºC (Fig. 4.2.15).

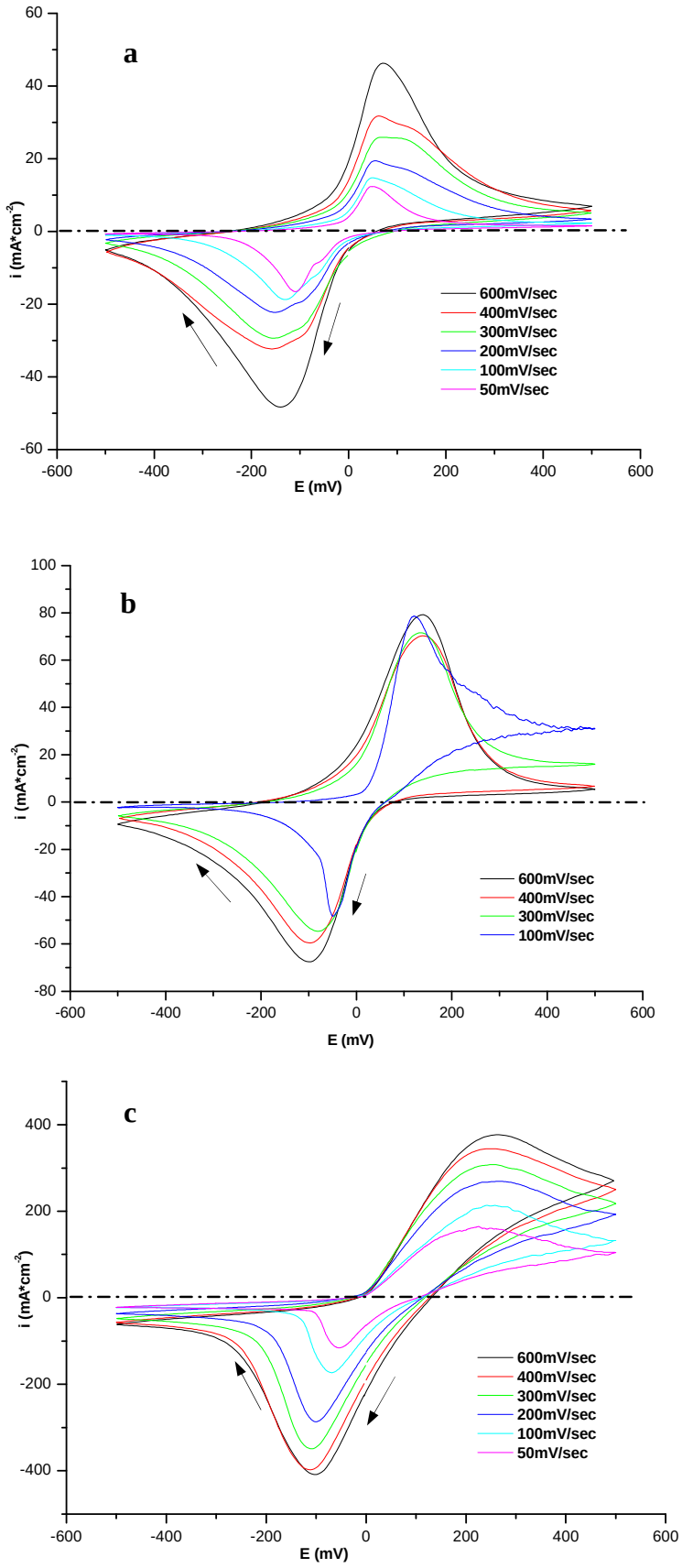

Figure 4.2.15: Cyclic voltammograms (3rd cycle) in FLiNaK-K_2TiF_6 (3 mol%)-TiF_3 (1.5 mol%) at different scan rates (WE - Pt wire, A=0.16 cm^2; quasi RE - Pt wire) (a) T=600ºC, (b) T=650ºC and (c) T=700ºC

In order to get more information on the system, the influence of the scan rate on the peak height (i_p) and peak potential (E_p) were studied (Fig. 4.2.16 and 4.2.17).

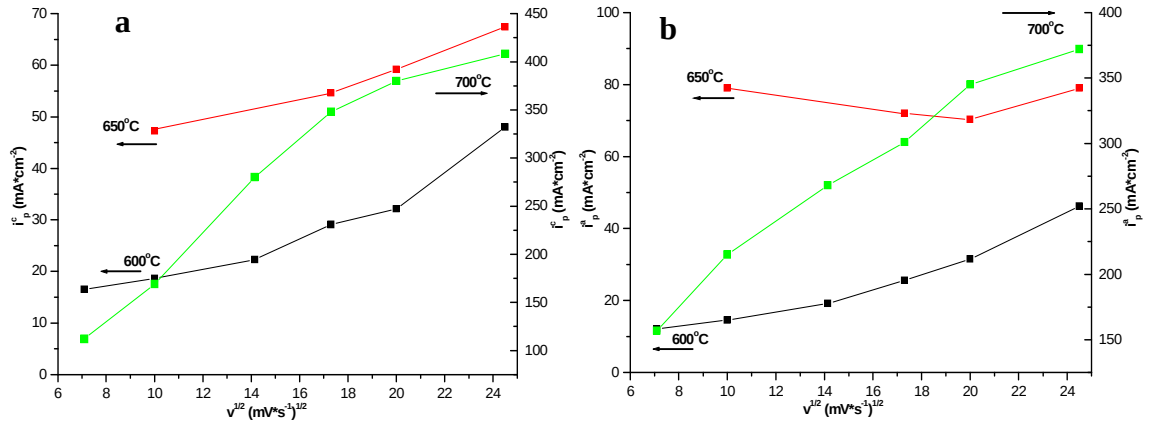

Fig. 4.2.16 Current (a) of the cathodic peak (i_p^c) and (b) of the anodic peak (i_p^a) as a function of the square root of the scan rates in FLiNaK-K_2TiF_6 (3 mol%)-TiF_3 (1.5 mol%) melt at the temperatures 600ºC, 650ºC and 700ºC (3rd cycle)

Figures 4.2.16 show the sweep rate dependence of the cathodic and anodic peaks current density. A linear relation was found between i_p^c, i_p^a and $v^{1/2}$ at 700ºC. A significant deviation from linearity was observed at lower temperatures. The non-linear increase of i_p with $v^{1/2}$ indicates weak adsorption of the reactant.

A plot of cathodic peak potential E_p^c and anodic peak potential E_p^a obtained from cyclic voltammograms (Fig. 4.2.15) as a function of scan rates for the reduction TiF_6^{2-} at Pt electrode is shown in Fig. 4.2.17.

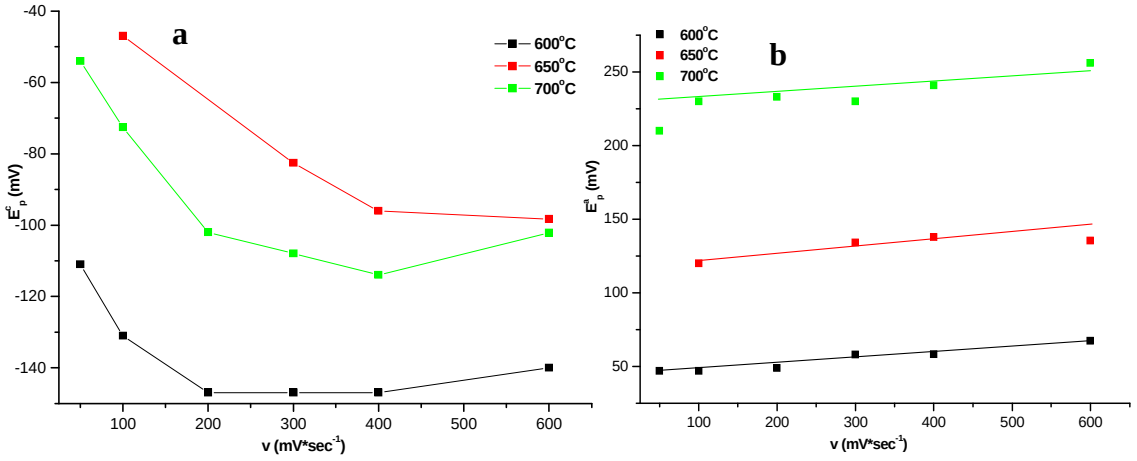

Figure 4.2.17: Potential of (a) the cathodic peak (E_p^c) and (b) of the anodic peak (E_p^a) as a function of scan rates in FLiNaK-K_2TiF_6 (3 mol%) -TiF_3 (1.5 mol%) melt at the temperatures 600ºC, 650ºC and 700ºC (3rd cycle)

As one can see in Fig. 4.2.17 the peak potentials vary with applied sweep rate indicating the irreversibility of the process.

To determine the electrode reaction reversibility also the ratio of $|i_p^a/i_p^c|$ which should be equal to 1 (unity) was calculated (Table 4.2.4).

Table 4.2.4: Diagnostic criterion for cyclic voltammograms of a reversible process: absolute values of current ratio of anodic and cathodic peaks

v (mV·s^{-1})	**i_p^a/i_p^c**		
	600ºC	650ºC	700ºC
100	0.78	1.31	1.3
300	0.88	1.30	1.1
400	0.96	1.19	0.91
600	0.98	1.17	0.90

The ratio close to one (0.98) was obtained for the voltammetric curve recorded at the scan rate of 600 mV·sec^{-1} at 600°C, indicating the reversibility of the reduction process of TiF_6^{2-} species. This ratio decreases with decreasing scan rate, indicating that the product of electroreduction enters into a subsequent chemical reaction. The ratio >1 was obtained for cyclic voltammograms recorded at the scan range of 100-600 mV·sec^{-1} at temperatures 650°C and 700°C, suggesting that the continuously accumulation of Ti^{3+} species occurs, resulting in higher anodic peak for the oxidation process of Ti^{3+} species to Ti^{4+}.

Plotting the ratio of cathodically consumed charge vs. the anodically one, as a function of temperature, (Fig. 4.2.18) one can observe that the charge ratio linearly decreases with increase the temperature at the scan rate of 100 mV·sec^{-1} and remains constant in the temperature range of 600-650°C at the scan rate of 600 mV·sec^{-1}.

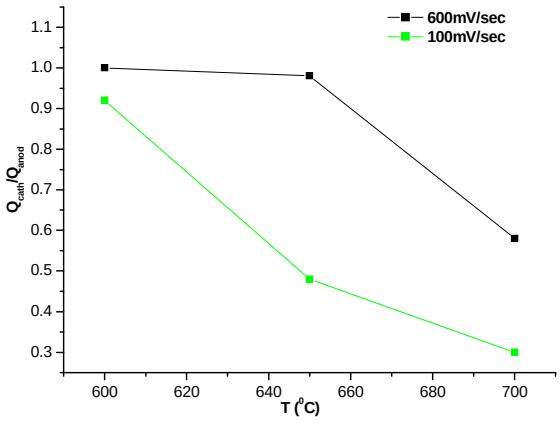

Figure 4.2.18: Ratio of the cathodic/anodic charge vs. temperature for the peaks of cathodic and anodic reaction (green line - scan rate 100 mV·s^{-1} and black line - scan rate 600 mV·s^{-1})

This electroanalysis for the range of the sweep rate 100-600 mV·sec^{-1} at 600-700°C allowed us to indicate that the process of the electrochemical reduction of Ti(IV) fluoride complexes to Ti(III) in a FLiNaK electrolyte changes from a quasi-reversible behaviour at 600ºC (at the scan rates of < 600 mV·sec^{-1}) to the irreversible process at 700ºC.

The number of electrons exchanged during the reversible reduction process of TiF_6^{2-} species at 600ºC (for the scan rate 600 mV·sec^{-1}) was evaluated applying the equations (4.2.8). From the data $E_p^a = 0.072\ V$ and $E_p^c = -0.139\ V$ at 600 mV·sec^{-1}, the calculated number of electrons *n* was equal to be 0.81. The diffusion coefficient of Ti(IV) species at 600ºC (scan rate 600 mV·sec^{-1}) has been calculated using the equation (4.2.9). The value of the diffusion coefficient for TiF_6^{2-} at 600°C was found to be 8.8 ·10^{-8} cm^2·s^{-1}. The value of the diffusion coefficient for TiF_6^{2-} at 700°C were calculated applying equation (4.2.2) and (4.2.3) and summarized in Table 4.2.5.

Table 4.2.5: Kinetic parameters of electrochemically active species (TiF_6^{2-}) in FLiNaK electrolyte with TiF_3 (1.5 mol%) (WE-Pt wire, A_{cath}=0.16 cm^2, T=700°C)

ν (V·s^{-1})	**i_p^c (A·cm^{-2})**	**$-E_p^c$ (V)**	**$-E_{p/2}^c$ (V)**	**αn**	**D (cm^2·s^{-1})**
0.1	0.17	0.068	0.0003	2.31	6.92·10^{-7}
0.2	0.28	0.102	0.013	1.74	5.2·10^{-7}
0.3	0.35	0.108	0.01	1.58	5.0·10^{-7}
0.4	0.38	0.114	0.02	1.65	5.0·10^{-7}

The activation energy of the overall reaction in the temperature range of 600-700ºC, calculated from the data in Fig. 4.2.19 and Eq.(4.2.6) is equal to 166 kJ·mol^{-1}.

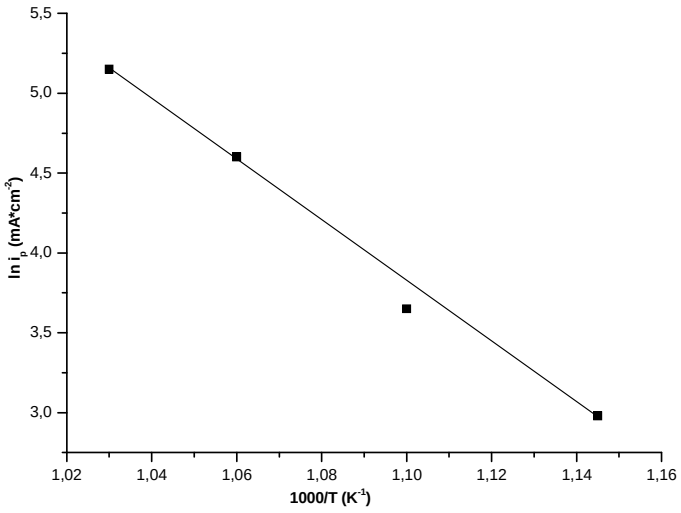

Figure 4.2.19: Arhenius plot of peak currents for the reduction of the Ti (IV) species (scan rate 100 $mV \cdot s^{-1}$)

4.2.5 The effect of temperature on the electrochemical reduction of Ti(IV) species out of FLiNaK electrolyte in the presence of Ti wire

4.2.5.1 Cyclic voltammograms at different temperature

The influence of the temperature on the reduction mechanism of Ti(IV) species in the presence of a Ti wire in the electrolyte was investigated by recording cyclic voltammograms in FLiNaK electrolyte in the temperature range of 600-700ºC. A representative selection of voltammograms is depicted in Fig. 4.2.20. The voltammograms are initially scanned in the cathodic direction, starting at 0 V vs. Pt quasi reference electrode.

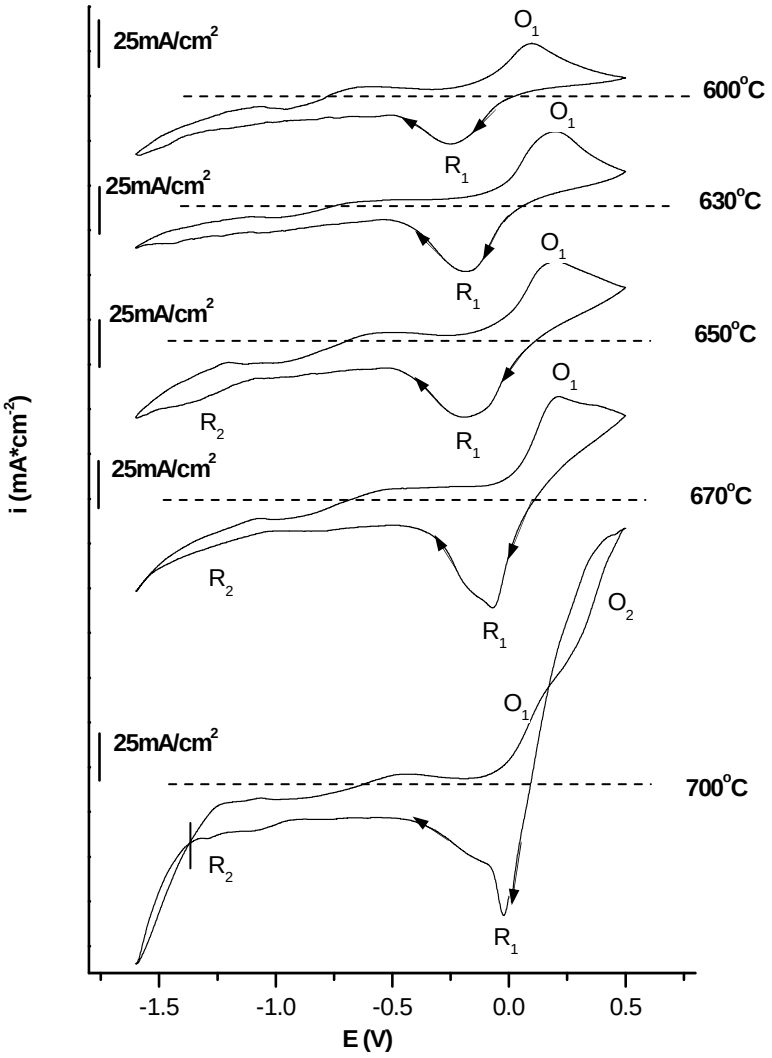

Figure 4.2.20: Cyclic voltammograms (3rd cycle) in FLiNaK-K_2TiF_6 (3 mol%)-Ti wire molten salt system at different temperatures (WE-Pt wire, A=0.16 cm^2; quasi RE-Pt wire, scan rate 100 $mV \cdot s^{-1}$)

The current flow is significantly lower than in the case of two previous systems. At the temperature < 630ºC the cyclic voltammogram exhibits one reduction at -0.24 V and the corresponding oxidation peaks at 0.1 V. Enhancement the temperature up to 670ºC causes appear of one additional minor cathodic peak at -1.35 V. Thus, it can be considered that at temperatures < 630ºC only the reduction of Ti(IV) species to Ti(III) takes place. Increasing the temperature up to 700ºC leads to the second reduction process, namely, Ti^{3+} to Ti^{3+-x+} complex. Similar to the situation in FLiNaK-K_2TiF_6 (3mol%)-TiF_3 (1.5mol%) molten salt system at 700ºC the voltammogram exhibits a characteristic cross-over current behaviour but not only in cathodic brunch also in the anodic one. This current loop in the cathodic direction is typical for nucleation processes, in this case formation of Ti^0. The second oxidation peak appeared at temperature of 700°C (~0.35 V) may be tentatively

ascribed to the dissolution of Pt-Ti alloy. The increase in temperature causes a slight shift of the potential values of the reduction peaks toward lower value due to the enhanced diffusion of the electrochemically active species toward the cathode.

Plotting the ratio of cathodically consumed charge vs. the anodically one, as a function of temperature, (Fig. 4.2.21) one can see that the charge ratio linearly decreases with increase of the temperature indicating a higher degree in irreversibility.

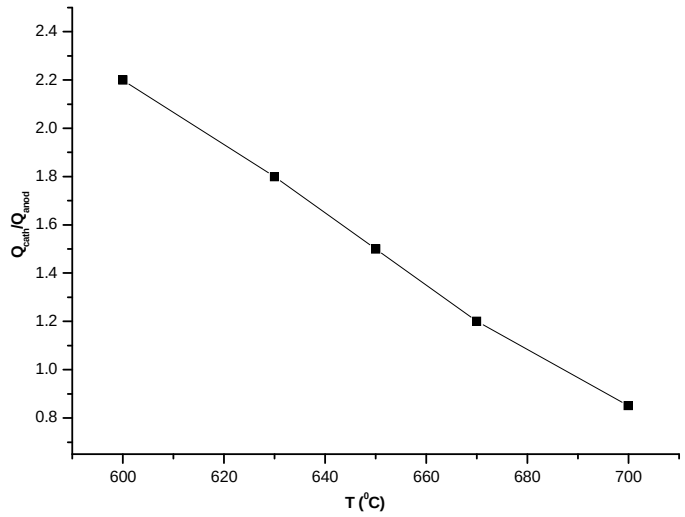

Figure 4.2.21: Ratio of the cathodic/anodic charge vs. temperature for the peaks of cathodic and anodic reaction (scan rate 100 $mV \cdot s^{-1}$)

4.2.5.2 Characteristics of the electrode reactions in FLiNaK-K_2TiF_6-Ti wire

A comparison of cyclic voltammograms of Ti (IV) species in FLiNaK electrolyte in the presence of Ti wire for the first reduction peak (R_1 in Fig.4.2.20) at various sweeping potentials is shown in Fig. 4.2.22.

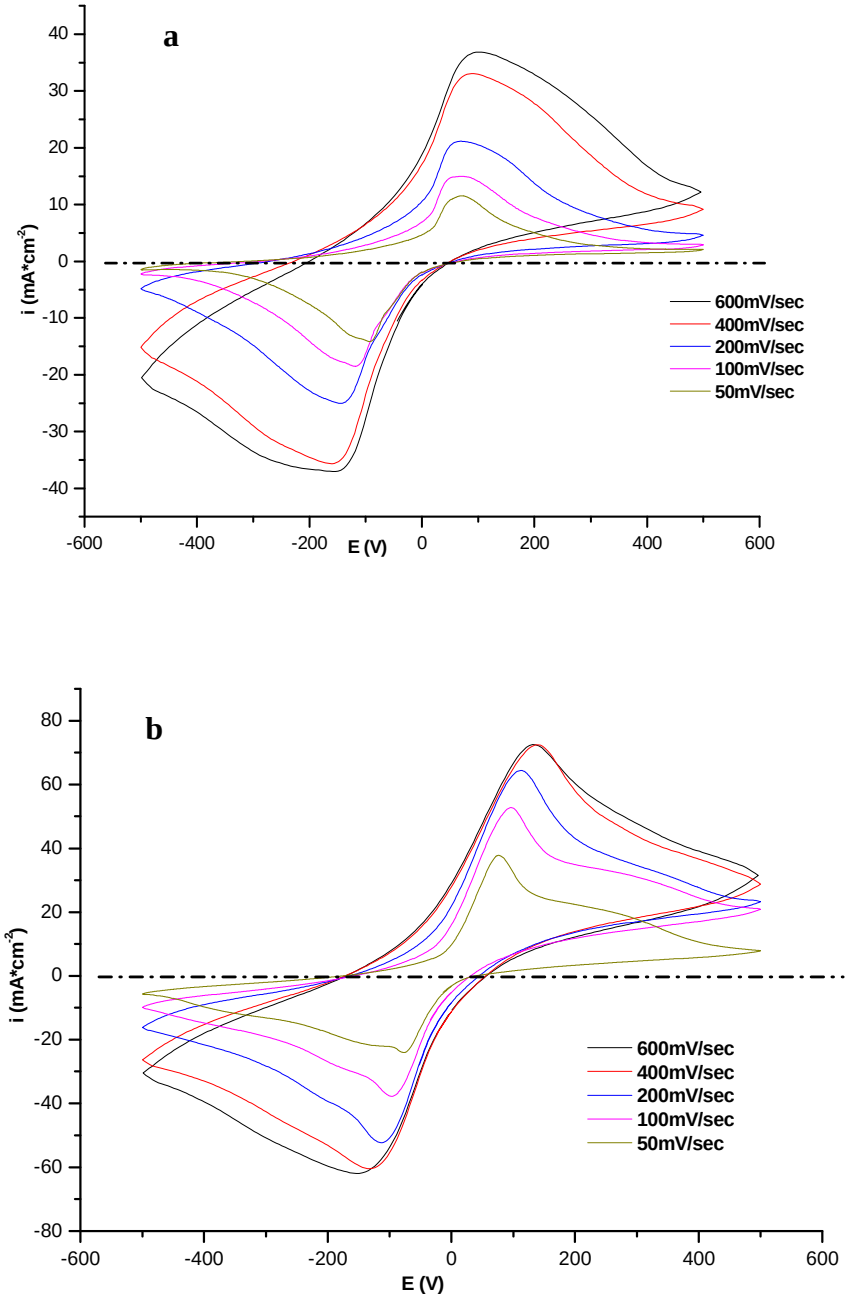

Figure 4.2.22: Cyclic voltammograms (3rd cycle) in FLiNaK-K_2TiF_6 (3mol%)-Ti wire at different scan rates (WE - Pt wire, A=0.16 cm^2; quasi RE - Pt wire) (a) T=600ºC and (b) T=650ºC

One can observe that at the temperatures 600ºC and 650ºC the cathodic peak potential (E_p^c) depends on the polarization rate (Fig. 4.2.23 a), i.e., an increase in the sweep rate shifts the E_p^c in the cathodic direction.

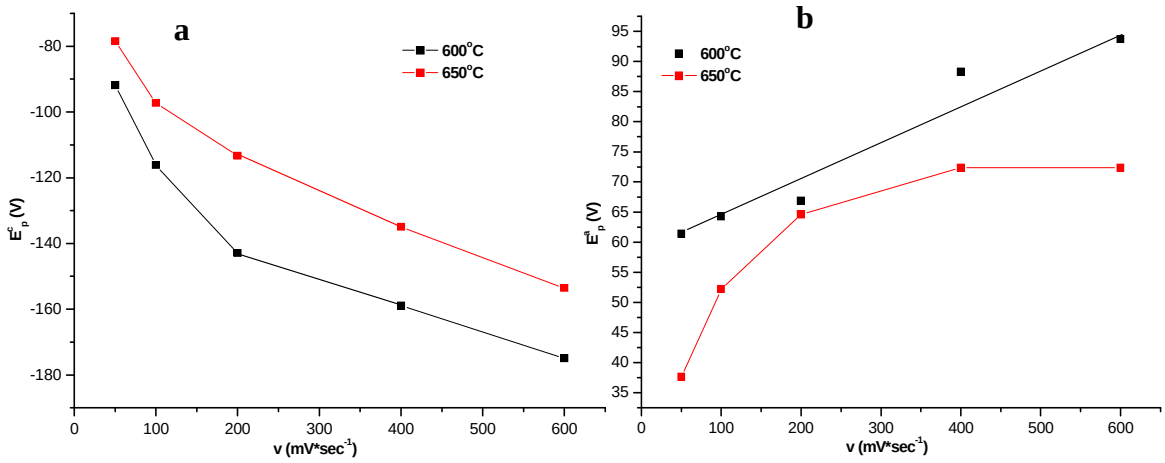

Figure 4.2.23: Potential (a) of the cathodic peak (E_p^c) and (b) of the anodic peak (E_p^a) as a function of scan rates in FLiNaK-K_2TiF_6 (3 mol%) in the presence of Ti wire melt at 600 and 650ºC (3rd scan)

Fig. 4.2.24 demonstrates that the dependence of the cathodic peak current i_p^c is not directly proportional to the square root of the scan rate, as expected for a reversible reaction.

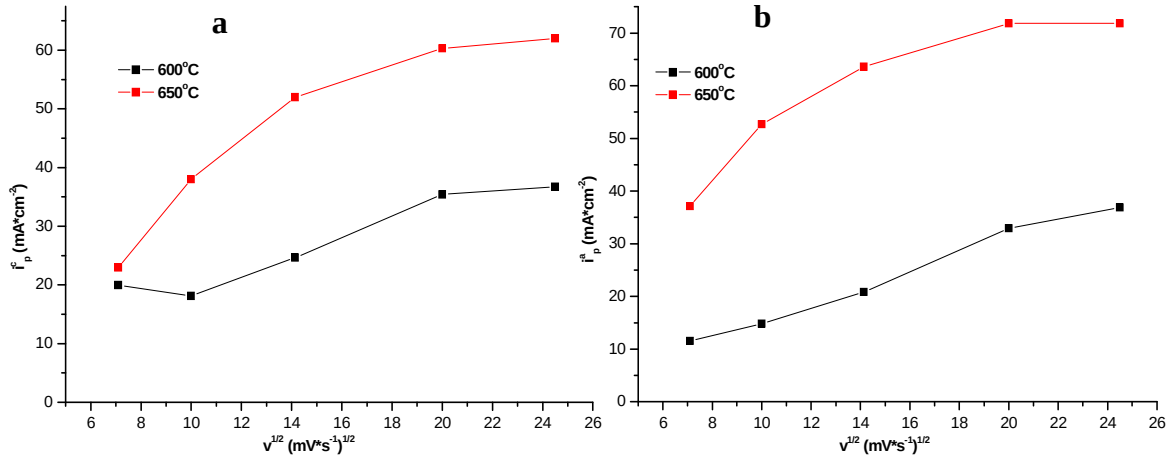

Figure 4.2.24: Current of (a) the cathodic peak (i_p^c) and (b) of the anodic peak (i_p^a) as a function of the square root of the scan rates in FLiNaK-K_2TiF_6 (3 mol%) in the presence of Ti wire melt at 600 and 650ºC (3rd cycle)

To determine the electrode reaction reversibility also the ratio of $|i_p^a/i_p^c|$ which should be equal to 1 (unity) was calculated (Table 4.2.6).

Table 4.2.6: Diagnostic criterion for cyclic voltammograms of a reversible process: absolute values of current ratio of anodic and cathodic peaks

ν (mV·s^{-1})	**i_p^a/i_p^c**	
	600ºC	650ºC
50	0.58	1.62
100	0.82	1.39
200	0.84	1.23
400	0.93	1.19
600	1.0	1.16

The ratio of anodic to cathodic peak current *(i_p^a/i_p^c)* is 1.0 for 600ºC at the scan rate of 600 mV·sec^{-1}. This ratio decrease with decreasing scan rate, indicating that another process is taking place together with the diffusion, e.g. chemical reaction following charge transfer. Probably, besides the process of the electrolytic reduction of Ti (IV) to Ti (III) species, a disproportionation of TiF_6^{2-} occurs in the near-electrode layer:

$$3TiF_6^{2-} + Ti + 6F^- \rightarrow 4TiF_6^{3-}$$

takes place, resulting in an increase of the concentration of Ti(III) species. The ratio >1 was obtained for cyclic voltammograms recorded at the scan range of 50-600 mV·sec^{-1} at temperature of 650°C, suggesting that the continuously accumulation of Ti^{3+} species occurs, resulting in higher anodic peak for the oxidation process of Ti^{3+} species to Ti^{4+}.

Based on the cyclic voltammograms (Fig. 4.2.20) and electroanalysis one can assume that the process of the electrochemical reduction of Ti(IV) fluoride complexes to Ti(III) in a FLiNaK electrolyte in the presence of Ti wire changes from a quasi-reversible behaviour at 600ºC (at the scan rates of < 600 mV·sec^{-1}) to the irreversible process at 700ºC. The number of electrons exchanged during the reversible reduction process of TiF_6^{2-} species at 600ºC (for the scan rate 600 mV·sec^{-1}) was evaluated applying the equations (4.2.8). From the data $E_p^a = 0.08\ V$ and $E_p^c = -0.146\ V$ at 600 mV·sec^{-1}, the calculated number of electrons *n* was equal to be 0.75. The diffusion coefficient of Ti(IV) species at 600ºC (scan rate 600 mV·sec^{-1}) has been calculated using the equation (4.2.9). The value of the diffusion coefficient for TiF_6^{2-} at 600°C was found to be $1.24 \cdot 10^{-8}$ cm^2·s^{-1}. The value of the diffusion coefficient for TiF_6^{2-} at 700°C calculated applying equation (4.2.2) was equal to be $1.78 \cdot 10^{-7}$ cm^2·s^{-1}.

The activation energy of the overall reaction in the temperature range of 600-700ºC, calculated from the data in Fig. 4.2.25 and Eq.(4.2.6) is equal to 66.5 kJ·mol^{-1}.

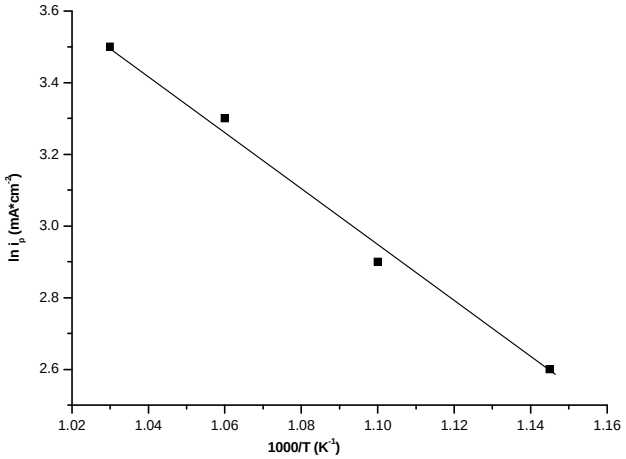

Figure 4.2.25: Arrhenius plot of peak currents for the reduction of the Ti (IV) species (scan rate 100 mV·s^{-1})

4.2.6 FTIR spectroscopy of Ti (IV) species

Method of FTIR spectroscopy was used for the identification of the electrochemical active species of Ti (IV) and Ti (III) in FLiNaK electrolyte in the solid state.

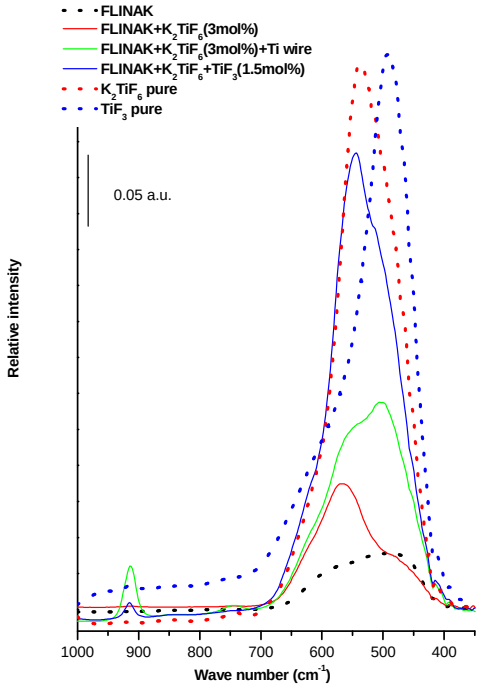

Figure 4.2.26: FTIR absorption spectra of FLiNaK, K_2TiF_6, TiF_3, FLiNaK-K_2TiF_6 (3 mol%), FLiNaK-K_2TiF_6(3 mol%)-Ti wire, FLiNaK-K_2TiF_6 (3 mol%)-TiF_3(1.5 mol%)

The FTIR spectrum of FLiNaK-K_2TiF_6 (3 mol%) measured in the solid state (Fig. 4.2.26, curve-2) demonstrates the presence of $[TiF_6]^{2-}$ octahedral complexes with a typical vibrational feature of 544 cm^{-1}.

As can be seen in Fig. 4.2.26 (curve-3) the spectrum exhibits three bands. The peak at 547 cm^{-1} demonstrates the presence of $[TiF_6]^{2-}$ octahedral species. The peak at 503 cm^{-1} is tentatively assigned to the vibration of the possible formed $[TiF_6]^{3-}$ complex confirming the disproportional reaction:

$$3TiF_6^{2-} + Ti + 6F^- \rightarrow 4TiF_6^{3-}$$

The band at 914 cm^{-1} corresponds to the titanium oxyfluoride impurities, $[TiOF_5]^{3-}$.

FTIR spectrum of FLiNaK-K_2TiF_6 (3 mol%)-TiF_3 (1.5 mol%) in solid state (Fig. 4.2.26, curve - 4) demonstrates the presence of $[TiF_6]^{2-}$ octahedral complexes (544 cm^{-1}) and $[TiOF_5]^{3-}$ at 914 cm^{-1}.

4.2.7 Effect of the temperature on the electrochemical reduction of B(III) and Ti(IV) species

The influence of the temperature on the reduction mechanism of Ti(IV) and B(III) species out of FLiNaK electrolyte was investigated by recording cyclic in the temperature range of 600-700ºC (Fig. 4.2.27). The electrode potential was scanned from 0 V (vs. Pt quasi reference electrode) in the negative direction at a scan rate of 100 $mV \cdot sec^{-1}$.

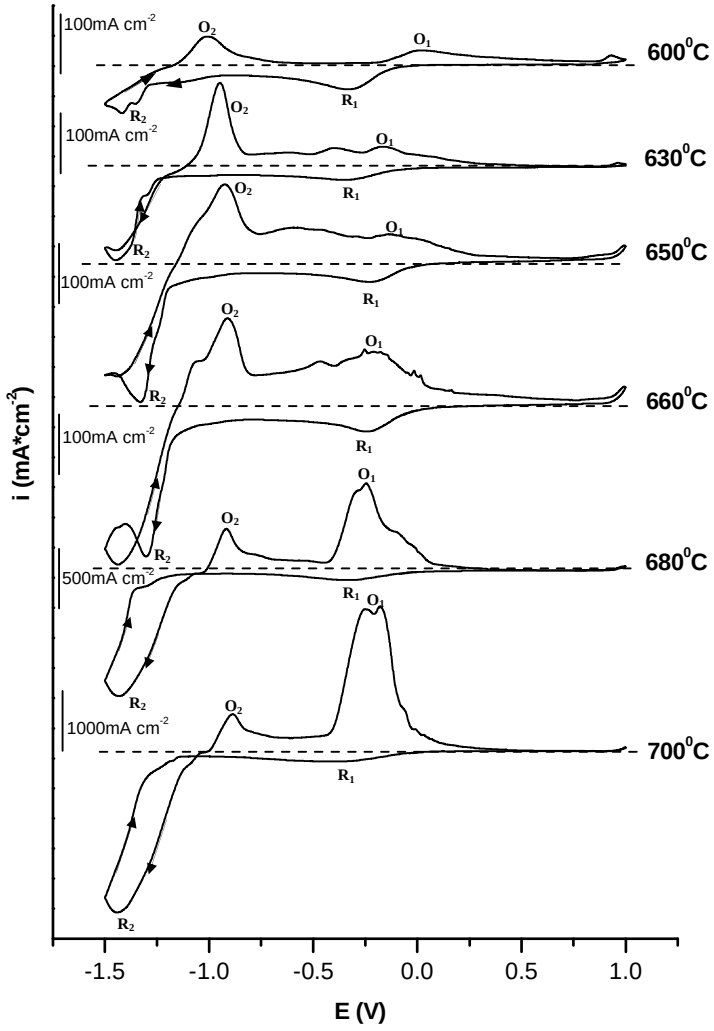

Figure 4.2.27: Cyclic voltammograms (3rd cycle) in FLiNaK-K_2TiF_6 (3 mol%)-KBF_4 (6 mol%) molten salt system at different temperatures (WE - Pt wire, A=0.16 cm^2; quasi RE-Pt wire, scan rate 100 $mV \cdot s^{-1}$)

The change of the form of the voltammetric curves caused by the addition of KBF_4 to the FLiNaK-K_2TiF_6 electrolyte can be seen in Fig. 4.2.27. Besides the first reduction peak at ~0.3 V (attributed to the reduction of Ti(IV) to Ti(III) species), which also was detected on the voltammetric curves in the system FLiNaK-K_2TiF_6 (Fig. 4.2.8), the second reduction peak is observed at -1.35 V due to the reduction of Ti(III) and of B(III) species, leading to TiB_2 formation via Ti^0 and B^0. The oxidation peak O_2 corresponds to the oxidation of Ti, which is not consumed in the formation of TiB_2. At the temperature ≥ 630ºC one can see that the anodic scan crosses over the cathodic scan resulting in a current loop, which is typical for continuous nucleation and formation of a new product, in this case TiB_2.

4.2.8 FTIR spectroscopy of Ti (IV) and B(III) species

FTIR-emission spectra of KBF_4, K_2TiF_6, pure FLiNaK, FLiNaK-K_2TiF_6, FLiNaK-KBF_4, FLiNaK-K_2TiF_6-KBF_4 (Fig. 4.2.28) melts have been recorded in solid states to estimate the structure of the electrochemical active species of titanium (IV) and boron (III).

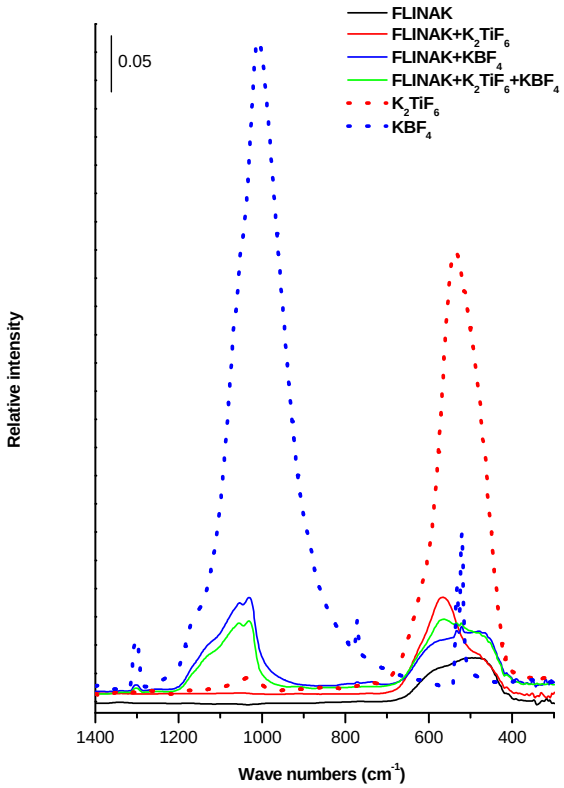

Figure 4.2.28: FTIR absorption spectra of FLiNaK, K_2TiF_6, KBF_4, FLiNaK-K_2TiF_6 (3 mol%), FLiNaK-KBF_4 (6 mol%), FLiNaK-K_2TiF_6 (3 mol%)-KBF_4 (6 mol%)

As can be seen in Fig. 4.2.28 (curve 2), the FTIR spectrum of FLiNaK-K_2TiF_6 (3 mol%) indicates the presence of $[TiF_6]^{2-}$ octahedral complexes at 568 cm^{-1} in the quenched samples. In curve 3 (Fig. 4.2.28), in the FTIR spectrum of FLiNaK-KBF_4 (6 mol%) the bands at 1051 cm^{-1}, 1032 cm^{-1} and 526 cm^{-1} correspond to the vibration of the BF_4^- anions. In curve 4 (Fig. 4.2.28), in the FTIR spectrum of FLiNaK-K_2TiF_6 (3 mol%)-KBF_4 (6 mol%), similar vibrational features as in the case of FLiNaK-K_2TiF_6 (3 mol%) and FLiNaK-KBF_4 (6 mol%) are detected, indicating, that there is no chemical reaction involving the starting compounds leading to significant changes of the electrolyte composition.

4.3. Morphology and mechanical properties of TiB_2 layer deposited from chloride-fluoride melt via pulse plating compared with TiB_2 layer deposited via direct current procedure

4.3.1 Introduction

The first investigation on the optimization of the process of electrochemical TiB_2 deposition and improving the quality of the coatings by applying pulse plating mode was published by Ett and Pessine [13]. The authors established that the electrodeposition with PIC produces coatings with better quality, showing less cracks and better adhesion to the graphite substrate compared with those obtained by CCP. Further work of other scientists [15, 16] also indicates improvements of the process of TiB_2 coatings via pulse plating techniques.

This chapter is focused on the investigation of the effect of the current mode on the mechanical properties and morphology of the TiB_2 coatings.

The eutectic mixture of NaCl - KCl - NaF was used as a solvent for the electrochemical active substances K_2TiF_6 and KBF_4 taken in molar ratio 1:3, which concentration in the melt was adjusted at 12-14 wt.%. The electrodeposition was performed at a temperature of 700ºC ± 10ºC in argon atmosphere. The applied pulse sequences are depicted in Fig. 3.5 (b and d). The deposition time was adjusted to 10-30 min, depending on the required thickness of the TiB_2 layers.

4.3.2 Morphology of TiB_2 coating

It was found that in the PIC mode the cathodic peak current applied should be within the limits $0.2 < -i_1 < 0.7$ A·cm^{-2}, in order to obtain dense and homogeneous coatings (Fig. 4.3.1a). The coatings growth not homogeneous at current densities < -0.2 A·cm^{-2} and, when $-i_1 > 0.7$ A·cm^{-2}, the coatings exhibit low adhesion to the substrate and a spherolitic growth is observed (Fig. 4.3.1b). For improving the homogeneity, the time of the pause (τ_2) is recommended to be longer than the time of current flow (τ_1). In comparison to DC procedures, the time of deposition of a layer with a thickness in the range up to 40 μm can be decreased by a factor of 3 in the considered PIC mode. It could be assumed that applying DC a side electrode reaction, e.g. reduction of Ti(IV) to Ti(III) takes place in the charge transfer.

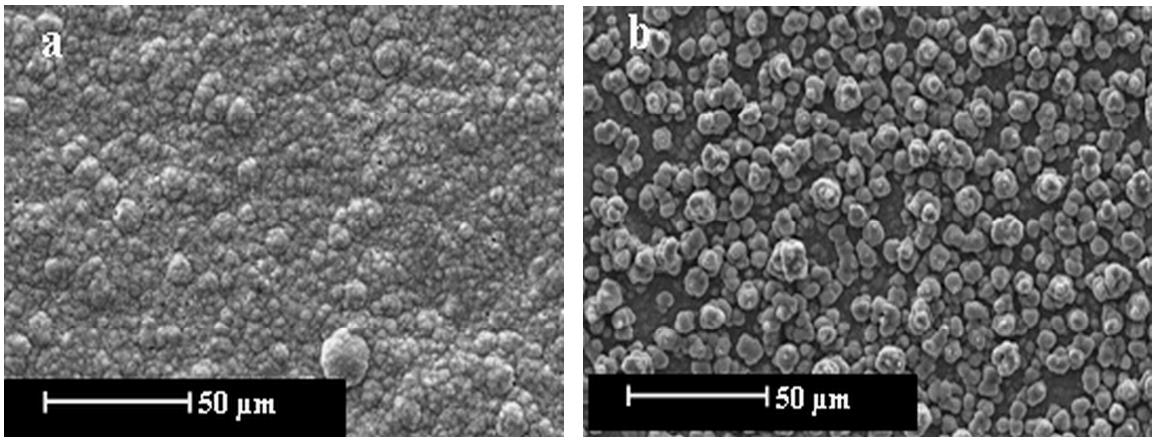

Figure 4.3.1: SEM images of samples (20 kV accelerating voltage, secondary electrons) on Mo substrate obtained in PIC mode with the following parameters: ν=53 Hz; τ_2/τ_1 =1.5; T=700ºC; t_{tot}=10 min (a) i_1=-0.36 A·cm^{-2}, (b) i_1=-0.76 A·cm^{-2}

Changing the deposition process to the PRC mode by introducing of one anodic cycle every five cathodic cycles results in decreasing essentially the roughness (from Ra values of 300-350 nm to Ra values of 100-150 nm) of the deposit, especially for stainless steel substrates. In addition, a significant grain refinement was achieved (reducing the average grain size from the range of 15-20 µm to a grain size < 4 µm). Beside this, the shape of the grains was changed from a more regular one to one with edges and well expressed large crystal faces. Fig. 4.3.2 shows this effect. For achieving a grain size of the TiB_2 coating < 4 µm, the optimal ratio between t_{on} and t_{off} (τ_1/τ_2) is about 4. For lower values of this ratio (< 3), roughness increases, and for higher values (> 5) the inhomogeneous coatings were obtained.

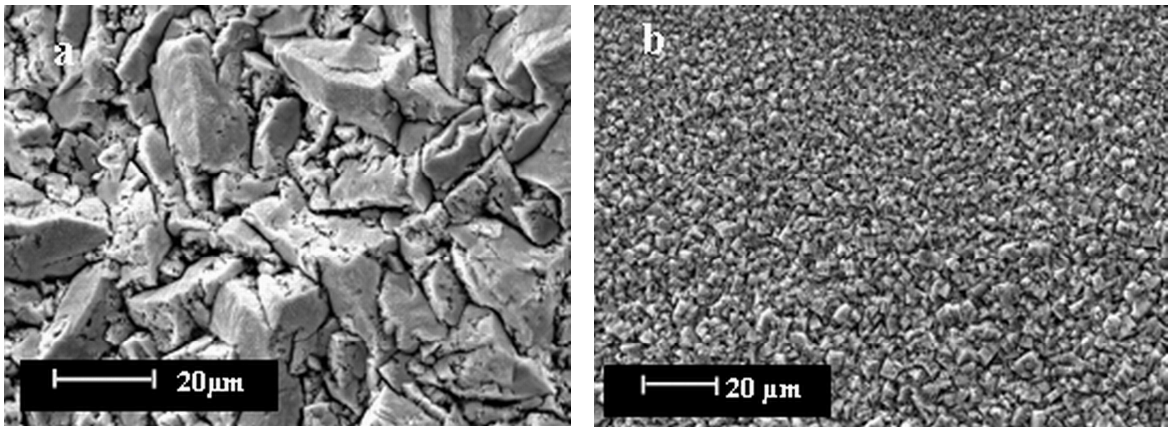

Figure 4.3.2 SEM images of a TiB_2 layer (20 kV accelerating voltage, secondary electrons) obtained on steel substrate (a) PIC mode, t_{tot}=30 min; T=700°C; i_1 =-0.35 A·cm^{-2}; ν=100 Hz, τ_2/τ_1=1.5, (b) PRC mode, each 5-th cathodic cycle of the previous pulse sequence is replaced by one anodic cycle, t_{tot}=30 min; T=700°C; i_3=-i_1= 0.35 A·cm^{-2}; ν=100 Hz, τ_1/τ_2=4

The value of current density is also important for the PRC mode. It was found, that for the sequence of 5 cathodic pulses followed by one anodic pulse, $-i_1$ in the range between 0.33 and 0.38 A·cm^{-2}, with 0.35 A·cm^{-2} as an optimum value, delivers appropriate results with respect to roughness and homogeneity. Increase the average current density to values > 0.38 A·cm^{-2} results in a rough coating with nodular shape of crystals like that shown in Fig. 4.3.3.

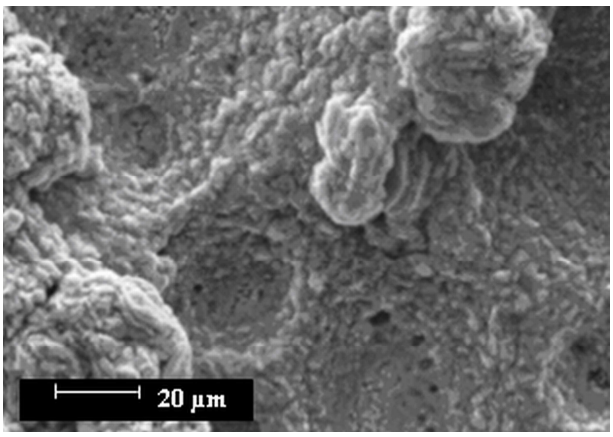

Figure 4.3.3: SEM image of a TiB_2 layer (20 kV accelerating voltage, secondary electrons) on steel substrate obtained in the PRC mode with the following parameters: 5 cathodic cycles plus one anodic cycle, t_{tot}=10 min; T=700°C; $i_{3=}$ i_1=0.75 A·cm^{-2}; ν=100 Hz; τ_1/τ_2=4

The pulse plating procedure allows a deposition of even smooth layers onto the surfaces of different substrates with complex configuration, which is not possible with DC plating. As an example, Fig. 4.4.4 shows good plated edges on steel and tungsten carbide substrates.

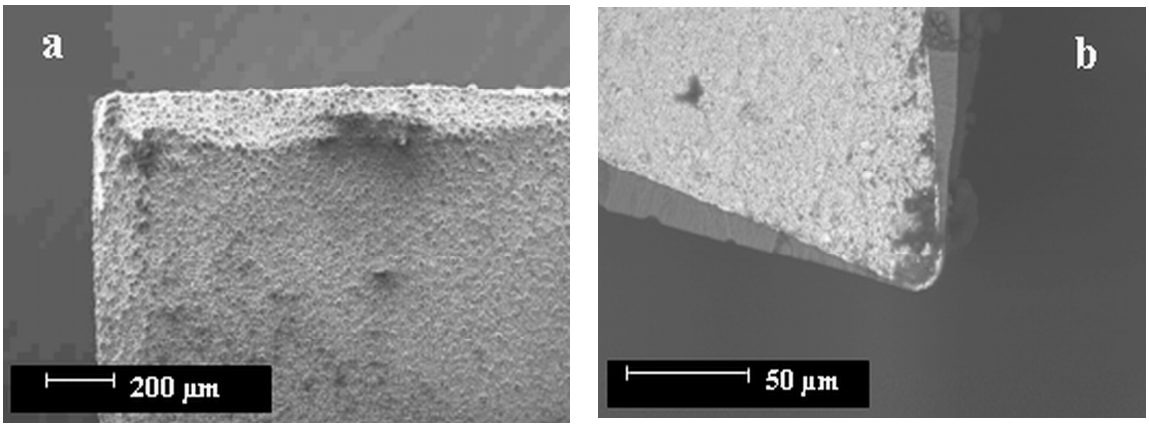

Figure 4.4.4: SEM images of the samples (a) steel substrate coated with TiB_2 layer using PIC mode, (20 kV accelerating voltage, secondary electrons) t_{tot}= 10 sec; T=700°C; i_1=-0.5 A·cm^2; ν=50 Hz; τ_2/τ_1=2, (b) cross section of WC substrate coated with TiB_2 layer using PRC mode, (20 kV accelerate voltage, backscattered electrons), 5 cathodic cycles plus one anodic cycle, t_{tot}=10 min; T=700°C; $i_{3=}$-i_1=0.3 A·cm^{-2}; ν=100 Hz; τ_1/τ_2=4

Concerning TiB_2 deposition, pulse plating permits to deposit high quality coatings onto various substrates when appropriate combinations of pulse magnitudes and sequences are established. The DC plating technique, where only one parameter, the current density, can be varied, has much less possibilities for optimization. This conclusion becomes especially clear when we consider some physical properties of TiB_2 coatings like roughness, hardness and residual stress produced at different regimes of electrodeposition.

4.3.3 Roughness of TiB_2 coating

DC plated samples show typical Ra values in the range of 400 to 1300 nm, Ra values < 400 nm are not observed, except for very thin layers. An AFM image of an example of a highly crystalline and rough (Ra=520 nm) sample on steel substrate is shown in Fig. 4.4.5.

When pulse plating is used, the roughness is highly decreased, and typical Ra values below 350 nm down to 95nm are obtained. Fig. 4.4.6 shows an example with a Ra value of 230 nm.

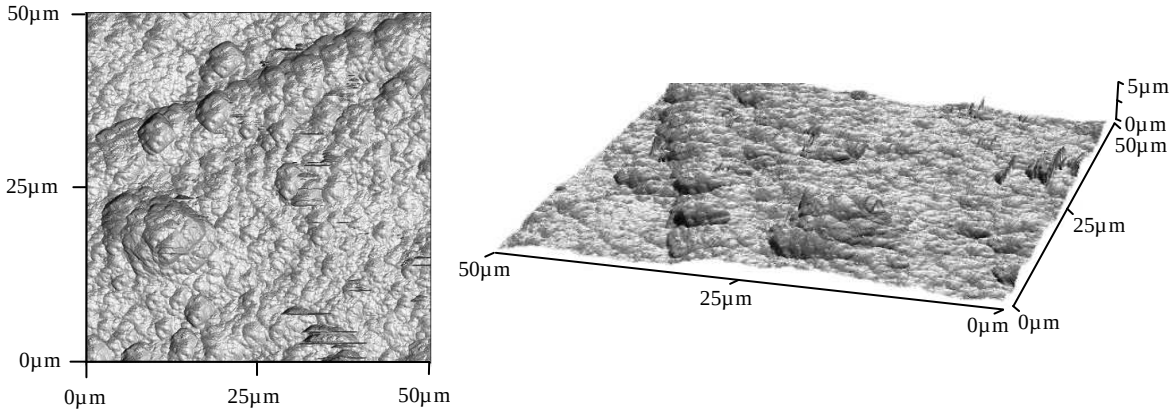

Figure 4.4.5: AFM images of the TiB_2 coating (thickness 20 µm) deposited on steel (Ra of the substrate 1703±20 nm) in DC mode: t_{tot}=90 min, T=700°C, i_1=-0.03 A·cm^{-2}

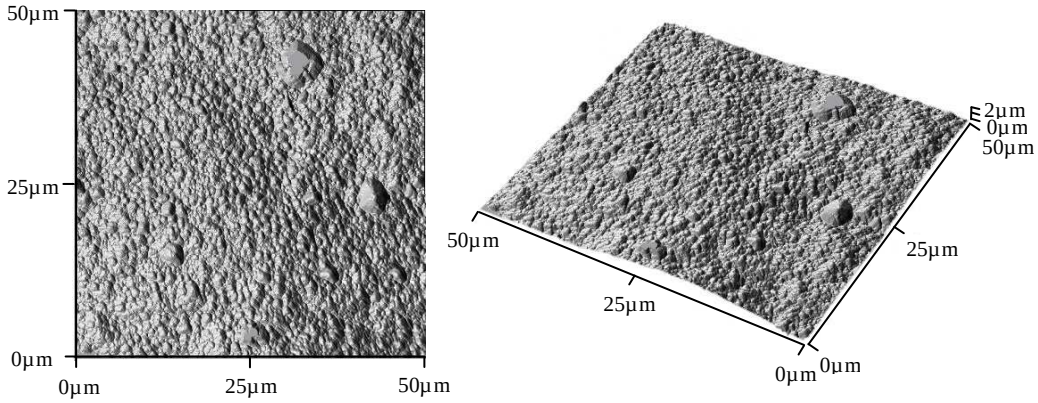

Figure 4.4.6: AFM images of the TiB_2 coating (thickness 20 µm) deposited on steel (Ra of the substrate 1703±20 nm) by PIC electrodeposition: t_{tot}=10 min; T=700°C; i_1=-0.45 A·cm^{-2}; ν=100 Hz; τ_2/τ_1=2.

An important point to emphasize is that uneven deposition or the growth of dendrites might appear even when the pulsed plating techniques was used, similar to some effects observed on DC coated samples. However, this problem can be overcome by the appropriate choice of the PIC or PRC modes.

In particular, the roughness has shown to depend on the pulse frequencies. Typical results obtained are presented in Fig. 4.4.7, where the average Ra values of the coatings as a function of the frequency are plotted. The lowest Ra values were obtained in the case of PRC plating for a frequency of 100 Hz.

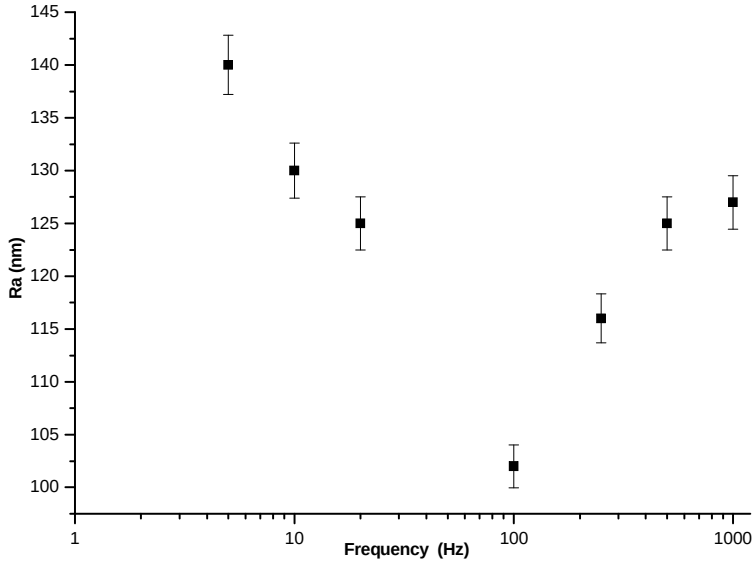

Figure 4.4.7 Ra values as a function of the pulse frequency in PRC mode of TiB_2 deposition (thickness 20 µm) on Mo substrates (Ra of the substrate 2490±20 nm). Conditions: one anodic peak per 5 cathodics, t_{tot}=10 min; T=700°C; i_3=-i_1=0.3 A·cm^{-2}, τ_1/τ_2=4

The curve exhibits a minimum two separating regions: the average roughness decreases sharply when the frequency decreases up to 100 Hz and the roughness increases more slowly in the frequency range of 100-1000 Hz, demonstrating that this property is no longer improved by high frequencies. The shape of the plot in Fig. 4.4.7 can be explained by the influence of diffusion layer thickness on tertiary current distribution (Fig. 2.8).

At low frequencies, the time-on is quite long; as a result, during each pulse the diffusion layer grows leading to a "microprofile". This means that the peaks are more accessible to diffusion layer than the recesses, giving rise to a tertiary current distribution [102]. As the result, the rougher coatings are observed at lower frequencies.

With increase the frequencies the thickness of the diffusion layer is reduced leading to the change of the "microprofile" into a "macroprofile", notably forming smoother coatings. SEM images of the coatings, corresponding samples prepared with a frequency of 10, 100 and 1000 Hz (samples of Fig. 4.4.7), are presented in Fig. 4.4.8. In all cases, the surface was smooth, but for higher frequencies the structure of the layer is finer compared with the coating prepared at lower frequencies. The grain size for the samples prepared with a frequency of 100 Hz is significantly lower (ranging < 2 μm), than for the samples prepared with a frequency of 10 Hz.

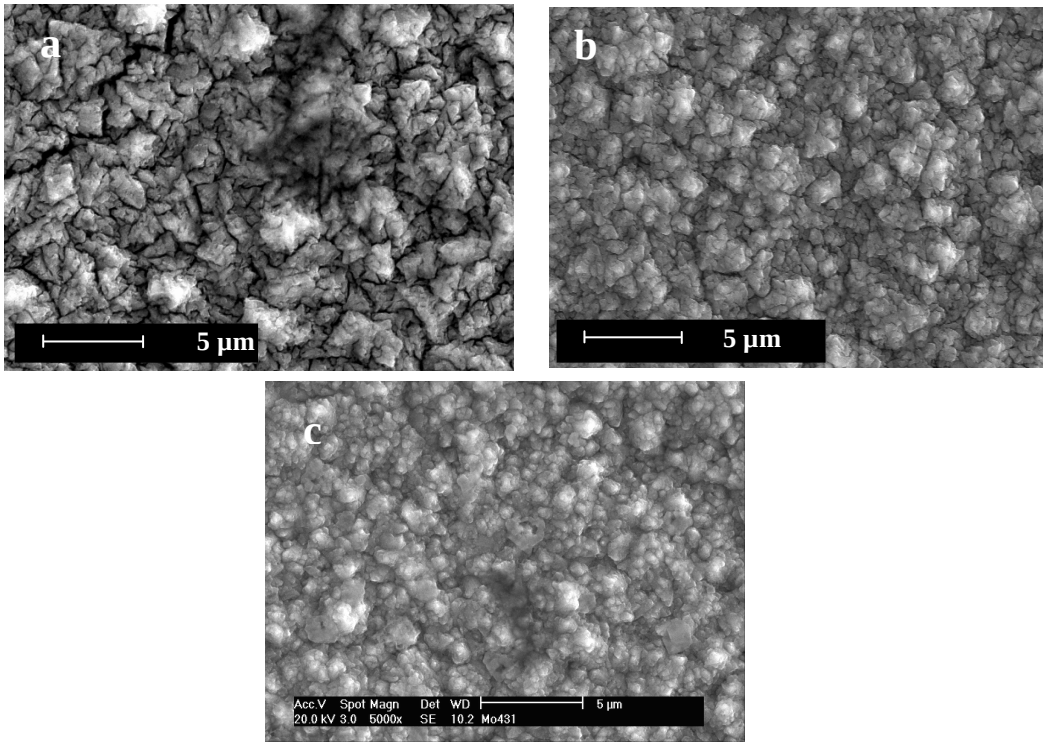

Figure 4.4.8: SEM images of samples (20 kV accelerating voltage, secondary electrons) obtained on Mo substrates (Ra of the substrate 2490±20 nm); roughness variation with the pulse frequency in PRC mode of deposition (a) ν=10 Hz; Ra=130±5 nm, (b) ν=100 Hz; Ra=102±5 nm, (c) ν=1000 Hz; Ra=127±5 nm

Taking into the consideration that the current density was equal in all experiments, the difference in the grain size could be explained by the nucleation process beginning again at each pulse. Increase the frequency causes the enhancement of the number pulses leading to the increase of the number of nuclei and continuous formation of small grains. As a result, a uniform distribution of the electrodeposited coating with smaller grain size and a finer microstructure onto the surface of the cathode is observed.

The optimal ratio between $cycle_{cat}$ /$cycle_{an}$ was 5/1. More frequent anodic cycles decrease the homogeneity of the layer and increase the duration of the deposition, while less frequent anodic cycles increase the roughness of the surface.

4.3.4 Microhardness

The microhardness values for bulk TiB_2 material, which were reported in the literature [120-122], range from 1646 to 3400 $HV_{0.05}$. Evidently, such differences stems from both the experimental procedure and origin of the material as well. Anyway, the obtained values for electrochemical coatings fall into this range. Such microhardness is on the desired level for a cutting tool.

Practically no correlation has been found between microhardness and the method of deposition. In both modes (DC and PIC, PRC), the microhardness of the coatings depends mainly on current density exhibiting a minimum at 0.3 $A \cdot cm^{-2}$ [71]. The reason for such behavior is not quite understood yet. Whereas grain size refinement at the increase of current density could account for an increase in microhardness, the lowering in the values at lower current densities is not clear.

In the case of changing the frequency between 10 Hz – 100 Hz in the PIC mode (Fig. 4.4.9), it is observed that the hardness increases as the frequency increases up to 100 Hz. The highest hardness value (~2250 MPa) was found for a pulse frequency of 100 Hz, correlated to the lowest roughness values in the case of PRC mode.

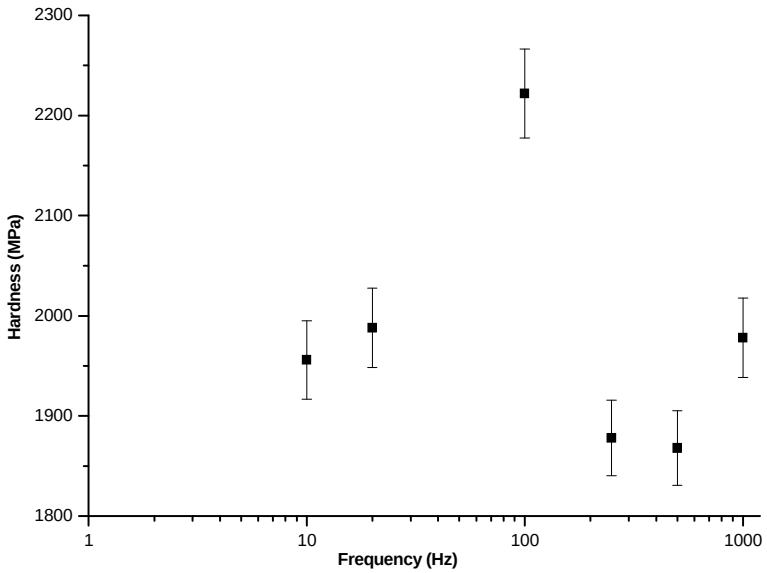

Figure 4.4.9: Microhardness dependence (load 1.0 N) on the pulse frequency of TiB_2 coatings deposited on Mo substrates in PIC mode: t_{tot}=10 min, T=700°C; i_1=-0.5 A·cm^{-2}

As it has been mentioned before, during short pulses at higher frequency a very thin pulsating diffusion layer has been formed leading to the enhanced nucleation rate and formation denser, more homogeneous and finer grained deposits. As the results, coatings with lower porosity and correspondingly higher hardness values are observed. Also the value of the grain size for the coatings prepared with a frequency of 100 Hz is significantly lower compared to coatings prepared with a frequency of 10 Hz. Thus, the highest value of microhardness at the frequency of 100 Hz can be explained by Hall-Petch law, as the grain size decreases, the microhardness of deposits will increase. Further increase the frequency up to 1000 Hz does not influence on the grain size, but significantly decrease the on-time and correspondently the thickness of the coatings, resulting in decrease of the hardness.

4.3.5 Stress

The resulting values of residual stress are in the range of -0.7 GPa to -2.2 GPa. In Fig. 4.4.10 the relationship of the residual stress in TiB_2 layers deposited with different thickness on Mo substrates is presented.

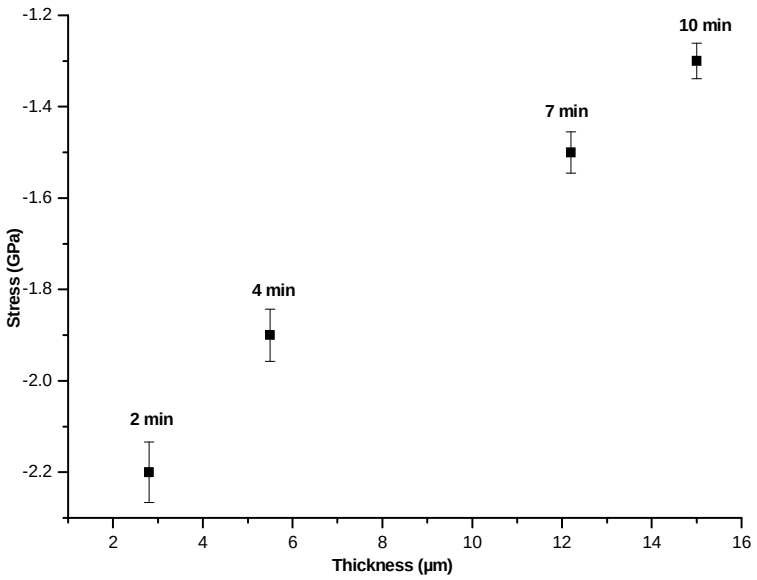

Figure 4.4.10: Residual stress dependence on the thickness of the TiB_2 layer on Mo substrate in PIC mode of deposition. Conditions: time of deposition 2 min, 4 min, 7 min, 10 min; T=700°C; i_1 = -0.5 A·cm^{-2}, τ_2/τ_1=1.5

The highest value of the stress is observed at the lowest thickness of the coating. As the thickness increases the stress values decreases to a value of -1.3 GPa for a layer of 15 µm. Due to the difference structure in the lattice structure of the TiB_2 (P6/mmm) [123] compared to Mo (Im-3m) [124] the thinner layers generate a higher stress, also enhanced by the mismatch between the thermal expansion coefficients of Mo, $\alpha=4.8\times10^{-6}$ K^{-1} [125] and TiB_2, $\alpha=7.8\text{-}8\times10^{-6}$ K^{-1} [2]) since during cooling down the samples, stress is induced into the layer. Within the thicker layers, there is more possibility in stress reducing relaxation during the cooling period. Any extrapolation towards thin coatings is thus risky. In Fig. 4.4.11, the dependence of the residual stress values on the frequency in the case of PIC deposition procedure for TiB_2 layer with a thickness ranging between 20 and 25 µm is shown.

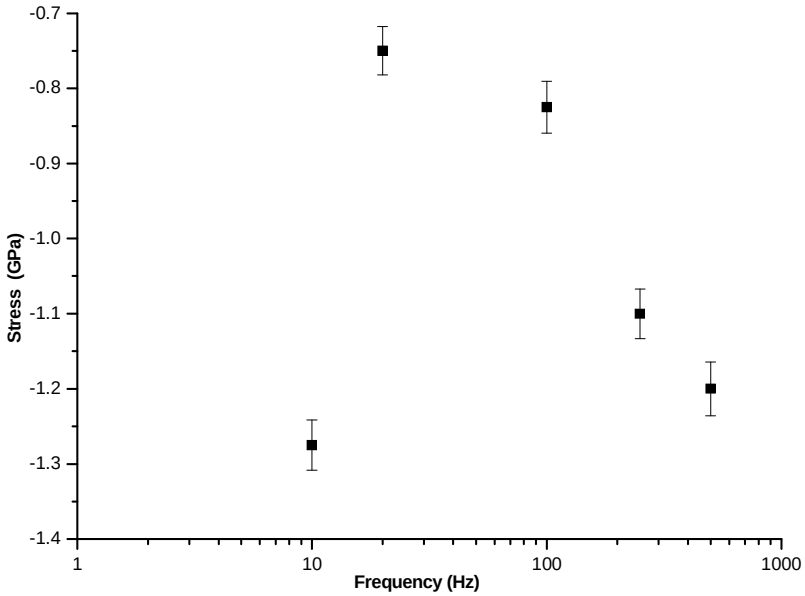

Figure 4.4.11: Residual stress dependence on the frequency of the TiB_2 layer (thickness between 20-25 μm) deposited on Mo substrate in PIC mode: t_{tot}=15 min, T=700°C; i_1=-0.5 A·cm^{-2}, τ_2/τ_1=1.5

The lowest values were measured for samples obtained using frequencies of 20 and 100 Hz. The negative sign of the stresses found indicates a compressive type of stresses in the coatings. These values are comparable to reported values for TiB_2 layers produced by magnetron sputtering on graphite [126] and other substrates [127,128]. Similarly to the roughness (Fig. 4.4.7), the residual stress of the layer depends on the pulse frequency in the PP deposition. The lowest values were observed for samples obtained at pulse frequencies of 20 and 100 Hz.

4.3.6 Current efficiency

Fig. 4.4.12 presents the current efficiency values obtained of TiB_2 layers as functions of the pulse frequency.

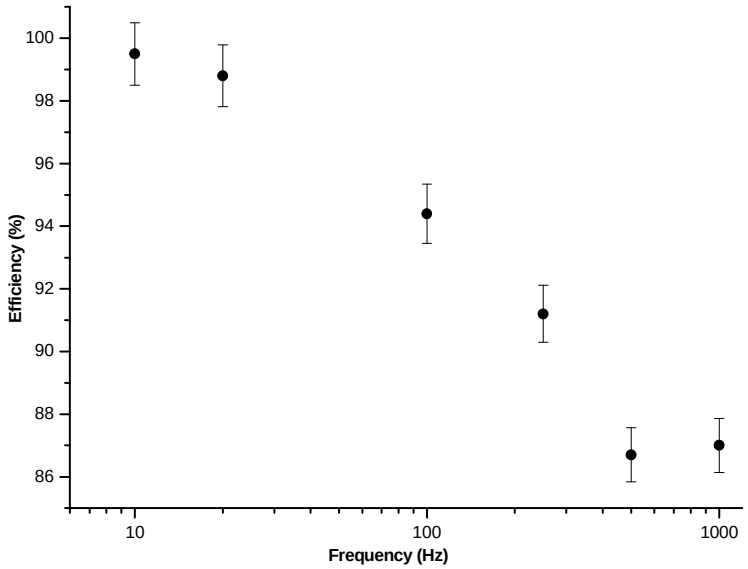

Figure 4.4.12: Efficiency dependence on the pulse frequency of TiB_2 coatings deposited on Mo substrates in PIC mode: t_{tot}=10 min, T=700°C; i_1=-0.5 A·cm^{-2}

As one can see, the current efficiency decreases as the pulse frequency increases from 99% at 10 Hz to 87% at 1000 Hz. One can suggest that increase of the pulse frequency leads to the losses of the current on the side electrode reaction, e.g. reduction of Ti (IV) to Ti (III) species.

4.4 Electrochemical deposition of TiB_2 coatings out of FLINAK electrolyte: influence of additive, pre-treatment of the substrate, temperature and current distribution on the quality of the layer

4.4.1 Electrochemical synthesis of TiB_2 layers out of FLiNaK electrolyte in the presence of $TaCl_5$ additive

FLiNaK was used as the supporting electrolyte. Active components, K_2TiF_6, KBF_4 and $TaCl_5$ were taken at molar ratio of 1:2:0.06 for CV measurements and 1:5:0.06 for the electrochemical deposition to get an excess of volatile component KBF_4. The electrodeposition was performed at a temperature of 650ºC ± 10ºC in argon atmosphere. The pulse sequences which were used see in Fig. 3.5 (a and f). The experiment lasted 20 min.

4.4.1.1 Cyclic voltammetry

Based on the results presented in Fig. 4.1.3, the electrochemical window for the further investigations was defined between -1.5 V and +1.0 V vs. Pt quasi reference electrode. Cyclic voltammograms were measured in FLiNaK-K_2TiF_6, FLiNaK-KBF_4, FLiNaK-$TaCl_5$, FLiNaK-K_2TiF_6-KBF_4, FLiNaK-$TaCl_5$-KBF_4 and FLiNaK-K_2TiF_6-KBF_4-$TaCl_5$ systems at 650ºC using a scan rate of 100 $mV \cdot sec^{-1}$, additional studies were performed in the FLiNaK-K_2TiF_6 system at 5 $mV \cdot sec^{-1}$ (Fig. 4.4.1). The voltammograms are initially scanned in the cathodic direction, starting at 0 V vs. Pt quasi reference electrode.

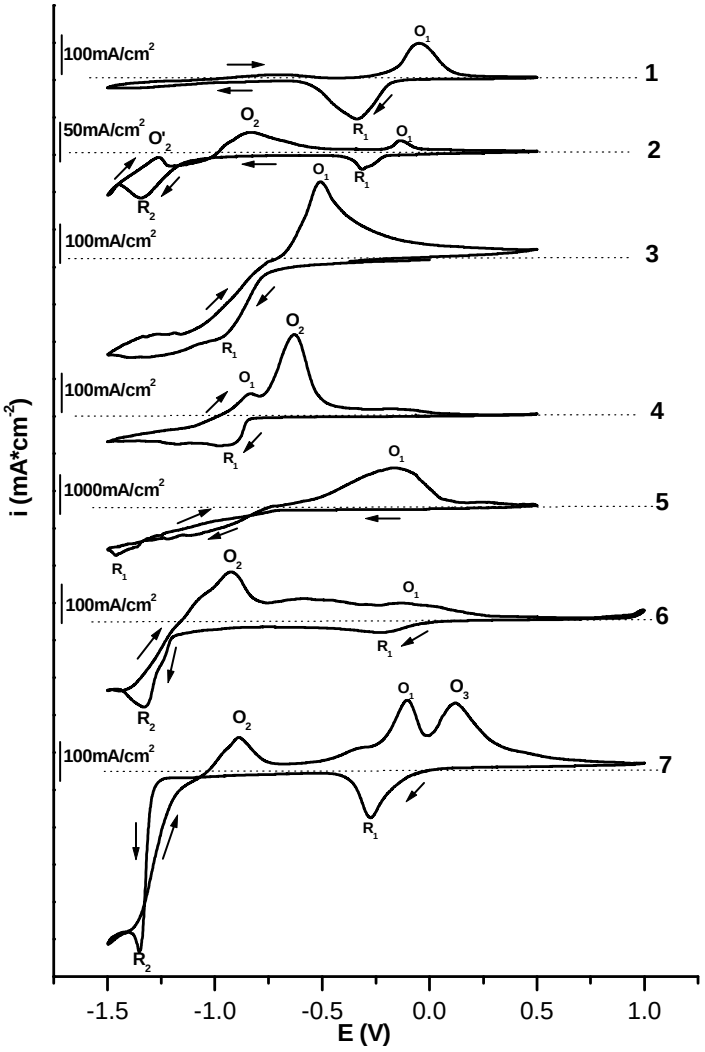

Figure 4.4.1: Cyclic voltammograms in different molten salt systems at 650ºC (WE-Pt wire, A=0.16 cm^2; quasi RE-Pt wire, CE-glassy carbon crucible; scan rate 100 $mV \cdot s^{-1}$). Curve 1: FLiNaK-K_2TiF_6 (3 mol%) scan rate 100 mV sec^{-1}; Curve 2: FLiNaK-K_2TiF_6 (3 mol%), scan rate 5 $mV \cdot s^{-1}$; Curve 3: FLiNaK-KBF_4 (6 mol%); Curve 4: FLiNaK-$TaCl_5$ (0.2 mol%); Curve 5: FLiNaK-$TaCl_5$ (3 mol%)-KBF_4 (6 mol%) Curve 6: FLiNaK-K_2TiF_6 (3 mol%)- KBF_4 (6 mol%); Curve 7: FLiNaK- K_2TiF_6 (3 mol%)- KBF_4 (6 mol%)- $TaCl_5$ (0.2 mol%)

The cathodic behaviour of Ti(IV) species in FLiNaK electrolyte at a scan rate of 100 $mV \cdot sec^{-1}$ and 5 $mV \cdot sec^{-1}$ is shown in Fig. 4.4.1 (curves 1 and 2). One cathodic peak (at -0.35 V) and its corresponding anodic peak (at -0.05 V) are observed in cyclic voltammogram recorded at 100 $mV \cdot s^{-1}$ (curve 1), attributed to the one-electron reversible charge transfer process involving the reduction of Ti(IV) species to Ti(III) species. At the lower scan rate, 5 $mV \cdot s^{-1}$, two more additional cathodic peaks are observed (curve 2), R_2 at a potential of -1.35 V and a broad peak (R_2') between -1.25 V and -1.0 V. R_2 can be attributed to the three-electron irreversible charge transfer process involving the reduction

of Ti^{3+} species to Ti^{o}. The current flow within the potential range of R_2' can be assigned to a reduction reaction of electroactive species containing $Ti^{(3+ - x+)}$ (x < 3). This attribution is still under discussion and needs further experimental work. The broad oxidation peak (O_2) at -0.8 V can be assigned to the oxidation of Ti^{o} or $Ti^{(3+ - x+)}$ (x < 3) species.

Curve 3 (Fig. 4.4.1) demonstrates the cathodic behaviour of B(III) species in FLINAK electrolyte. It can be seen that the reduction of B(III) species to B^{o} occurs in one step at potentials more cathodic than -0.8 V. This finding is in good agreement with literature data [129] according to which the electrochemical reduction of B(III) species proceeds in a single charge transfer step: $BF_4^- + 3e^- \rightarrow B^0 + 4F^-$.

Curve 4 (Fig. 4.4.1) is typical for the cathodic behaviour of Ta(V) species in FLINAK electrolyte. The peak R_1 at -0.9 V is attributed to the reduction of Ta(V) species. Based on the voltammogram, one can assume that the reduction of Ta(V) ions to metallic state proceeds in a single multi-electron step, that was also confirmed by Polyakova et al. [130].

Curve 5 (Fig. 4.4.1) demonstrates the cathodic behaviour of a mixture of Ta(V) and B(III) species in FLiNaK electrolyte. The reduction reaction starting at -0.75 V and the peak R_1 at -1.45 V, corresponding to the TaB_2 formation, is only weakly expressed. The single reduction peaks of Ta^{5+} and B^{3+} species diminish, the current density is by a factor of ten higher as in the case of FLiNaK-$TaCl_5$ electrolyte (curve 4), related to the higher Ta content and to a possible catalytic behaviour of (the mixture or) the nuclei of TaB_2 on the further reaction. A typical cross-over of the direct (in cathodic direction) and the reverse scanning (in the anodic direction) curve is observed, which demonstrates the irreversibility of the nucleation step in the direct scan. Thus, this cross-over is considered to be a proof of the formation of a new solid phase, in our case TaB_2 [115]. The current density is by a factor of ten higher as in the case of FLiNaK-$TaCl_5$ electrolyte, indicating a catalytic behaviour of (the mixture or) the nuclei of TaB_2 on the further reaction. The oxidation peak shifts by more than 500 mV in the anodic direction, giving an evidence for the high stability of TaB_2 against oxidation.

Curve 6 (Fig. 4.4.1) is characteristic for the cathodic behaviour of Ti(IV) and B(III) species in the FLiNaK electrolyte at 650ºC. The reduction reactions of Ti(III) species and of B(III) species occur in the potential range -1.2 to -1.4 V, leading to TiB_2 formation. The peak R_1 at -0.3 V can be attributed to the reversible reduction of Ti(IV) to Ti(III). The reduction peak R_2 at -1.35 V is positioned at the same potential as in curve 2 and corresponds to the reduction of Ti^{3+} species to Ti^{o}. A shoulder in the cyclic voltammogram at approximately

-1.24 V can be assigned to the reduction of an actually unknown B-containing complex. The phenomena of shifting the reduction potential of an electroactive species to higher overvoltages via complex forming is well known in polarographic work and is probably the cause for the shift of the B^{3+}/B^{o} couple to higher voltage values in comparison to curve 3. As in the case of curve 5 (Fig. 4.4.1), a cross-over of the direct and the reverse voltage scan is observed, attributed to the formation of the new solid phase TiB_2.

Curve 7 (Fig. 4.4.1) is typical for the Ti(IV)/B(III) system with the addition of a small amount of Ta(V) species in the FLiNaK electrolyte. Beside the characteristic, well expressed reduction peak R_1 at -0.3 V (reduction of Ti(IV) species to Ti(III) species), the current flow in the reduction peak R_2 at -1.4 V (attributed to TiB_2-TaB_2 formation) is significantly higher compared to curve 6 measured at similar electrolyte composition. The potentials of the formation of the individual compounds TiB_2 and TaB_2 (Fig. 4.4.1, curve 5 and 6) are close, resulting in simultaneous co-deposition of these compounds. As in the case of an electrolyte composition of FLiNaK-K_2TiF_6-KBF_4 (curve 6), the shift of the reduction potentials of the individual compounds can be explained by the formation of complex species of unknown composition. Addition of $TaCl_5$ to the FLiNaK-K_2TiF_6-KBF_4 system promotes the increase of the cathodic peaks in height by a factor of 2, indicating that the Ta(V) species acts as a catalyst for the reduction of Ti(IV) to Ti(III) species, and more Ti^{3+} species are available at higher cathodic potentials for the reduction reaction Ti^{3+}/Ti^{o}. Additional evidence of this fact based on the findings that the melt after the CV measurements was coloured deeply violet in the case of FLiNaK-K_2TiF_6-KBF_4-$TaCl_5$ system compared to a light blue colour in the case of the FLiNaK-K_2TiF_6-KBF_4 system. The violet colour is typical for Ti^{3+} species, and due to the addition of a small amount of $TaCl_5$ the concentration of the Ti^{3+} containing complex species is significantly enhanced. Also, as one can see in the curves 5 and 6, the cross-over of the direct and the reverse scanning curve is observed, which is attributed to the formation of a new solid phase TiB_2 or TaB_2. The voltammograms 5-7 in Fig. 4.4.1 indicate that the deposition of TiB_2 and TaB_2 occurs simultaneously in the same potential range (1.2-1.4 V), thus a co-deposition of the compounds takes place.

Thermodynamic data of the formation of TiB_2 and TaB_2 compounds (Table 4.4.1) indicates that at 650ºC the free energy of TiB_2 formation is more negative in comparison with the values of TaB_2, therefore at the same temperature the growing of TiB_2 is thermodynamically favoured compared to TaB_2.

Table 4.4.1: Standard free enthalpies of formation of TiB_2 and TaB_2 compounds

Compound	ΔG^o (kJ/mol) (T in K)	ΔG^o (kJ/mol) at 923K	Reference
TiB_2	-279.49 + 0.028·T	-253.65	[131]
TaB_2	-190.1 + 0.047·T	-146.72	[132]

4.4.1.2 Phase analysis and chemical composition of the coatings

The X-ray diffraction pattern of a TiB_2 layer deposited using the PIC mode shows the same peak positions and intensity ratios as a pattern calculated according to JCPDS-PDF 00-035-0741 data. The additional diffraction peaks can be attributed to the Mo substrate (Fig. 4.4.2).

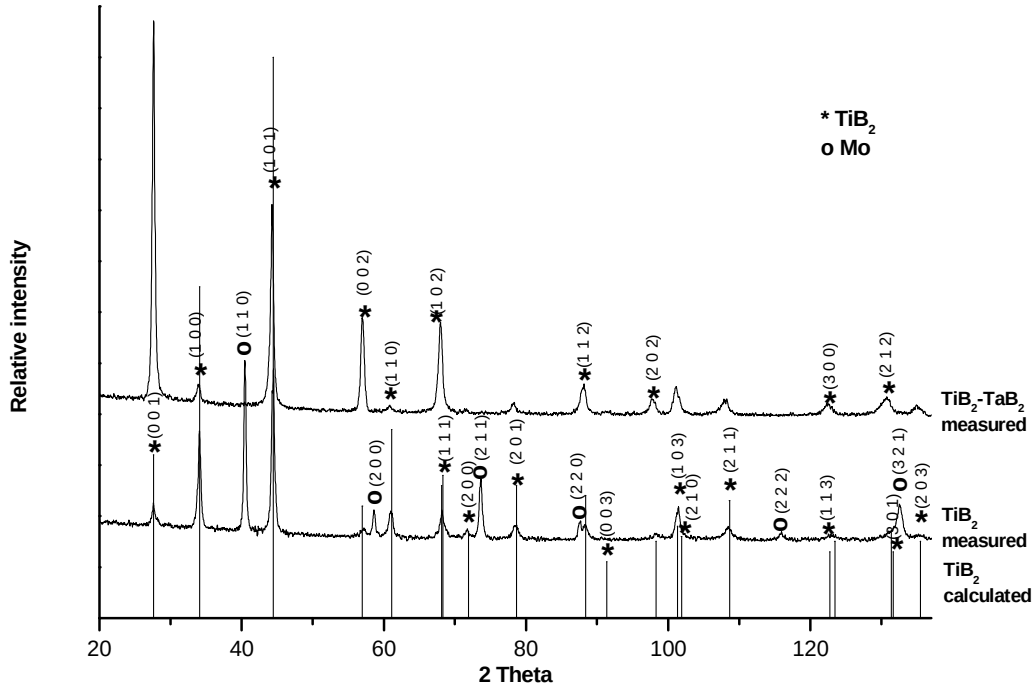

Figure 4.4.2: X-ray diffraction pattern of the TiB_2 (25 µm) and TiB_2-TaB_2 (30 µm) coatings on Mo substrate, electrochemically deposited out of FLiNaK electrolyte via PIC mode with the following parameters: ν=55 Hz; T=650ºC; t_{tot}=30 min; i_{av}=-0.08 A·cm^{-2}, τ_{on}/τ_{off} =2.6; Bragg-Brentano geometry, CuKα radiation

In the case of the presence of $TaCl_5$ in the electrolyte, and using the same amount of charge the TiB_2 phase exhibits a strong (001) texture and no reflections attributed to the Mo substrate were detected. This fact can be explained by a higher porosity of the pure TiB_2

layer compared to the TiB_2-TaB_2 layer and on the higher X-ray absorption coefficient of TaB_2. Pure TaB_2 phase was not detectable by XRD measurements in the TiB_2 deposits, possible due to the overlapping of diffraction peaks related to the similar lattice structure of TiB_2 and TaB_2 (Fig. 4.4.3). A pure Ta was also not detectable.

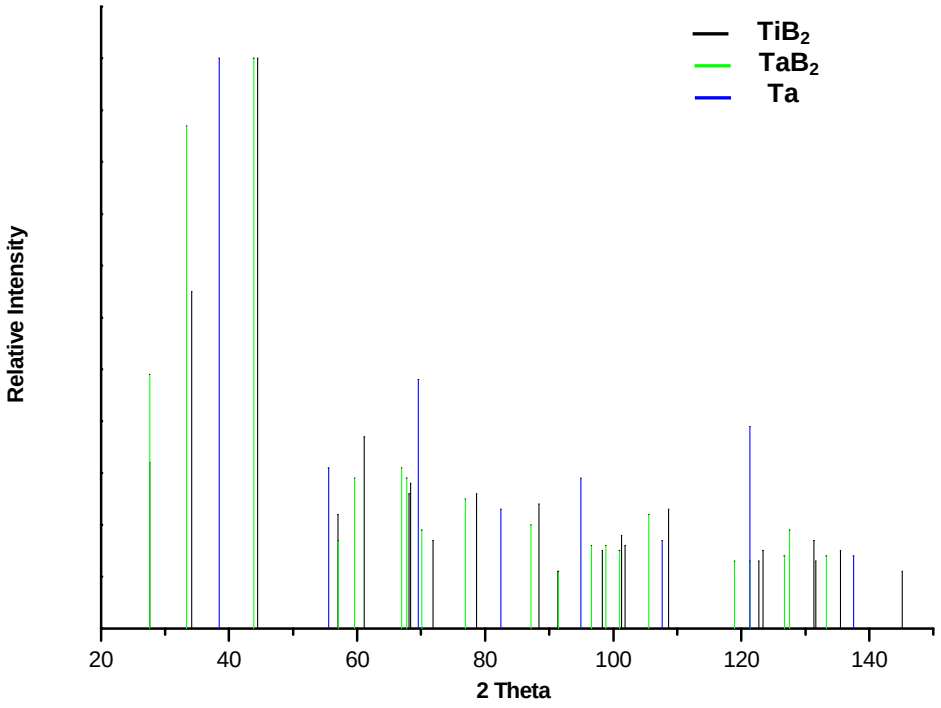

Fig. 4.4.3 X-ray diffraction pattern of the TiB_2, TaB_2 and Ta [123, 124, 133]

However, on the base of the Rietveld refinement of the lattice parameters it can be assumed that some of the lattice positions of Ti are substituted by Ta, forming partly TaB_2 in the TiB_2 deposits. The lattice constants of a pure TiB_2 deposit were a=3.03 Å and c =3.22 Å, which are in good agreement with those mentioned in the literature of a=3.03034 Å and c =3.22953 Å [134]. In the case of the TaB_2 co-deposition, an extension of the lattice parameter a up to 3.074 Å was observed. The *c*-values are ranging within 3.224-3.231 Å. This change in the lattice parameters *a* confirms the above mentioned assumption that the structure of the deposit becomes more similar to TaB_2, having the parameters a= 3.09803 Å and c=3.22660 Å as a pure phase [135].

The EDX analyses indicate values from 0.5 at% up to 10 at% of Ta in the TiB_2 coatings, depending on the points of measurement in the layered structure. Fig. 4.4.4 shows the cross-section (SEM picture, BSE backscattered electrons) of a TiB_2-TaB_2 layer deposited on a Mo substrate. The deposited layer is homogeneous, dense, thick, adherent

and free of pores and cracks. The coating with an even thickness on the substrate forms a columnar type structure. Some fractures, visible in the picture, were caused by the preparation procedure of the cross section of the sample. Due to the thermal expansion coefficient of TaB_2 (5.1×10^{-6} K^{-1}) [121] which is closer to Mo (4.8×10^{-6} K^{-1}) [125] in comparison with TiB_2 (7.8×10^{-6} K^{-1}) [136] and the layers-by-layers structure (Fig. 4.4.4), the TiB_2-TaB_2 deposit exhibits a significantly better adhesion to the substrate than a pure TiB_2 layer (Fig.4.4.5).

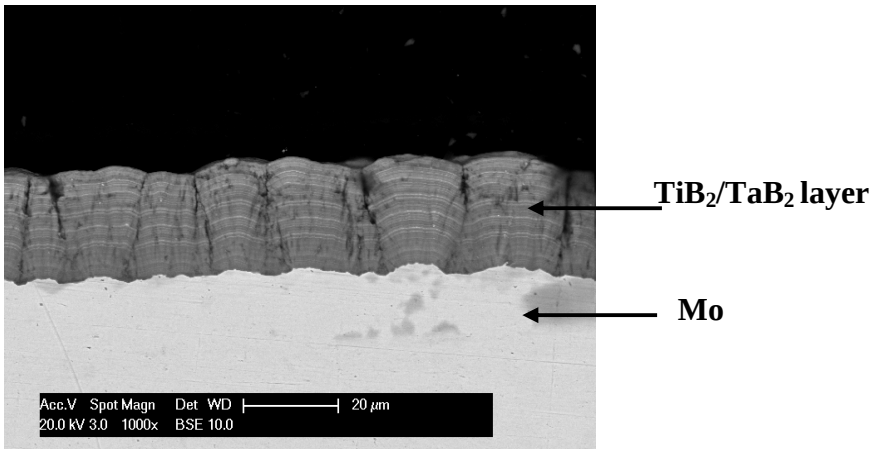

Figure 4.4.4: SEM image (20 kV accelerating voltage, backscattered electrons) of the cross-section of the TiB_2-TaB_2 layer on Mo substrate obtained in PIC mode with the following parameters: ν=55 Hz; T=650ºC; t_{tot}=15 min; i_{aver}=-0.08 A·cm^{-2}, τ_{on}/τ_{off} =2.6

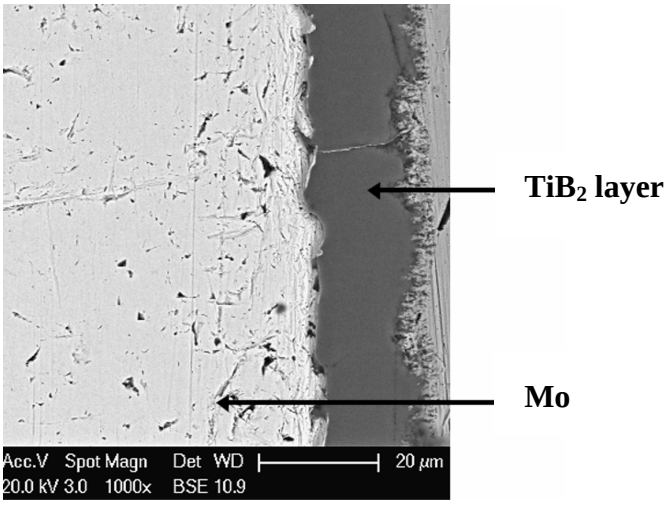

Figure 4.4.5: SEM image (20 kV accelerating voltage, backscattered electrons) of the cross-section of the TiB_2 layer on Mo substrate obtained in PIC mode with the following parameters: ν=55 Hz; T=650ºC; t_{tot}=15 min; i_{aver}=-0.08 A·cm^{-2}, τ_{on}/τ_{off} =2.6

The distribution of TaB_2 throughout the TiB_2 layer is non-uniform. The coating consists of alternating sandwich-like layers exhibiting thickness in the range of 100-1000 nm, and

different intensities of the back scattered electrons, indicating different content of TaB_2 deposited during the oscillating reaction (Fig. 4.4.6). TaB_2 backscatters based on the higher atomic weight of Ta (180.95 $g \cdot mol^{-1}$) compared to the lighter Ti (47.87 $g \cdot mol^{-1}$) significantly more electrons, resulting in features with higher brightness in the BSE-pictures.

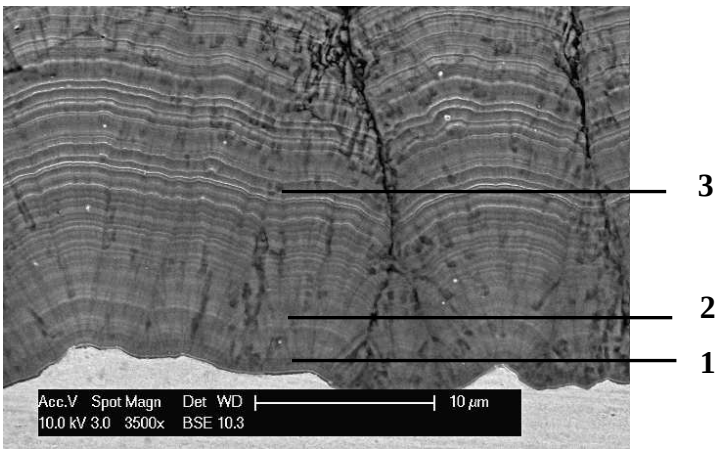

Figure 4.4.6: SEM image (10 kV accelerating voltage, backscattered electrons) of a cross-section of the TiB_2-TaB_2 layer deposited on Mo substrate via PIC mode (for parameters see Fig. 4.61) prepared by ion etching; results of EDX analysis summarized in Table 4.4.2

Table 4.4.2 represents the atomic concentration of elements in the layer in three different regions exhibiting different intensity of the backscattered electrons.

Table 4.4.2: Elemental analysis of the cross section of a TiB_2-TaB_2 coating (positions as indicated in Fig. 4.4.6)

Position in Fig. 4.4.6	Element	At %
1	B	70.3
	Ti	27.3
	Ta	2.4
2	B	68.4
	Ti	28.3
	Ta	3.3
3	B	68.2
	Ti	27.6
	Ta	4.2

The quantity of TaB_2 in the TiB_2 layer increases from an inner region of the deposit to the outer one (Table 4.4.2). The analysis of the layers deposited and cyclic voltammetry measurements allow assuming that at the beginning of the deposition process the forming of TiB_2 layers occurs, and at that time, when all Ti^{3+} (and B^{3+}) species in the diffusion layer at the cathode are reduced, and consumed in the building process of TiB_2, Ta^{n+} complex species are enriched in the interface, reduced and incorporated in the TiB_2 structure. Thus, these two processes alternate each other during the electrodeposition, and as a result, layers with different contents of TaB_2 are generated alternatively at the substrate and oscillating in the composition.

The GDOES analyses demonstrate an overall content of 5-6 at% of Ta in the layer, but due to the restricted depth resolution (it is determined by the sputtering rate), the different composition of the layered structure can not be resolved (Fig. 4.4.7).

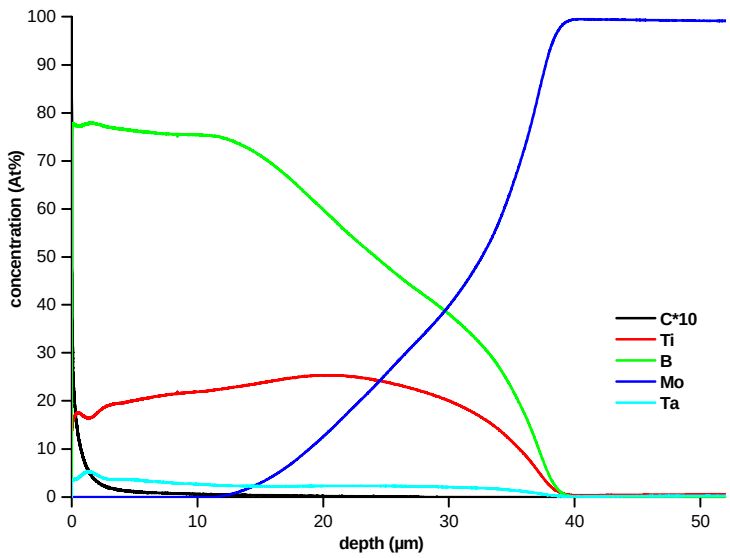

Figure 4.4.7: GDOES analysis of a 30 µm thick TiB_2-TaB_2 coating on Mo substrate obtained via PIC mode with the following parameters: ν=55 Hz; T=650ºC; t_{tot}=15 min; i_{aver}=-0.08 A·cm^{-2}, τ_{on}/τ_{off} =2.6

The coating thickness is approximately 30 µm. Concentration of B decreases closer to the substrate. Interstitial impurities like O_2, H_2 or N_2 were not detectable using this GDOES analysis procedure. Some quantity of C (< 0.5%) is detectable in the outer region of the coating, probably due to reactions of the glassy carbon crucible. An intermediate layer between Mo substrate and TiB_2 coating was not detectable.

4.4.1.3 Surface morphology

The co-deposition of TaB_2 in the TiB_2 layer has not significant influence on the morphology of the layer. In both cases the SEM characterisation of the coatings shows that the layer consists of spherical particles (Fig. 4.4.8).

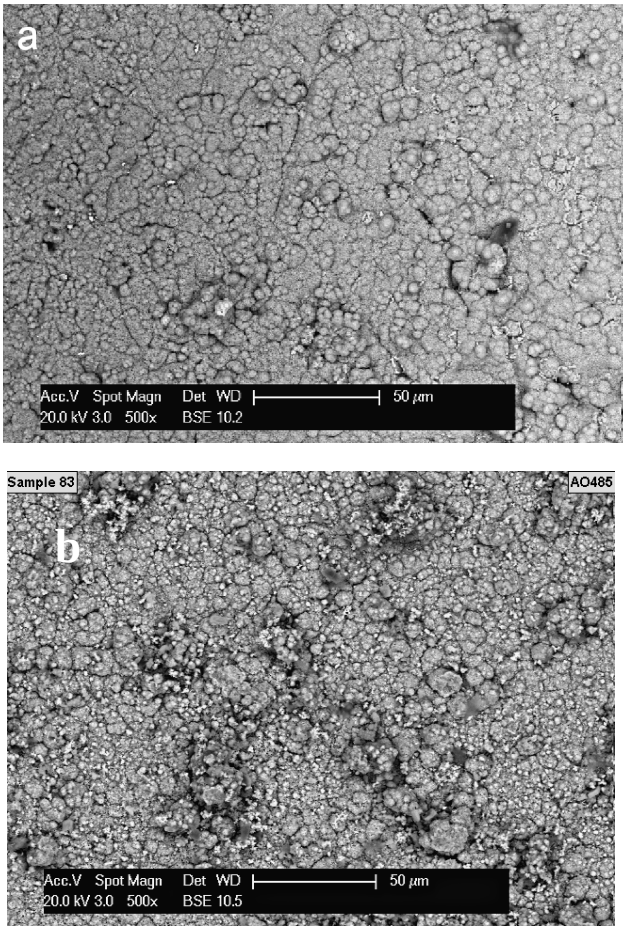

Figure 4.4.8: SEM images of (a) TiB_2-TaB_2 layer and (b) TiB_2 on Mo substrates (20 kV accelerating voltage, backscattered electrons), obtained in PIC mode with the following parameters: ν=55 Hz; T=650ºC; t_{tot}=20 min; i_{aver}=-0.07 A/cm^2,τ_{on}/τ_{off} =0.8

4.4.1.4 Grain size, lattice parameters and thickness of the coatings

The grain size and lattice parameters of the TiB_2-TaB_2 and TiB_2 layers prepared using PIC and PP procedures are summarized in Table 4.4.3.

Table 4.4.3: Crystallite size and cell parameters of the TiB_2-TaB_2 and TiB_2 layer obtained in (a) PIC mode with the following parameters: ν=55 Hz; T=650ºC; t_{tot}=20 min; i_{aver}=-0.07 A/cm^2,τ_{on}/τ_{off} =0.8; (b) pre-pulse plating with the following parameters: ν=55 Hz; T=650ºC; t_{tot}=20 min; i_{aver}=-0.09 A/cm^2,τ_{on}/τ_{off} =2.6

Coating	Mode of deposit	Crystallite size (nm)	Lattice parameter (Å) a	c	Cell volume(Å^3)
a	TiB_2-TaB_2 (Ta 0.25wt%)	53±5	3.04674	3.23136	25.97
a	TiB_2-TaB_2 (Ta 0.6wt%)	10±1	3.0738	3.2109	26.27
a	TiB_2	120±5	3.02896	3.22849	25.65
b	TiB_2-TaB_2 (Ta 0.3wt%)	35±5	3.03735	3.22885	25.79
b	TiB_2	96±5	3.02976	3.22792	25.66
Theoretical values	TiB_2 [134]		3.03034	3.22953	25.7
Theoretical values	TaB_2 [135]		3.09803	3.22660	26.8

Adding of Ta-species to the electrolyte and therefore a TaB_2 co-deposition in the TiB_2 layer leads to the formation of deposits of significantly lower crystallite size (Fig. 4.4.9).

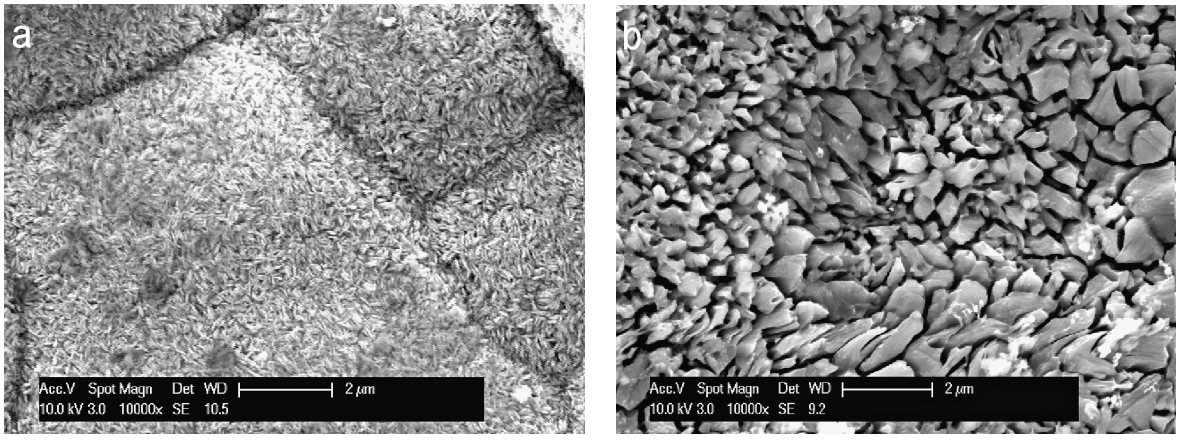

Figure 4.4.9: SEM images of (a) TiB_2-TaB_2 layer and (b) TiB_2 layer on Mo substrates (10 kV accelerating voltage, secondary electrons), obtained in PIC mode with the following parameters: ν=55 Hz; T=650ºC; t_{tot}=20 min; i_{aver}=-0.07 A/cm^2,τ_{on}/τ_{off} =0.8

It is well known that in electrochemical deposition processes the crystallite size depends on two factors: nucleation scan and grain growth scan. If the nucleation rate is faster than the grain growth rate, the grain size will get smaller. The growth mechanism of TiB_2 layer with the TaB_2 co-deposition is not fully understood, but one can suggest that co-deposition of TaB_2 inhibits surface diffusion of ad - atoms toward growth centres, thus promoting nucleation and reduction of the grain size. It can also explain the preferred <001> orientation of TiB_2-TaB_2 coatings which was mentioned above. It is assumed that during the initial electrocrystallization the layer is composed of fine grains with random texture due to the formation of randomly oriented nuclei. As the electrodeposition process continues the coating exhibits the (001) texture due to the non-equilibrium growth based on partial co-deposition of TaB_2 in the TiB_2 layer.

The continuous formation of randomly oriented nuclei and furthermore of small grains leads to the uniform distribution of the layer on the substrate, and as a result, the roughness of TiB_2-TaB_2 coating is significantly lower (Fig. 4.4.10) in comparison with pure TiB_2 layers (Fig. 4.4.11).

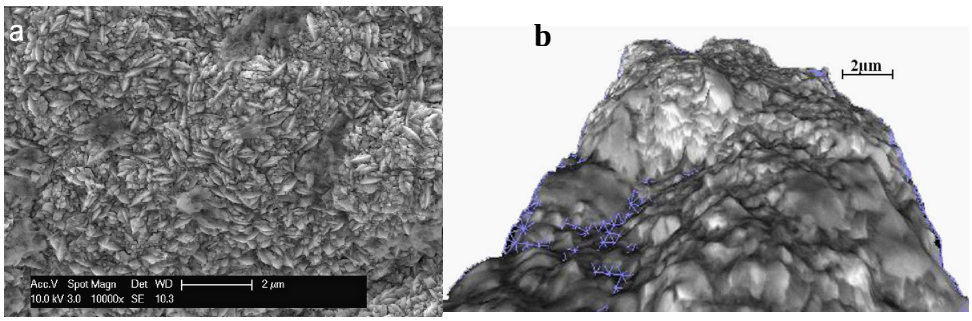

Figure 4.4.10: (a) SEM image and (b) 3D SEM reconstruction of a 32 µm thick TiB_2-TaB_2 layer (Ra=0.2 µm) deposited on Mo substrate (Ra=2.5 µm) (10 kV accelerating voltage, secondary electrons) in PIC mode with the following parameters: ν=55 Hz; T=650ºC; t_{tot}=20 min; i_{aver}=-0.09 A/cm^2,τ_{on}/τ_{off} =0.8

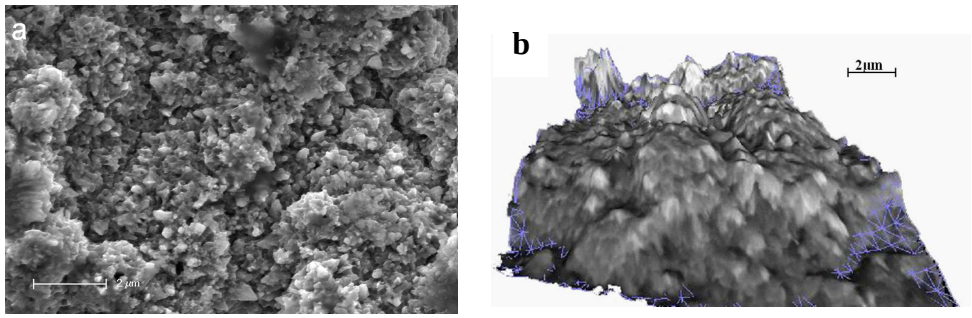

Figure 4.4.11: (a) SEM image and (b) 3D SEM reconstruction of a 25 µm thick TiB_2 layer (Ra=0.4 µm) deposited on Mo substrate (Ra=2.5 µm) (10 kV accelerating voltage, secondary electrons) in PIC mode with the following parameters: ν=55 Hz; T=650ºC; t_{tot}=20 min; i_{aver}=-0.09 A/cm^2,τ_{on}/τ_{off} =0.8

As one can see the nucleation rate is preponderant at the presence of $TaCl_5$ in the electrolyte, i.e. the continuous formation of small grains is observed, leading to a uniform distribution of the electrodeposited layer and as a result to lower roughness of TiB_2-TaB_2 coatings.

At the same average current densities and consumed charges, the TiB_2-TaB_2 coatings are always thicker in comparison with TiB_2 coatings (Table 4.4.4).

Table 4.4.4: Thickness of TiB_2 and TiB_2-TaB_2 layers deposited on Mo substrate at different average current densities (PIC, ν=55 Hz) t_{tot}= 20 min, τ_{on}/τ_{off} =0.8

Coating	Average current density ($A \cdot cm^{-2}$)	Thickness experimental (µm)	Thickness theoretical (µm)
TiB_2	0.06	7	11
TiB_2-TaB_2	0.06	11	11
TiB_2	0.08	14	15
TiB_2-TaB_2	0.08	20	15
TiB_2	0.11	15	21
TiB_2-TaB_2	0.11	22	21

Based on the observations of the quenched electrolytes after the deposition procedure (Fig. 4.4.12) and cyclic voltammetry measurements (Fig. 4.4.13), one can conclude that at the same current densities Ta^{5+} species enhance significantly the charge efficiency of the overall electrochemical reaction and influences via complex forming the equilibrium of the Ti^{4+}/Ti^{3+} complex species. A higher amount of Ti^{3+} species results in a higher amount of Ti complex species at the interface, and therefore in an improved charge efficiency resulting in a higher thickness of the TiB_2-TaB_2 layer.

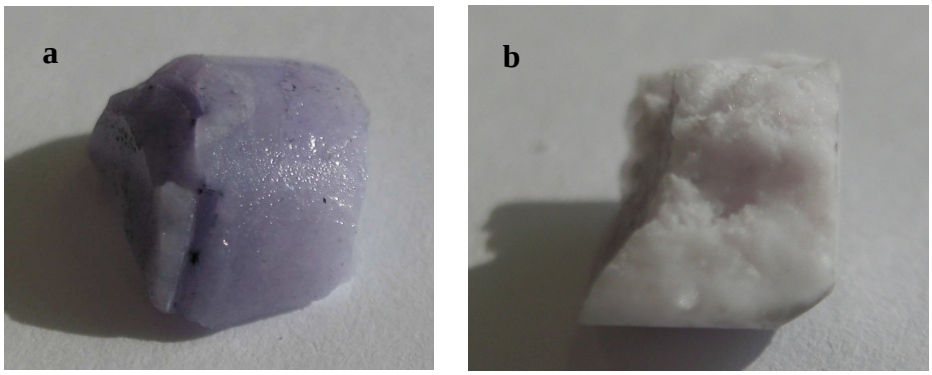

Figure 4.4.12: Optical aspect of the colour of the electrolytes after the electrochemical deposition process (a) FLiNaK-K_2TiF_6-KBF_4-$TaCl_5$ and (b) FLiNaK-K_2TiF_6-KBF_4

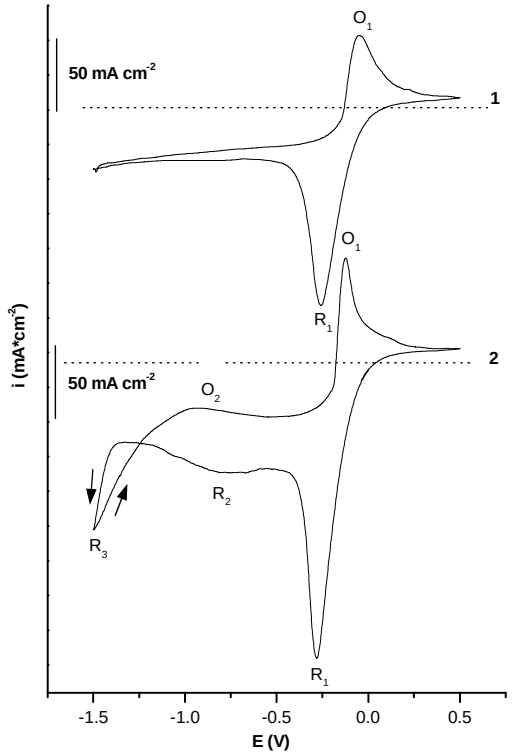

Figure 4.4.13: Cyclic voltammograms in different molten salt systems at 650ºC (WE-Pt wire, A=0.16 cm^2; quasi RE-Pt wire, CE-glassy carbon crucible; scan rate 100 $mV \cdot s^{-1}$). Curve 1: FLiNaK-K_2TiF_6 (3 mol%); Curve 2: FLiNaK-K_2TiF_6 (3 mol%)-$TaCl_5$(0.2 mol%)

One can observe that $TaCl_5$ additive significantly changes the mechanism of the reduction of Ti (IV) species in FLiNaK electrolyte, leading to the change of the mechanism of TiB_2 formation. Based on the results described in chapter 4.2 (Fig. 4.2.8, 4.2.16, 4.2.24) and cyclic voltamogramms (Fig. 4.4.1, curve 1 and 2) it follows, that for reduction of Ti(IV) species to metallic Ti two conditions are necessary: the initial presence of Ti(III) species in the electrolyte (or Ti wire, which initiates the disproportional reaction since increase the quantity of Ti(III) species in the electrolyte) or lower scan rate of CV measurements to accumulate enough quantity of Ti (III) species at the electrode surface for further reduction process (reduction Ti(III) to metallic Ti). Fig. 4.4.13 demonstrates the electrochemical behaviour of Ti(IV) species in the presence of $TaCl_5$ additive in the FLiNaK electrolyte. Beside the reduction peak R_1 at -0.3 V attributed to the Ti(IV) to Ti(III) reduction process, two more additional cathodic peaks are observed. The first one at -0.9 V can be assigned to the reduction of Ta(IV) species to Ta and the second one at -1.5 V - to the formation of Ti_xTa_y alloy. Thus, one can say that the presence of Ta^{5+} species in the electrolyte acts as a catalyst for the reduction of Ti(IV) to Ti(III) species, and more Ti^{3+} species are available at higher cathodic potentials for the reduction reaction Ti^{3+}/Ti^{o}.

In spite of the fact that the values of hardness of TaB_2 (HV=2100) [137] are lower in comparison with TiB_2 (HV=3000) [2], a negative influence of TaB_2 co-deposition in TiB_2 layer on the values of hardness was not observed. The average micro hardness is in the HV=2500-3300 range for all samples. This value is similar with those obtained for TiB_2 coatings without TaB_2 co-deposition. Considering the Hall-Petch correlation [138], this experimental finding can be explained, since hardness increases with a decrease in grain size.

Process of the electrodeposition of TiB_2 coatings from HT molten salts is sufficiently complicated, depending on many factors such as substrate, temperature, mode and density of the applied current. Using the same parameters, the reproducibility of the quality of TiB_2 coatings was not always achieved. The co-deposition of TaB_2 in TiB_2 layer demonstrates the substantial improvements of the properties of TiB_2 coatings, and makes the electrochemical deposition process highly reproducible (Fig. 4.4.14).

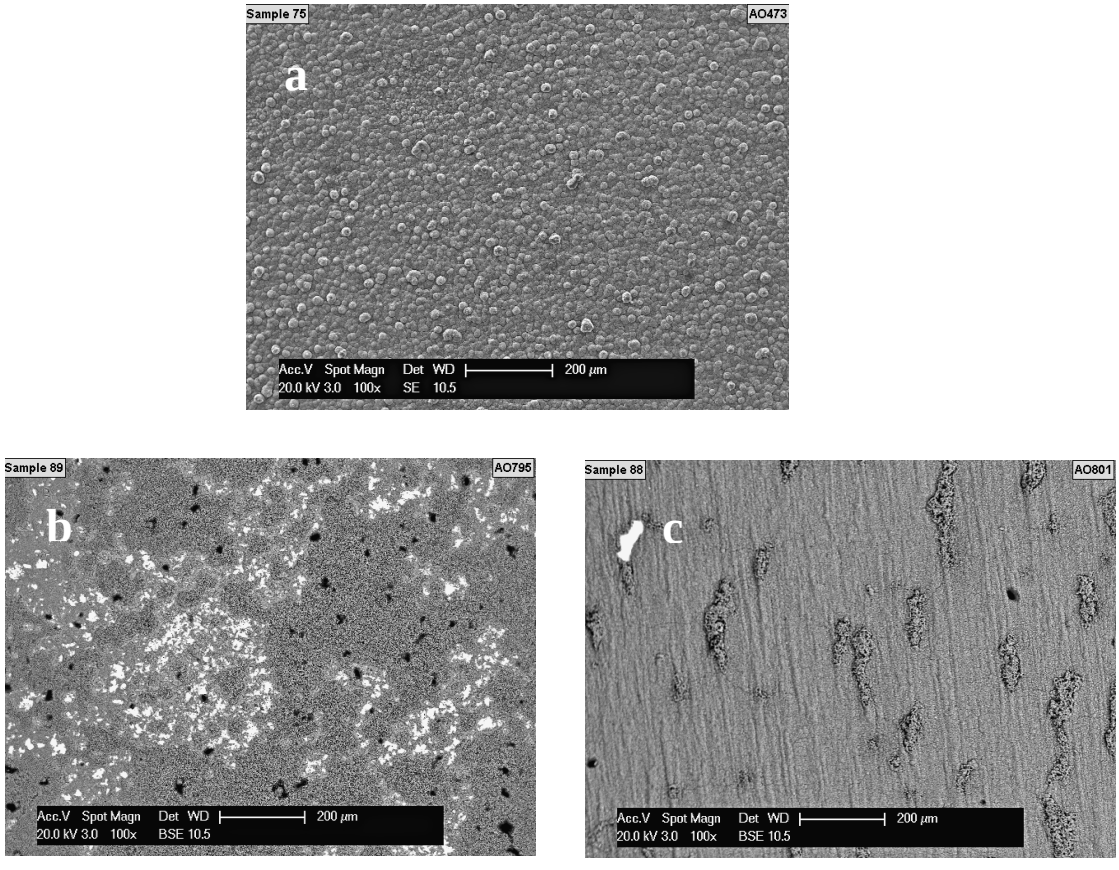

Figure 4.4.14: SEM images of (a) TiB_2-TaB_2 layer (20 kV accelerating voltage, scattered electrons) (b) and (c) TiB_2 layer (20 kV accelerating voltage, backscattered electrons) on Mo substrates obtained in PIC mode with the following parameters: ν=55 Hz; T=650ºC; t_{tot}=20 min; i_{aver}=-0.07 A·cm^{-2};$\tau_{on}/_{off}$ =0.8

As one can see, TiB_2 layers of different quality were obtained under the same parameters out of FLiNaK electrolyte with and without additive of $TaCl_5$. The TiB_2-TaB_2 coating is found to be homogeneous, dense, without cracks and pores in the presence of $TaCl_5$ additive in the electrolyte (Fig. 4.4.14 a). When $TaCl_5$ was not added to the electrolyte, not uniformly layer of TiB_2 was obtained in one case and layer with dendrites was obtained in another case (Fig. 4.4.14 b and c).

4.4.2 Effect of the substrate pre-treatment on morphology, quality and adhesion of the TiB_2 layer

The effect of substrate pre-treatment on morphology, quality and adhesion of the TiB_2 layer was studied. As mentioned in [138] the Mo is one of the most difficult refractory metals to coat with adherent, functionally thick acceptable deposits. The reason of this is that Mo has a thin naturally protective oxide film which reforms quite quickly when exposed to air. Mo has quite large heat of oxide formation (MoO_3 heat of formation=-180 kcal·mol^{-1}) [139], while the higher the negative heat of formation, the higher the affinity for oxygen. The authors have been tried different methods of pre-treatment and improving the adhesion of the substrate, such as pickling in concentrated acids, mechanical roughening, intermediate strike coatings, displacement films, anodic oxidation, heating after plating, plasma etching and non of them got more or less optimal results. They suggest [138] to use augmented energy physical vapour deposition to provide an initial adherent coating and afterwards over this to deposit layers by electrolysis to final thickness. This provides excellent adhesion. In this work it was not possible to use such method. That is why we tried two different surface pre-treatments (pickled and sandblasted) and studied it influence on the quality of the coating.

For the investigation, Mo substrates pre-treated by pickling and sandblasting were used for the deposition TiB_2 layer out of FLiNaK electrolyte at 650ºC. The pulse sequences which were used see in Fig. 3.5 (e and f). The experiment lasted 20 min.

Fig. 4.4.15 demonstrates an optical aspect of the samples covered with TiB_2 layer on different pre-treated substrates.

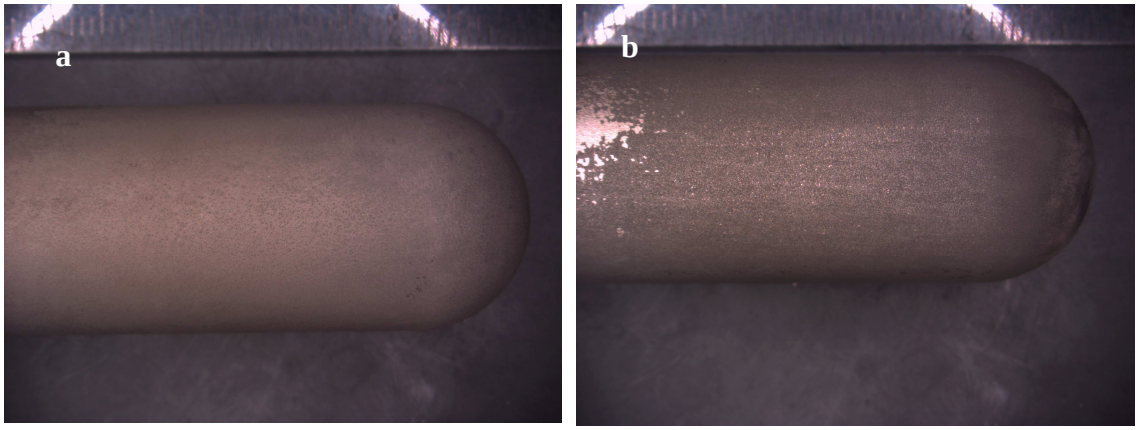

Figure 4.4.15: Optical images of the cylinders coated with TiB_2 (a) sandblasted and (b) pickled substrate

As can be seen in Fig. 4.4.15 (a) the TiB_2 coating on sandblasted substrate is homogeneous, even and dense in comparison with the sample in Fig. 4.4.15 (b), which has uncoated areas because of the loosely adherent. Slight scratching of such sample has removed the coating. Thus, the coating interface adhesion is not strong. The SEM micrographs of the TiB_2 coatings deposited on the different pre-treated substrates and EDX results are shown in Fig. 4.4.16 and Fig. 4.4.17.

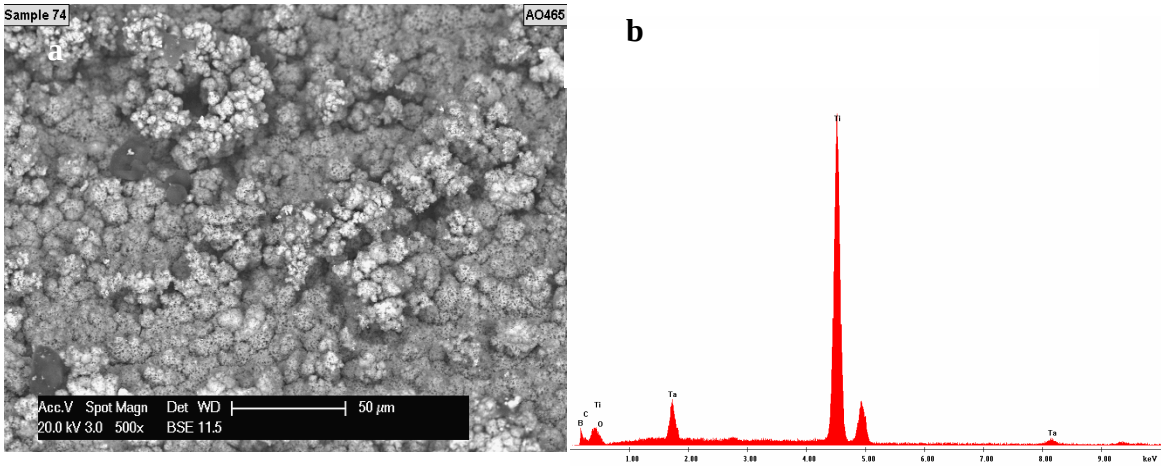

Figure 4.4.16: (a) SEM image (20 kV accelerating voltage, backscattered electrons) and (b) EDX analysis of TiB_2 coating deposited on Mo sandblasted substrate in pulse plating mode with the following parameters: ν=55 Hz; i_1=-0.18 A·cm^{-2}, i_2=-0.09 A·cm^{-2}, t_{tot}=15 min

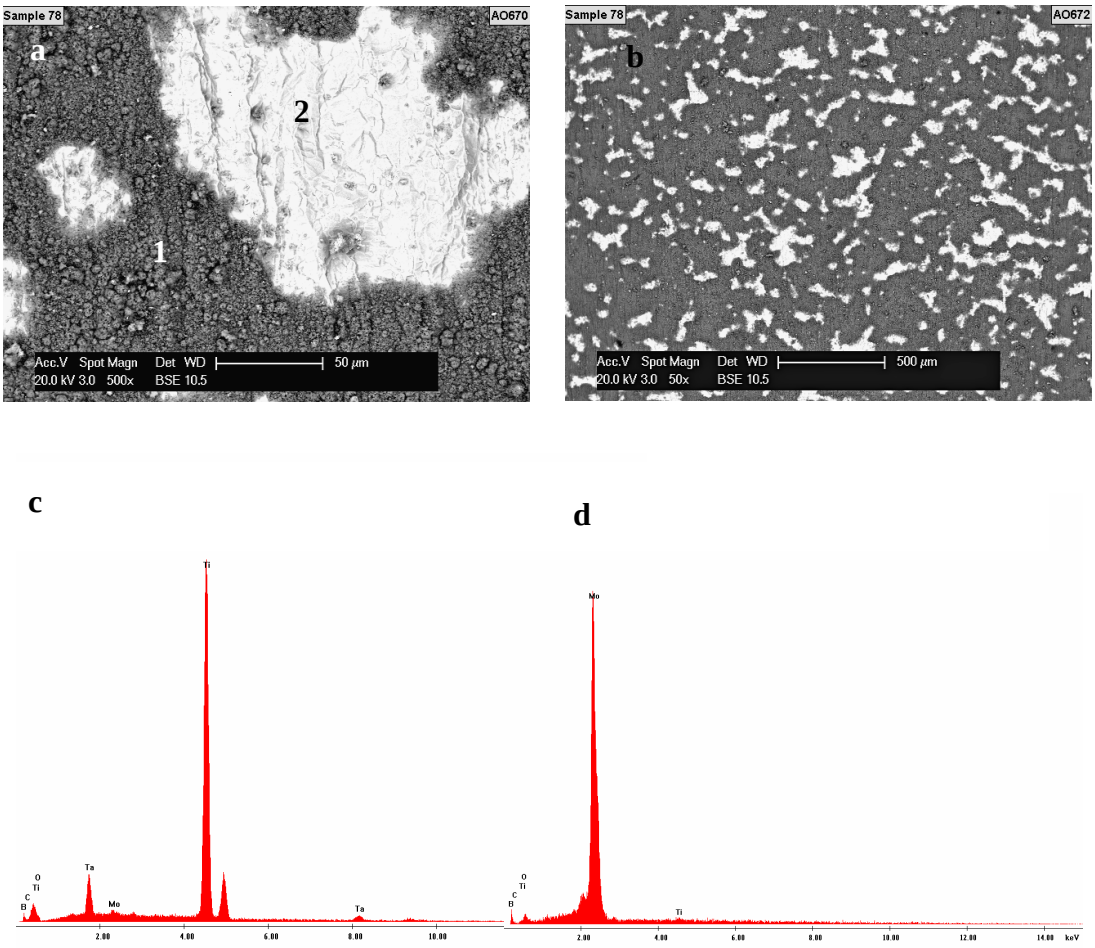

Figure 4.4.17: (a) SEM image (20 kV accelerating voltage, backscattered electrons) (500x), (b) (50x), (c) and (d) EDX analysis of TiB_2 coating deposited on Mo pickled substrate in pulse plating mode with the following parameters: ν=55 Hz; i_1=-0.18 A·cm^{-2}, i_2=-0.09 A·cm^{-2}, t_{tot}=15 min; (c)- point 1 in (a); (d)- point 2 in (a)

One can see in Fig. 4.4.17 (a and b), the Mo substrate was largely exposed with some island deposits scattered on the surface. The weak adhesion of TiB_2 layer on the substrate pre-treated by pickling can also be seen in the results of a simple scotch tape test (Fig. 4.4.18).

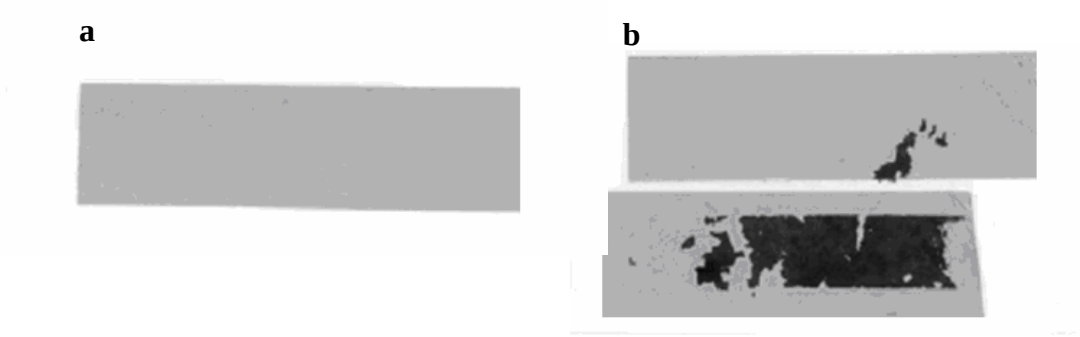

Figure 4.4.18: Scotch tapes after the test (a) sandblasted pre-treatment, (b) pickled pre-treatment

TiB_2 layers coated on sandblasted pre-treated substrate (Fig. 4.4.18 a) exhibits fairly good adhesion; none of the coating was removed by the tape test. In the case of pickled pre-treated substrate (Fig. 4.4.18 b) some part of the coating was removed by the tape test, indicating non-adherent deposition. Better adhesion of the sandblasted substrate in comparison with pickled one can be explained by following: during the mechanical pre-treatment the surface to be coated becomes roughed. Surface roughening forms microgrooves on the substrate which are filled by the coating material, and this mechanical interlocking provides better adhesion.

In addition, using the same parameters the coating of TiB_2 obtained on the sandblasted substrate is denser and thicker (δ=30 µm) in comparison with TiB_2 layer on pickled substrate (δ=20 µm). This is also visible in X-ray diffraction (Fig. 4.4.19).

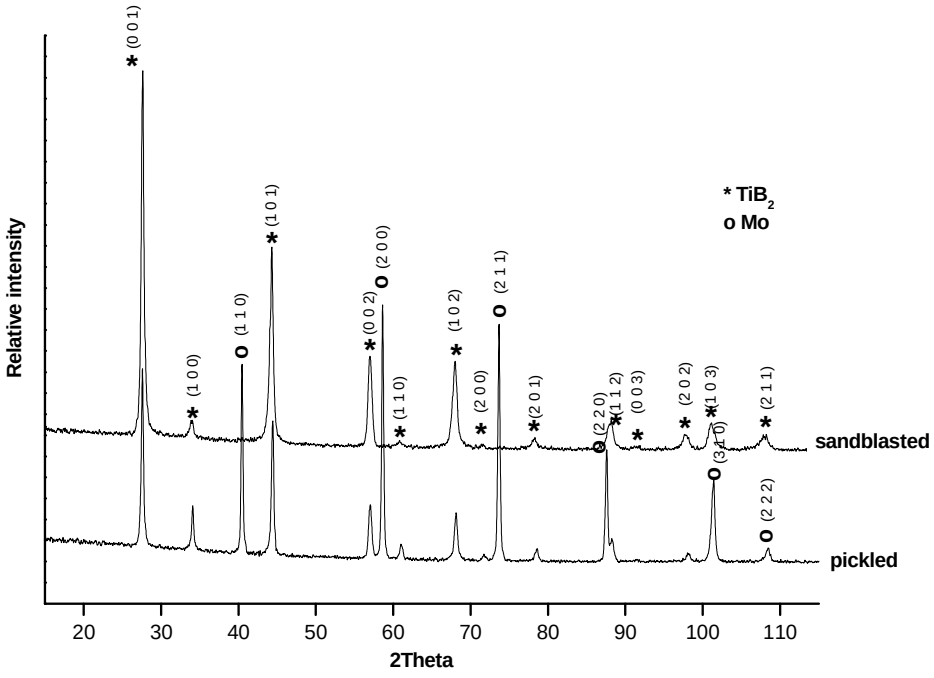

Figure 4.4.19: X-ray diffraction pattern of the TiB_2 (30 µm) coating deposited on the sandblasted pre-treated substrate and TiB_2 (20 µm) coating deposited on the pickled pre-treated out of FLiNaK electrolyte via pre-pulse plating: ν=55 Hz; T=650ºC; t_{tot}=20 min; i_{aver}=-0.08 A/cm^2,τ_{on}/τ_{off} =2.6

As one can observe in Fig. 4.4.19, using the same amount of charge for the deposition some peaks related to Mo substrate were detected by XRD measurements in the sample prepared by pickling pre-treatment. In the sample prepared by sandblasting pre-treatment no reflections attributed to the Mo substrate were detected. This fact can be explained by

different thickness of the layers (TiB_2 (30 µm) coating deposited on the sandblasted pre-treated substrate, and TiB_2 (20 µm) coating deposited on the pickled pre-treated).

The abrasion resistance of TiB_2 coatings plated on pickled and sandblasted pre-treated substrates was analysed by a sand blasting test using corundum grains of 500µm average size at 2.5 bar of pressurized air (Fig. 4.4.20).

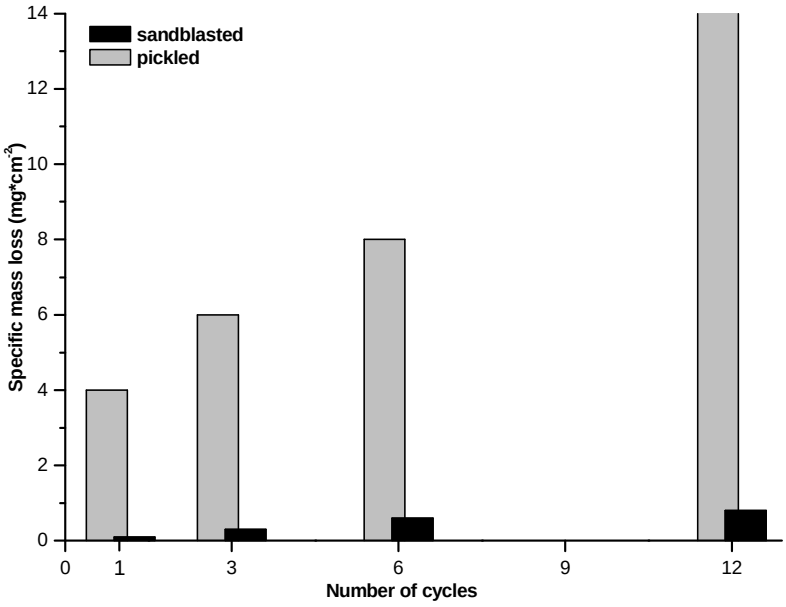

Figure 4.4.20: Specific mass loss values of TiB_2 coatings deposited on sandblasted and pickled substrates

As can be seen from Fig. 4.4.20 the difference on the abrasion resistance among the two types of specimens becomes greater as the number of cycles increases. TiB_2 coating being plated on pickled pre-treated substrate is eroded strongly compared to layer deposited on sandblasted pre-treated surface.

4.4.3 Effect of the temperature on the quality of TiB_2 layer

The working temperature of the process is dependent of the properties of the molten salt bath. At the low end it is limited by the melting point of the eutectic mixture and the high end by the gradual loss of coherence of the deposit once a critical temperature is exceeded.

The electrochemical deposition of TiB_2 coating on the Mo substrate was carried out in the temperature range of 570-700ºC via pulse plating for 20 minutes. It was established that the optimum temperature for the forming continuous, homogeneous layers of TiB_2 is 650±10ºC (Fig. 4.4.21 and 4.4.22).

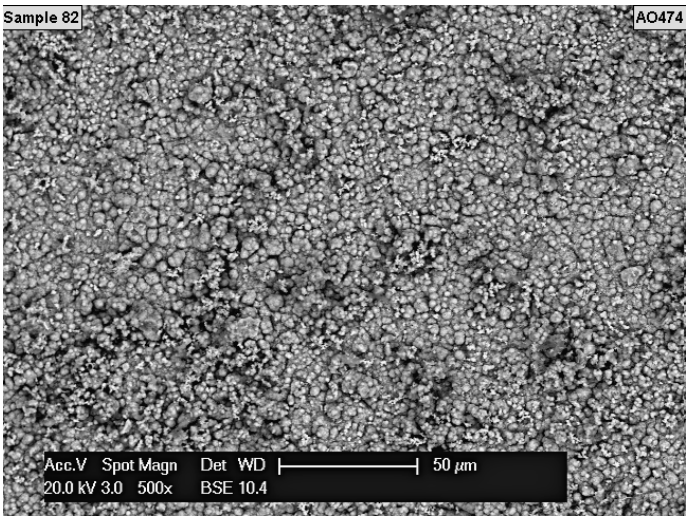

Figure 4.4.21: SEM image of TiB_2 coating (20 kV accelerating voltage, backscattered electrons) deposited on sandblasted substrate in pulse plating mode with the following parameters: ν=55 Hz; i_1=-0.09 A·cm^{-2}, i_2=-0.17 A·cm^{-2}, t_{tot}= 10 min, T=650ºC

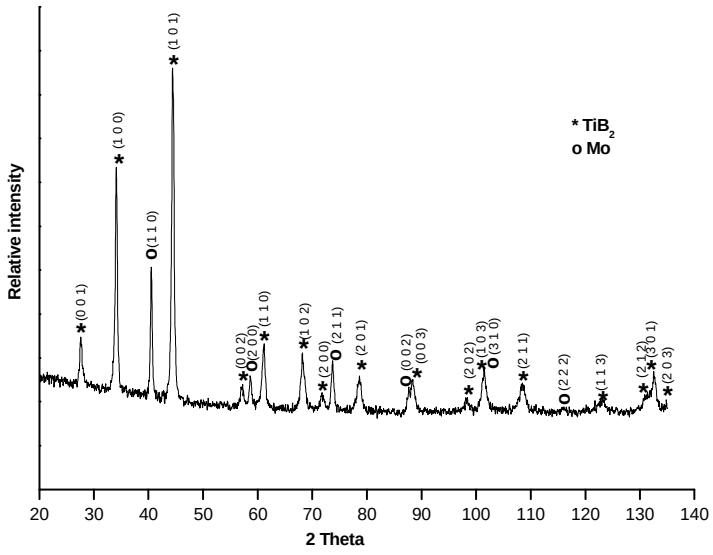

Figure 4.4.22: X-ray diffraction of the TiB_2 coating (for parameters see Fig. 4.4.21)

At the temperature range of 570-600ºC none of the coatings were obtained. Increase the temperature up to 630ºC produces coatings of low quality (Fig. 4.4.23 and 4.4.24). The layers were non continuous and with poor adhesion.

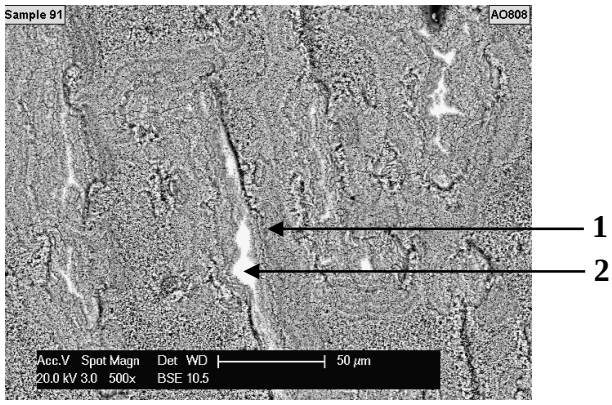

Figure 4.4.23: SEM image of TiB_2 coating (20 kV accelerating voltage, backscattered electrons) deposited on Mo sandblasted substrate in pulse plating mode with the following parameters: ν=55 Hz; i_1=-0.09 A·cm^{-2}, i_2=-0.17 A·cm^{-2}, t_{tot}= 10 min, T=600ºC

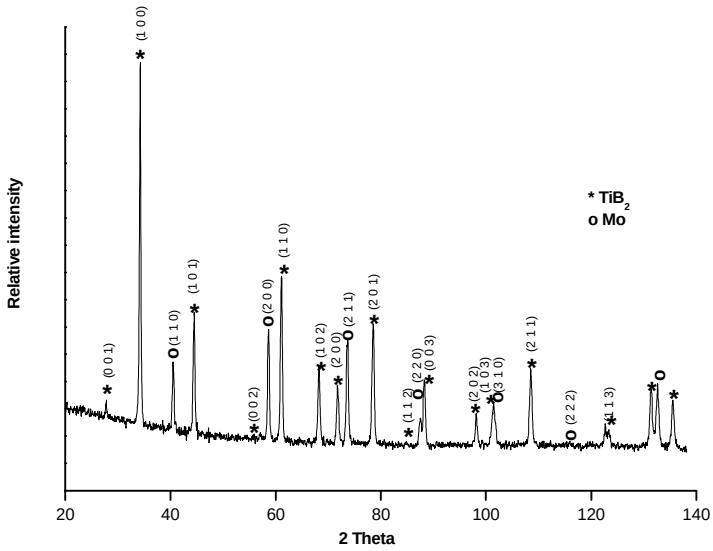

Figure 4.4.24: X-ray diffraction of the TiB_2 coating deposited on sandblasted substrate in pulse plating mode with the following parameters: ν=55 Hz; i_1=-0.09 A·cm^{-2}, i_2=-0.17 A·cm^{-2}, t_{tot}= 10 min, T=630ºC

Table 4.4.5 represents the atomic concentration of elements in the layer in three different stripes.

Table 4.4.5: Elemental analysis of TiB_2 layer

Position in Fig. 4.4.23	Element	At %
1	B	54.8
	Mo	0.5
	Ti	42.9
	O	1.8
2	B	57.8
	Mo	29.9
	Ti	1.3
	O	11.0

Further increase of the temperature up to 700ºC is not expedient as it diminishes the thermal stability of the cell, but do not increase the quality of the TiB_2 coatings.

4.4.5. Effect of the current distribution on the thickness of the layer

The thickness of TiB_2 coatings deposited on Mo plates and Mo cylinders was measured on 4 positions on the samples (Fig. 4.4.25) to reveal the deposition distribution of the layer.

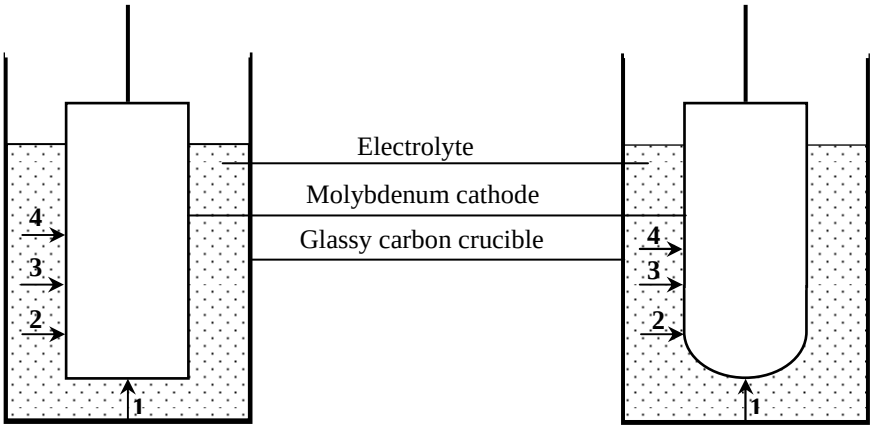

Figure 4.4.25: Sketch of the sample position in the cell

Obtained results about the thickness of the layers are depicted in Fig. 4.4.26.

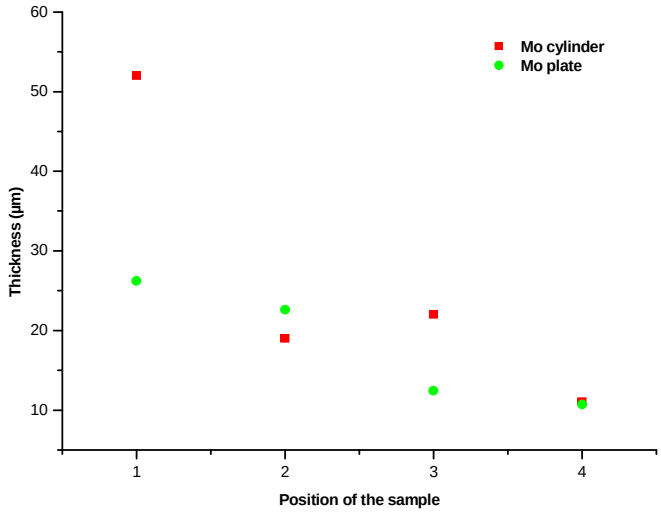

Figure 4.4.26: Thickness distribution of TiB_2 layer deposited on the sandblasted pre-treated Mo samples out of FLiNaK electrolyte via pre-pulse plating: ν=55 Hz; T=650ºC; t_{tot}=20 min; i_{aver}=-0.08 A·cm^{-2},τ_{on}/τ_{off} =2.6

Based on the results illustrated in Fig. 4.4.26, one can say that the deposition distribution depends on the current density distribution. As expected, the current density is higher at the point of the samples closer to the bottom of the crucible, resulting in the higher thickness of the deposits. In addition, the value of the thickness on the edge of the cathode
(Fig. 4.4.25 and 4.4.26, position 1 of the sample) of Mo cylinder two times higher in comparison with Mo plate. It could be explained by the concentration of electrical lines of force at edges and corners on the samples (Fig. 4.4.27), leading to higher current density at these points and resulting at higher thickness.

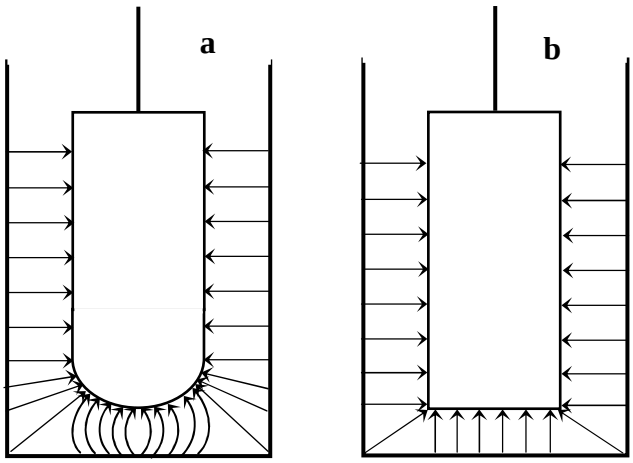

Figure 4.4.27: Primary current density distribution as a function of the electrical field between anode and cathode (a) cathode – Mo cylinder, (b) cathode – Mo plate

4.5 Stability of electroplated titanium diboride coatings in molten aluminum alloy at high temperature

4.5.1 Introduction

It is known, that metals as steel, Mo, W, Ti react easily with molten Al and Al alloys. The usage of these metals in aluminium production, melting and forming industry causes problem with long term stability which could be solved by means of protective coatings with materials resistive to corrosive action of the liquid metal. It is also known that many common materials are unstable when being exposed to liquid oxide melts [140 -142]. Thus, glass industry also demands for efficient protective coating of the tools working in such media. It is believed that the TiB_2 coatings can be used for such purposes. However, its stability in such media was not yet proven experimentally. The wettability of hot pressed TiB_2 substrates containing a different amount of impurities by molten aluminium drops were discussed in [143].

Thus, study of the behaviour of electrochemically plated TiB_2 coatings in molten Al alloy at 720ºC is the aim of this chapter.

4.5.2 Coating process

TiB_2 coatings were electrochemically deposited out of a FLiNaK melt at 650ºC as well as out of a chloride-fluoride melt at 700-710ºC. Electrochemical active additives, a mixture of K_2TiF_6 and KBF_4 in the molar ratio of 1:5, were added to the melts. Molybdenum cylinders (diameter 10 and 30 mm, length 7 cm, area 50 cm^2) were used as substrates. Periodically interrupted (PIC) and periodically reversed (PRC) current modes were used, with the best results being achieved in PRC mode when 1 anodic pulse follows by 5 cathodic ones (Fig. 3.5 b and d). The time of deposition for layers with thickness between 10 and 15 µm ranges between 15-20 min.

Dense, adherent, fine grain sized and homogeneous coatings up to 10 µm thickness were obtained by PIC electrodeposition from FLiNaK electrolyte. Fig. 4.5.1 shows the typical morphology of an electrochemically deposited TiB_2 coating on a Mo substrate.

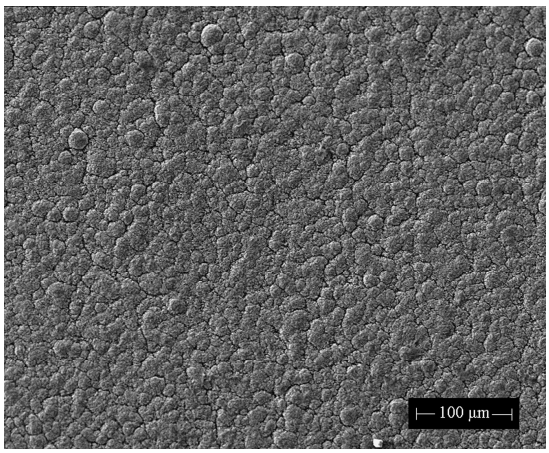

Figure 4.5.1: SEM image of the TiB_2 coating (Ra=820±20 nm) on Mo substrate (Ra=2490±20 nm) (20 kV accelerating voltage, secondary electrons) obtained in PIC mode with the following parameters: t_{dep}=20 min, $-i_1$=0.3 A·cm^{-2}, T=650ºC, τ_1/τ_2=0.8, H=55 Hz

The well crystallized TiB_2 layer exhibits a crystallite size of 25 nm. An XRD measurement of a representative sample is shown in Fig. 4.5.2.

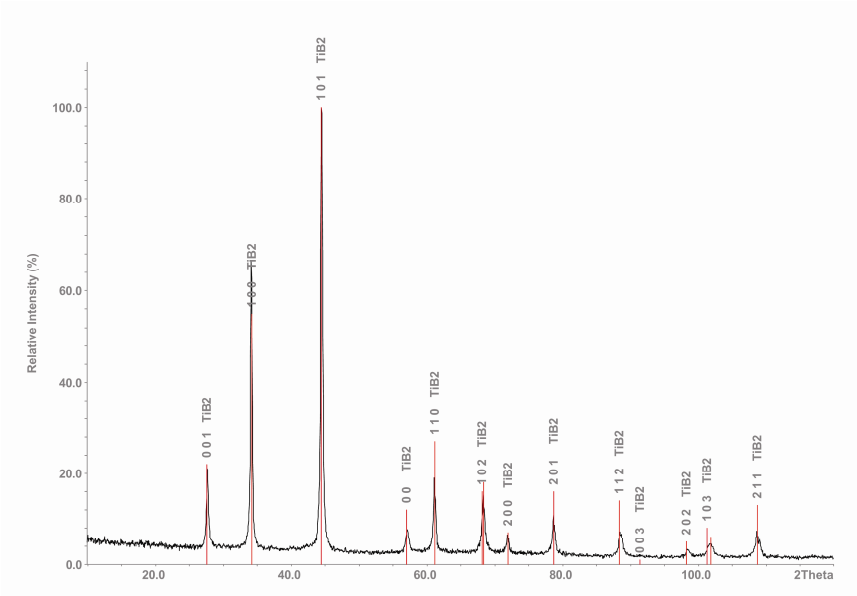

Figure 4.5.2: The X-ray diffraction pattern of TiB_2 coating on Mo substrate out of FLiNaK electrolyte

The TiB_2 phase exhibits a slight (101) texture; no reflections attributed to the Mo substrate were detected. After the electrochemical deposition process the samples were passed to corrosion tests.

4.5.3 Corrosion tests in molten Al alloys

The chemical resistance of the TiB_2 coatings on Mo cylinder was characterized by immersion tests in molten aluminium alloy (AlSi7Mg and Al9Si3Cu) in a furnace at 720ºC at air atmosphere under static conditions. Duration of the test was 168 and 24 hours.

Fig. 4.5.3 demonstrates a visual idea about the behavior of the samples in static test conditions.

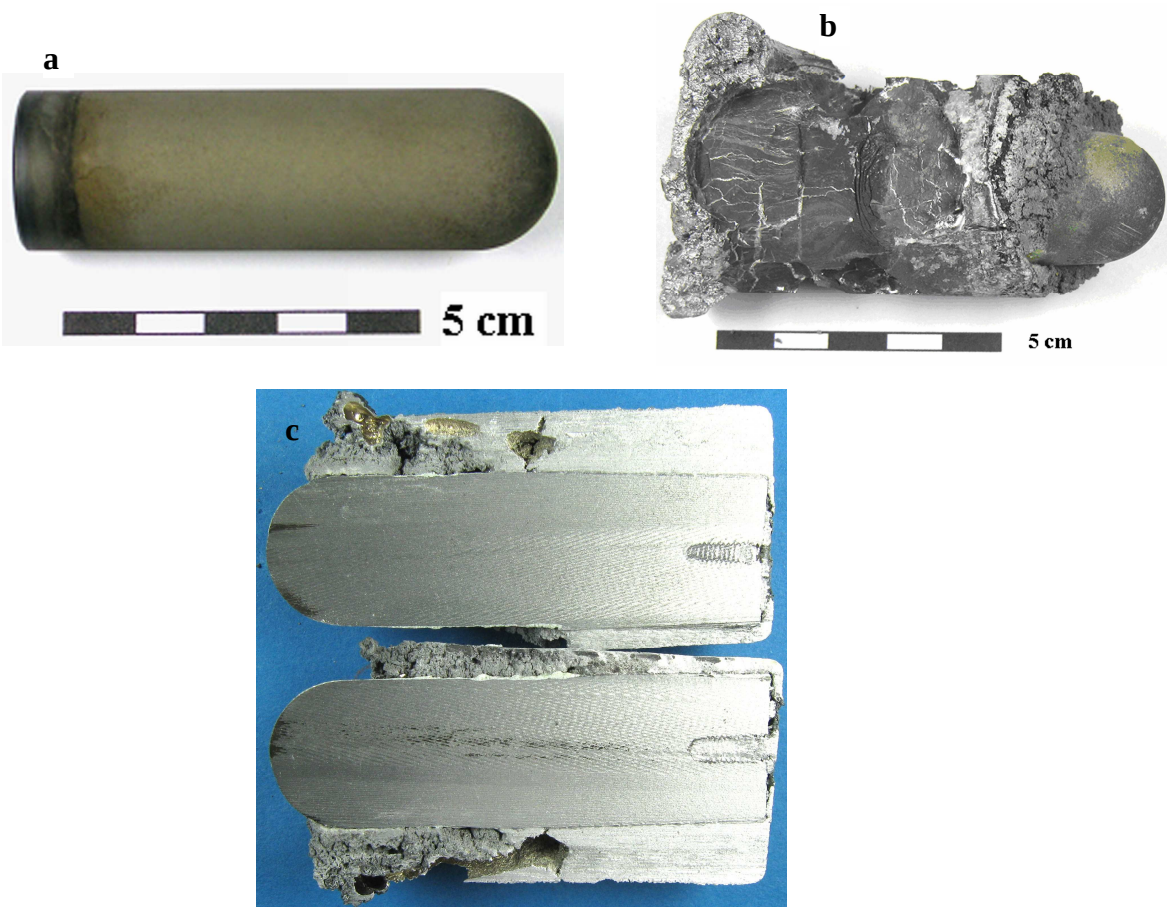

Figure 4.5.3: Optical images of the cylinder (a) before test, (b) after test and (c) longitudinal cut of the cylinder after the test

One can see from the picture (Fig. 4.5.3 c) no changes of the geometric dimensions were detectable.

Comparing the different sections of the cylinder, it can be seen that the coating remains adherent to the substrate on the part inside the melt and oxidizes on the part of the surface exposed to air (Fig. 4.5.4).

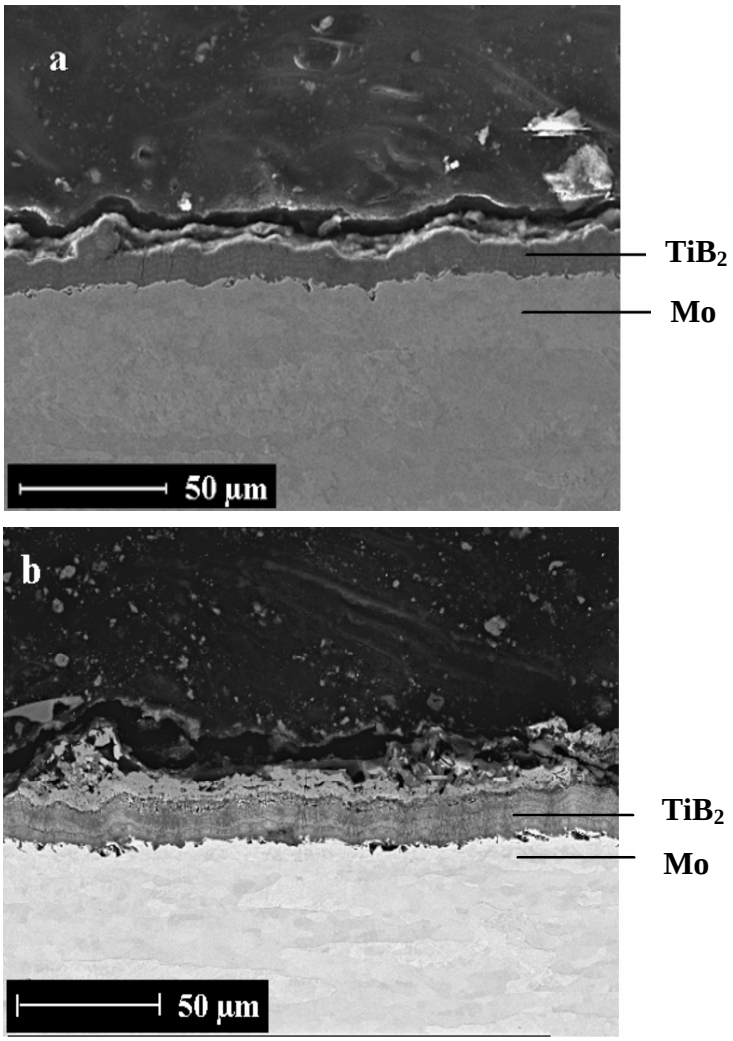

Figure 4.5.4: SEM images of a cross-section of the cylinder (a) part of the cylinder being inside the melt, (b) part of the cylinder being in air after a static corrosion test for 168 hours

Table 4.5.1 represents the EDX measurements of different parts of the cylinder after a static corrosion test.

Table 4.5.1 Elemental analysis of the cross section of TiB_2 coating on different parts of the Mo cylinder after static corrosion test

Part of the cylinder	Element	At %
Inside the melt	B	65.5
	O	2.4
	Si	2.7
	Ti	29.4
At air	B	58.3
	O	20.9
	Mo	0.1
	Ti	20.7

Hence the TiB_2 coating is stable inside the molten metal but is oxidized in air at temperatures above 700°C.

For the better clearness of the stability of TiB_2 layer in Al melt two Mo samples, being exposed to Al9Si3Cu liquid alloy at 720ºC for 24 h, are presented: uncoated (Fig. 4.5.5) and coated with TiB_2 (Fig. 4.5.6).

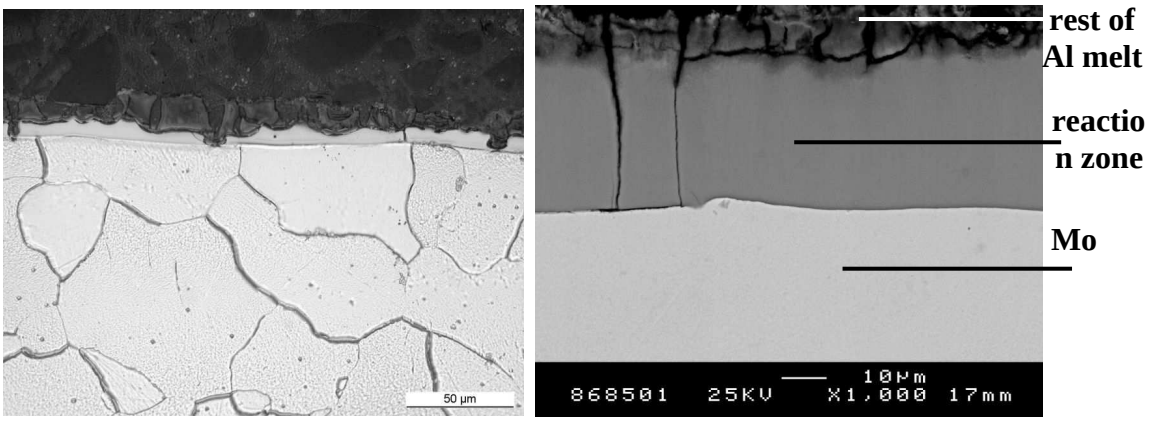

Figure 4.5.5: SEM images of a cross-section of an uncoated Mo cylinder after the static test

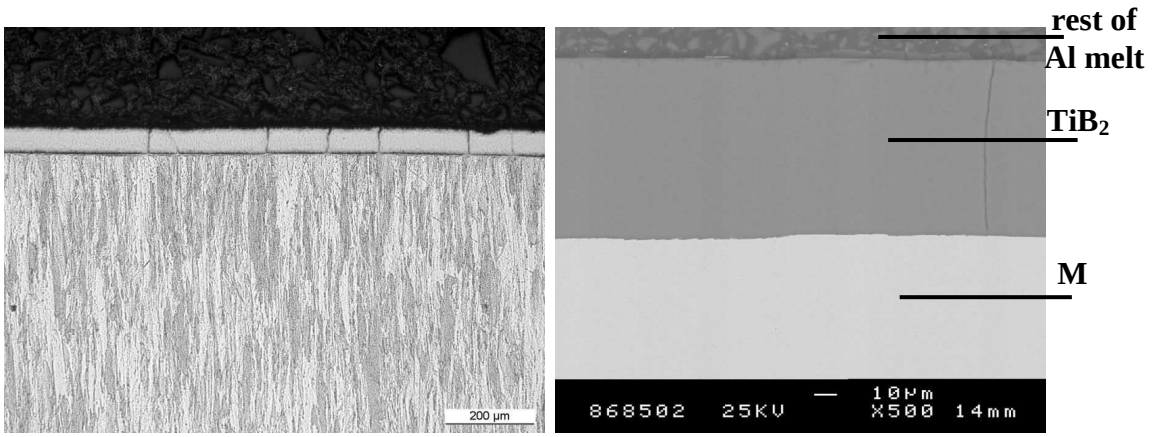

Figure 4.5.6: SEM images of a cross-section of a Mo cylinder coated with TiB_2 after the static test

One can see, as expected, a rather thick zone where the corrosion induced the loss of material is significant on the bare Mo substrates. On the contrary, TiB_2-coated samples show that the TiB_2 layer remains intact and well-adhered to the Mo surface. Thus, the coating is quite stable in molten Al alloy being an efficient protection treatment for Mo substrates.

5. Conclusions

5.1. FLiNaK electrolyte in comparison with other molten fluoride salts possesses the following advantages: high quality of the melt (the procedure of the drying gets lower content of the water), a wide electrochemical potential window, low melting point and temperature of the processes. Obviously, so high melting point of the electrolyte makes difficult for the purification of the initial compounds, resulting in forming oxyfluoride impurities and the decreasing of the electrochemical window of the supporting electrolyte. On the other hand, it can be that alkali metal cation (Li^+) greatly increases the electrochemical stability of the electrolyte in the cathodic regions.

5.2. The electrochemical behaviour of Ti(IV) and B(III) species in FLiNaK electrolyte were characterized by means of cyclic voltammetry in the temperature range of 600 - 700ºC. Based on the experimental data and electroanalysis it was established that the mechanism of the reduction of Ti(IV) species in FLiNaK electrolyte depends on the composition of the electrolyte and temperature of the process. The formation of Ti^0 is possible only at the temperatures ≥ 650ºC and more preferable in the presence of Ti(III) species in the melt. The electroanalysis for the range of the sweep rate 50-600 $mV \cdot sec^{-1}$ at 600-700°C allow us to indicate that the process of the electrochemical reduction of Ti(IV) fluoride complexes to Ti(III) in a FLiNaK electrolyte changes from a quasi-reversible behaviour at 600ºC (at the scan rates of < 600 $mV \cdot sec^{-1}$) to the irreversible process at 700ºC, due to producing an insoluble product on the electrode surface. A study of the electrochemical behavior of Ti(IV) species in FLiNaK electrolyte indicates that only the reduction process of Ti(IV) to Ti(III) species takes place at the temperatures < 650ºC.

In the studied temperature range the electrochemical reduction process of the B (III) species occurs via a single $3e^-$ consumed step. Based on the results of voltammetric studies, it could be assumed that in the temperature range of 600-700°C the change in the mechanism of the reduction of BF_4^- complexes in FLiNaK electrolyte takes place. The reduction process of BF_4^- species is quasi-reversible at low scan rates and temperatures < 650°C and irreversible at high scan rates ≥ 600 $mV \cdot s^{-1}$ and temperatures ≥ 650°C, i.e. it is controlled by the rate of charge transfer.

5.3. Electrodeposition of TiB_2 coatings in molten chloride-fluoride electrolyte (NaCl - KCl – NaF – K_2TiF_6 - KBF_4) at 700ºC was investigated. Pulse plating (PP) techniques in forms of periodically reversed (PRC) and periodically interrupted current (PIC) were applied – instead of traditional direct current (DC) procedure, which was also used for comparison - for the efficient deposition of the coatings onto molybdenum, stainless steel and tungsten carbide substrates with different geometries and surface areas. The effect of current density, frequency and pulse shape on the coatings properties was studied. Pulse plating technique can be usefully applied for coating of Mo, stainless steel and other substrates. In comparison with direct current, pulse plating has shown to improve the quality of the coating with respect to low roughness, and reducing undesirable edge effect that conduce to high residual stress in the layer. The coating with the lowest roughness (Ra=102±5 nm) was obtained by PRC pulse plating. The values of microhardness were in the range of 1800-2400 MPa depending on the pulse frequency in PIC electrolysis. The residual stresses are related to the frequency of deposition and vary in the range of -0.7 GPa to -1.3 GPa, being the minimum at pulse frequency of 20 and 100 Hz. The time for deposition of a 10 µm thick layer ranges between 10 and 20 min, depending on the method used. The best results were obtained with pulse reverse current (PRC) plating, though the pulse interrupted current (PIC) shows also very good results in many cases.

Plating conditions (pulse shape, sequence and frequency) were found to deposit TiB_2 smooth coating with low compressive stress and good wear resistance. Such coatings can be used for manufacturing cutting tools; especially those working in high temperature corrosive environment.

5.4. The additive of $TaCl_5$ in FLiNaK electrolyte influences positive on the electrochemical deposition process of TiB_2 and the properties of the layer.

- TiB_2-TaB_2 coatings of high quality were obtained in the presence of $TaCl_5$ additive in FLiNaK electrolyte at 650ºC via pulsed current plating.
- Cyclic voltammetry measurements and analysis of the coatings show the possibility of co-deposition of TiB_2-TaB_2 compounds in the same potential range in form of alternative layers due to the competitive alternative processes at the electrode, following each other during the electrochemical reduction.
- Due to incorporation of the TaB_2 in TiB_2 and the established layered structure a better matching to the thermal expansion coefficient was achieved, resulting in a better adhesion of the coating to the substrate. The process of the electrodeposition

of TiB_2 coatings from high temperature molten salts is sufficiently complicated, depending on many factors e.g., substrate, electrolyte composition, temperature, current mode and current density applied. Using the same parameters, reproducibility in the quality of TiB_2 coatings was not always achieved. Adding $TaCl_5$ to the molten salt electrolyte improves the process of TiB_2 electrodeposition successfully, making process highly reproducible and improving the properties of the coatings with respect to roughness, adhesion and grain size.

5.5. Among the two pre-treatment methods (pickling and sandblasting), the last one is more effective to obtain the coatings of high quality. Coatings deposited on the sandblasted substrates have better adhesion strength compared to that deposited on the pickled substrates.

5.6. The optimal temperature for the deposition of TiB_2 coatings of high quality was found to be 650°C. Based on the cyclic voltammograms and electrochemical deposition experiments it was indicated that forming of TiB_2 layers take place in the temperature range of 600-630ºC, but the diffusion rate of Mo into TiB_2 was not sufficiently rapid to effect a good bond. An increase of the temperature over 650ºC is not expedient due to the decrease of the thermal stability of the cell and deterioration of the conditions of forming TiB_2 layer.

5.7. The corrosion behaviour of molybdenum material, protected by electrochemically plated TiB_2 coatings, has been studied by static tests. The Mo cylinders, both coated and uncoated, were immersed in liquid aluminium alloys (AlSi7Mg and Al9Si3Cu) at air at 720ºC for 168 and 24 hours. The investigations showed that the TiB_2 coatings effectively protect Mo surface against corrosion in molten Al alloys media. No changes of the geometric dimensions were detectable. No visible traces of corrosion were detected on the liquid metal – TiB_2 interface in corrosion tests in static conditions. Hence the TiB_2 coating is stable inside the molten metal but is oxidized in air at temperatures above 700ºC.

Literature index

1. G. Samsonov, *Plenum Press Handbooks of High Temperature Materials*, Plenum Press, New York (1964)
2. R. Telle, L. Sigl, K. Takagi, in *Handbook of ceramic materials*, R. Riedel (Ed.) V.2, Wiley-VCH, Weinheim (2000)
3. M. Berger, E. Coronel, E. Olsson, *Surface & Coatings Technology*, 185 (2004) 240
4. K. Seitz, S. Sussbrich, M. Hornung, H. Kuhn, F. Hiltman, *U.S. Patent* No.6,645,568 B1, (2003)
5. V. Shapoval, V. Malyshev, I. Novoselova, K. Kushkhov, *Usp.Khim*., 64:2 (1995) 133
6. V. Gurin, *Usp.Khim*., 41:4 (1972) 616
7. M. Makyta, K. Matiasovsky, V. Taranenko, *Electrochim. Acta*, 34 (1989) 861.
8. M. Makyta and T. Utigard, *Light metals* (1993), TMS, Denver, 1137
9. V. Malyshev, I. Noveselova, V. Shapoval, *Zh. Prikl. Khim*., 69:8 (1996) 1233
10. F. Lantelme, A. Barhoun, Ei. M. Zahidi, J. H. von Barner, *Plasmas & Ions*, 2 (1999) 133
11. V. Taranenko, I. Zarutskii, V. Shapoval, M Makyta and K. Matiašovský, *Electrochim. Acta*, 37 (1992) 263
12. M. F. Souto, J. Sytchev, A. Köpf, R. Krendelsberger, G. E. Nauer, G. Kaptay, in Molten Salts XIII, H. C. Delong, R. W. Brandshaw, M. Matsunaga, G. R. Stafford, P. Trulove, Editors, PV 2002-19, p.857, *The Electrochemical Society Proceedings Series*, Pennington, USA (2002)
13. G. Ett and E. J. Pessine, *Electrochim. Acta*, 44 (1999) 2859
14. H.-P. Martinz, M. Sulik, M. Kathrein, G. E. Nauer, R. Krendelsberger, A. Pascual, G. Winkler, *Plansee Berichte*, HM77, (2005) 1029
15. J. Li and B. Li, *Materials Letters*, 61:25 (2007) 4711
16. J. Li, B. Li, L. Jiang, Zh. Dong, Y. Ye, *Rare Metals*, 25: 2 (2006) 111
17. N. Rybakova, M. Souto, H.-P. Martinz, Y. Andriyko, W. Artner, J. Godinho, G.E. Nauer, *Corrosion Science*, 51 (2009) 1315
18. N. Rybakova, M. Souto, Y. Andriyko, W. Artner, J. Godinho, G. E. Nauer, *J. Electrochem. Soc.*, 156:4 (2009) 131
19. V. Malyshev, H. Kushkhov, V. Shapoval, *J. Appl. Electrochemistry* 32 (2002) 573

20. V. Malyshev, *Protection of Metals*, 40:6 (2004) 525
21. L. E. Toth, *Transition Metal Carbides and Nitrides*, Refractory Materials, Vol 7, Margrave JL (Ed.). Academic Press: New York, (1971) 5-11
22. N. B. Dahotre, P. Kadolkar, S. Shah, *Surf. Interface Anal*., 31 (2001) 659
23. H. Goldschmidt, *Interstitial Alloys*. Plenum Press: New York (1967), 289–292, 337–340
24. D. Buell, C. Suryanarayana, D. Williamson, J. Moore, J. Disam, in *Elevated Temperature Coatings: Science and Technology III*, J. Hampikian, N. Dahotre (Eds), TMS, Warrendale, PA (1999), 361-370
25. A. Alexious, S. Shanmugam, J. Hampikian, in: *Elevated Temperature Coatings: Science and Technology III*, J. Hampikian, N. Dahotre (Eds). TMS:Warrendale, PA (1999), 330–331
26. R. Rowe, *Adv. Mater. Process*, 33 (1992) 150
27. R. Streiff, in: *Elevated Temperature Coatings: Science and Technology II*, N. Dahotre, J. Hampikian (Eds). TMS: Warrendale, PA (1996) 407
28. J. Murray, P. Liao, K. Spear, *Alloy Phase Diagram*, 7 (1986) 550
29. E. Rudy, S. Windisch, *Ternary Phase Equilibria in Transition Metal-Boron-Carbon-Silicon Systems*, Part I, V. VII, Technical Report N. AFML-TR-65-2, Wright Patterson Air Force Base, OH, USA, (1966)
30. W. B. Pearson, *The Crystal Chemistry and Physics of Metals and Alloys*, Wiley-Interscience, New York, (1972)
31. R. Cutler, *Engineering Material Handbook: Ceramic and Glasses*, Vol. 4, ASM International: Metals Park, OH, (1995), 787
32. A. Agarwal, N. Dahotre, in: *Elevated Temperature Coatings: Science and Technology III*, J. Hampikian, N. Dahotre (Eds), The Metallurgical Society of AIME, Warrendale, PA (1999)
33. G. Samsonov, T. Serebryakova, V. Neronov, *Boridy*, Atomizdat, (1975)
34. H. Oye, M. Sorlie, *Aluminum*, 2 (1994) 147
35. H. Wendt, K. Reuhl, *Aluminium, 7* (1985) 518
36. C. Ransley, *J. Metal*, 14 (1982) 129
37. C. Marvin, P. Wendelin, *Nucl. Sci. Abstr*., 22 (1968) 14
38. I. Campbell, C. Powell, D. Nowicki, H. Gonser, *J. Electrochemical. Soc*., 96 (1949) 318
39. A. McDonald Howard, R. Synder, *US Patent No*.3524543 (1970)

40. Kawecki Chemical Co., *Brit. Patent No*. 3508977 (1970)
41. D. S. Rickerby, A. Matthews, *Advanced surface Coatings – A Handbook of surface Engineering*, Blackie and Sons, London (1991)
42. K. Holmberg, A. Matthews, *Coatings Tribology: Properties, Mechanisms, Techniques and Applications in Surface Engineering, 56*, Elsevier, Amsterdam, The Netherlands, (2009) 560
43. Rointan F. Bunshah, in *Handbook of Hard Coatings: deposition technologies, properties and applications*, Rointan F. Bunshah (Ed), Noyes Publications (2001), 60
44. Rointan F. Bunshah, *in Handbook of Deposition Technologies for Films and Coatings*, 2nd Ed.: Science, Applications and Technology, Rointan F. Bunshah (Ed), Noyes Publications (1994) 134
45. M. Boulos, P. Fauchais, A. Vardelle and E. Pfender in *Plasma spraying: theory and applications*, R. Suryanarayanan (Ed.), 1993
46. D. Inman, D. Williams, *Future prospects for electrodepositing metals from high temperature inorganic melts*, Proceedings: Electrochemistry Symposium: The past, present and future, Plenum Press, New York (1977)
47. K. Spear, P. McDowell, F. McMahon, *J. Am. Ceram. Soc.*, 69 (1989) C4
48. S. Kuznetsov, *Journal of Electrochemistry*, 35:11 (1999), 1144
49. A. N. Baraboshkin, *Electrocrystallization from Molten Salts*, Moscow: Nauka (1976)
50. H. Kushkov, V. Shapoval, S. Devytkin, *Electrochemistry*, 57 (1991), 8 (in Russian)
51. H. Wendt, K. Reuhl, V. Schwarz, *Electrochim. Acta*, 37 (1992) 237
52. J. L. Andrieux, G. Weiss, *Mémoires présentés a la société chimique* (1948) 598.
53. J. L. Andrieux, *Ann. Chim*., 12 (1929) 423
54. J. L. Andrieux, *Thesis*, University of Paris (1929)
55. G. Meerson, M. Smirnov, *Khim. Redkih Elementov*, Akad. Nauk SSSR Inst. Obschei I Neorg. Khim, 2 (1995), 130-147
56. D. Stern, Q. McKenna, *USA Pat.* 2936268 (1960)
57. H. P. Nies, C. Morgen, G. Jones, *Brit. Patent* 861743 (1961)
58. D. Schlain, F.X. McCawley, C. Wyche, *J. Electrochemical Soc*., 116 (1969) 1227
59. A. Ganesan, V. Aravamuthan, M. Sundaram, R. Gangadharan, *Indian Chem. Journal*, (1972) 37

60. J. Gomes, K. Uchida, M.M. Wong, *Report Invest. No. 8053 of the US Bureau of Mines* (1975)
61. H. Giess, *German Pat.*, 2214633 (1972)
62. J.D. Kellner, *US Pat.* 3880729 (1975), C1. 204-39, C23b
63. M. Matiasovsky, K. Grjotheim, M. Makyta, *Metall* 42 (1988) 1196
64. H. Wendt, K. Reuhl, V. Schwarz, *J Appl. Electrochem*., 22 (1992) 161
65. V. Taranenko, V. Bidenko, I. Zarutskii, S. Devyatkin, *High-temperature electrochemical synthesis of borides of elements of the VI-A group in ionic melts*, in: Borides [in Russian], Institute for Problems of Materials Science, Kiev (1990) 55-61
66. M. Makyta, V. Danek, G.H. Haarberg, J. Thonstad, *J. Appl. Electrochem*., 26 (1996) 319
67. Shapoval V.I., Kaptay G., Deviatkin S.V. *High-Temperature Electrochemical Synthesis of Intermetallides of Titanium in Molten Salts* - published as Chapter 18 of the book: "Electrochemical Technology: Innovation and New Developments", N.Masuko, T.Osaka, and Y.Ito (Eds.); copublished by Kodanscha Ltd and Gordon and Breach Science Publishers S.A. (1996) 361-378
68. T. Yamamoto, T. Takenaka, M. Kawakami, *Materials Transactions*, JIM 37:3 (1996) 363-366
69. G. Ett, E.J. Pessine, *Plat. Surf. Finish.*, 87 (2000) 118
70. B. Tury, J. Sytchev, G. Kaptay, Morphology of titanium diboride obtained by electrochemical synthesis from molten chloro-fluoride melt – High temperature material processes 3 (1999) 117-126
71. U. Fastner, T. Steck, A. Pascual, G. Fafilek, G. E. Nauer, *Journal of Alloys and Compounds*, 452:1 (2008) 32-35
72. R.Krendelsberger, A.Pascual, M.F.Souto, J.Sytchev, G.E.Nauer, G.Kaptay: *Textures of TiB_2 coatings from molten salts* – Proc. of Int. Symp. on Ionic Liquids in Honour of Marcelle Gaune-Escard, France, 26-28 June (2003) 95-103
73. S. Devyatkin, G. Kaptay, V. Shapoval, I. Zarutskii, V. Lugovoi, S. Kuznetsov: *Deposition of Titanium, Zirconium and Hafnium Diboride Coatings by High-Temperature Electrochemical Synthesis from Chloro-Fluoride Melts* - in Refractory Metals in Molten Salts, ed. by D. Kerridge and E. Polyakov, Kluwer Academic Publishers, Netherlands (1998) 73-80

74. V. Shapoval, I. Zarutskii, V. Malyshev, N. Uskova, *Russian Chemical Reviews*, 11 (1999) 925-936
75. J.-C. Poignet, J. Fouletier, in: Materials Issues for Generation IV Systems, V. Ghetta, D. Gorse, D. Maziére, V. Pontikis (Ed.), Corsica, France (2007) 523-524
76. Kurt H. Stern, in: *Metallurgical and Ceramic Protective Coatings*, Kurt H. Stern (Ed.), Chapman and Hall, London (*1996*) 14
77. I. Galasiu, R. Galasiu, J. Thonstand, in *Nonaqueous electrochemistry*, D. Aurbach, (Ed.), Marcel Dekker, New York (1999) 461
78. C. K. Gupta, *Extractive metallurgy of molybdenum*, CRC Press, Boca Raton, Florida, (1992)
79. W. Powers, S. Cohem, N. Greene, *Nucl, Sci. Eng.*, 71 (1963) 200
80. D. Flin, F. McCawley, G. Smith., *US Bureau of Mines*, Report. Invest. 8332 (1979)
81. F. McCawley, C. Wynche, D. Shlain, *Pat. USA* 3713993 (1969)
82. F. McCawley, C. Wynche, D. Shlain, *Pat. USA* 3827954 (1968)
83. D. Schlain, E. McCawley, G. Smith, *Electrodeposition of titanium diboride coating*, Rep. Invest. No.8140, US Department of Interior, Bureau of Mines, Washington DC, 20240, (1976) 1-22
84. J. Gomes, K. Uchida, *Pat. USA* 3775271 (1972)
85. S. Devyatkin, G. Kaptay, E. Berecz, in: *Proc. Molten Salts*, Electrochem. Soc. Inc., N.Y.(1994) V.94-13, 584
86. S. Devyatkin, G. Kaptay, J-C. Poignet, J. Bouteillon, *Molten Salts Forum* 5-6 (1998) 331
87. I. Zarutskiy, V. Malishev, V. Shapoval, *Zh. Prikl. Khim*., 70 (1997) 1475
88. N. Komatsy, T. Arai, Y. Sugimoto, *Pat. Japan* 49-067847
89. N. Cook, Pat. 989807 *Gr. Britain. (1962)*
90. H. Giess, Pat. 2132251 *France. Publ. (1972)*
91. D. Lovering, R. Gale, *Molten Salt Techniques*, V. 1-4, Plenum Press, New York, 1983-1993
92. G. Lanz, *Molten Salts Handbook*, Academic Press Publishers, New York (1967)
93. S. White, U. Twardoch, *J. Appl. Electrochemistry* 17 (1987) 225
94. J. Perry, *Scale-up of cells to electrodeposit refractory metals using molten salts electrolytes*, Workshop, London, 7-8 July (1985)
95. D. Inman, *Molten Salt Chemistry*, G. Mamontov and R. Marassi (Eds.), *Riedel Publishing Company* (1987) 417

96. F. Cardarelli, P. Taxil, A. Savall, *Int. J. of Refractory Metals & Hard Materials* 14 (1996) 365
97. R. Pandey, S. Sahu, S. Chandra, *Handbook of Semiconductor Electrodeposition*, Marcel Dekker, New York (1996)
98. S. Senderoff, G. Mellors, *Science* 153 (1966) 1475
99. N. Cook, *Scientific American* 221 (1969) 38
100. D. Williams, "Assessment of Candidate Molten Salt Coolants for the NGNP/NHI Heat-Transfer Loop," Oak Ridge National Laboratory, ORNL/TM 69 (2006)
101. M. Matsumiya, W. Shin, N. Izu, N. Murayama, *J. Electroanal. Chem.* 528 (2002) 103
102. O. Dossenbach, in *Theory and Practice of Pulse Plating*, J.-C. Puippe, F. Leaman (Eds.), American Electroplaters and Surface Finishers Society, Orlando, FL (1989)
103. N. Ibl, in *Advances in Electrochemistry and Electrochemical Engineering*, Vol.2., C.W. Tobias and P. Delahay (Eds.), J. Wiley, New York (1962)
104. P. Chamelot, P. Taxil, D. Oquab, J. Serp, B. Lafage, *J. Electrochem. Soc*., 11 (2000)
105. M. Makyta, O.Patarak and T.Utigard, "*Electrochemical Synthesis of TiB_2 powders in molten salts"*, Proceedings of the International Symposium on Materials Performance, Edmonton, Alberta, August 23-27 (1992) 319-325
106. M. Makyta, K.Matiasovsky and P.Fellner, *Electrochimica Acta*, 29 (1984) 1653
107. S. Volkov, K. Yatsimirskii, *Spektroskopiya rasplavlennykh solei*, Naukova Dumka, Kiev (1977)
108. A. Agarwal, N. B. Dahotre, in *Intermetallic and Ceramic Coatings*, N. B. Dahorte (Ed.), Marcel Dekker, New York, (1999)
109. P. Angerer, P. Pessenda-Garcia, E. Neubauer, G. E. Nauer, *Z. Krist. Supp.*, 26 (2007) 235
110. J. van der Maas and T. Visser, in *Laboratory methods in vibrational spectroscopy*, 3rd Ed., H.A. Willis, J.H. van der Maas, R.G.J. Miller (Eds.), John Wiley & Sons, New York (1987)
111. A. Robin, J. de Lepinay, M.J. Barbier, *J. Appl. Electrochem*., 20 (1990) 289
112. J. Sangster, A. Pelton, *J. Phys. Chem*.,16:3 (1987) 509
113. P. Lidin, V. Molochko, L. Andreeva, *Chemical properties of inorganic compounds*, 3rd Ed., P.A. Lidin (Ed.), Moscow (2000)
114. K. Torlep and H. A. Oye, *J. Chem. Eng. Data* 25, (1980) 16

115. A. Bard, L. Faulkner, *Electrochemical Methods: Fundamentals and Applications*, 2nd Ed., John Wiley, New York (2001)
116. A. Fisher, *Electrode Dynamics*, Oxford University Press, Oxford, New York (1996) 3-5
117. R. Nicholson and I. Shain, *Anal Chem*., 36 (1964) 706
118. G. Mamantov, D. Manning, I. Dole, *J. Electroanal. Chem*., 9 (1965) 253
119. H. Nishimura, T. Hiramatsu, *Nippon Kinzoku Gakkaishi*, 21 (1957) 469
120. J. Steinebrunner, T. Emmerich, S. Heck, I. Munder. R. Steinbuch, *Surface and Coatings Technology*, 86 (1996) 748
121. R. Kieffer, F. Benesovsky, *Hartstoffe*, Springer, Vienna, (1968)
122. H. Holleck, *Vac. Sci. Technol*., A4 2663, (1986)
123. ICDD database, *file PDF* 00-035-0741
124. ICDD database, *file PDF* 00-042-1120
125. D. Lide, *Chemical Rubber Company Handbook of Chemistry and Physics*, CRC press, Boca Raton, Florida, USA, 79th edition, (1998)
126. I. Yoshizawa, R. Urao, Y. Hori, K. Akaishi, K. Kamada, *J. Nuclear Materials*, 103 (1981) 267
127. M. Berger, S. Hogmark, *Surface and Coatings Technology*, 149:1 (2002) 14
128. A. Perry, A. Tian, J. Treglio, C. Loomis, *Surface and Coatings Technology*, 68 (1994) 528
129. J. Li and B. Li, *Rare Metals*, 26:1 (2007) 28
130. L. Polyakova, G. Bukatova, E. Polyakov, *Russian J. Electrochem*., 29 :11 (1993) 1330
131. M. Kh. Karapet'yants and M. L. Karapet'yants, in *Thermodynamic Constants of Inorganic and Organic Compounds*, Humphrey Science Publishing, Ann Arbor, MI (1970)
132. G. Samsonov and I. Vinitskii, *in Handbook of Refractory Compounds*, Plenum, New York (1980)
133. ICDD database, *file PDF* 00-004-0788
134. H. Jehn and G. Reiners, *Charakterisierung dünner Schichten*, DIN-Fachbericht 39, Beuth-Verlag, Berlin, (1993) 134
135. *International Center for Diffraction Data Powder Diffraction File*, ASTM, Swarthmore, PA 19081, USA, CD-ROM (1992)
136. B. Rother and J. Vetter, *Plasma-Beschichtungsverfahren und Hartstoffschichten*,

Leipzig (1992) 171

137. H. Holleck, *J. Vac. Sci. Technol*., A4, (1986) p.2663
138. J. W. Dini, in *Electrodeposition: The materials science of coatings and substrates*, Noyes Publications, USA, New York (1993) p.122
139. *Handbook of Chemistry and Physics*, R.C. Weast (Ed.), Chemical Rubber Co., Cleveland, OH (1971)
140. G. Lai, *High-temperature corrosion of engineering alloys*, ASM International, Materials Park, OH (1990) 186
141. *Corrosion Data Survey*, Metals Section, 6th Ed., NACE, (1985), 156,169
142. A. Littner, B.G. Allemand, M. Francois, M. Vilasi, *Corrosion Science*, 48 (2006) 1426
143. D. Weirauch, J, W. Krafick, G. Ackart, P. Ownby, *Journal of Materials Science*, 40 (2005) 2301-2306

CURRICULUM VITAE

Dipl.-Ing. NATALIIA RYBAKOVA

(Diploma in Technical Electrochemistry)

Junior Researcher, PhD Student
CEST Centre of Electrochemical Surface Technology
Viktor-Kaplan str. 2
A-2700 Wiener Neustadt
Tel.: +43 (0) 2622/22266-48
+43 (0) 699 – 10 88 27 75 (mobile)
E-mail: nataliia.rybakova@cest.at

Personal Data

Date of Birth: 1983, October 2
Place of Birth: s.Balky, Ukraine
Citizenship: Ukrainian
Language Proficiency: English (fluent)
German (good)
Russian (mother tongues)
Ukrainian (fluent)

Education

June 2005	National Technical University of Ukraine "KPI" Bachelor in Chemical Technology and Engineering, KB#28181915
March 2007	National Technical University of Ukraine "KPI" Diploma in Technical Electrochemistry KB#30786887

Work Experience

Since 2006	Junior researcher, PhD Student CEST Centre of Electrochemical Surface Technology (formerly ECHEM Centre of Competence in Applied Electrochemistry), Wr. Neustadt, Austria
July 2004- August 2004	Laboratory assistant Kiev factory "Rostok"

Main Research Interests

- Electrochemistry and physical chemistry. Electrochemistry of molten salts.
- Electrochemical deposition of refractory metals and their compounds out of non aqueous electrolytes.
- Investigation of the mechanism of electrochemical reduction of refractory compounds and metals.
- Technological aspects of the chemical and electrochemical processes.

Publications

Articles

1. N. Rybakova, M. Souto, H.-P. Martinz, Y. Andriyko, W. Artner, José Godinho, G.E. Nauer, Stability of electroplated titanium diboride coatings in high temperature corrosive media, Corrosion Science, 51:6 (2009), 1315.
2. N. Rybakova, M. Souto, Y. Andriyko, W. Artner, José Godinho, G. E. Nauer, Morphology and mechanical properties of TiB_2 coatings deposited from chloride-fluoride melts by pulse electroplating, Journal of The Electrochemical Society, 156:131-137, (2009).
3. N. Rybakova, O. Babushkina, and G.E. Nauer, Electrochemical synthesis of TiB_2 layers out of FLiNaK electrolyte in the presence of $TaCl_5$ additive, Journal of The Electrochemical Society, 157:D593, (2010).

Proceeding

1. N. V. Rybakova, O. B. Babushkina, and G.E. Nauer, Electrochemical Investigation on the Synthesis of TiB_2 out of FLINAK Electrolyte: Electrochemistry of K_2TiF_6 and KBF_4, ECS Transactions - San Fransisco, CA" Volume 19, "Industrial Electrochemistry and Electrochemical Engineering (General) - 215th ECS Meeting", from the San Francisco, CA meeting.

Oral presentation

1. N. Rybakova, O. Babushkina, W. Artner, G. E. Nauer, Electrochemical synthesis of TiB_2 out of FLINAK electrolyte in the presence of $TaCl_5$ additive, 216th ECS Meeting, Vienna, Austria, October, 2009.
2. N. Rybakova and G. E. Nauer, Electrochemically deposited TiB_2 as corrosion protection layers in melts of Al and Al alloys, The 60th Annual Meeting of the International Society of Electrochemistry, Beijing, China, August, 2009.
3. N. Rybakova, Refractory compounds in high temperature molten salts, CEST´s monthly Seminar „Topics in applied electrochemistry", June, 2009.
4. N. Rybakova, Electrochemical synthesis of TiB_2 out of high temperature molten salts, University of Vienna, June, 2008.

Posters

1. O. B. Babushkina, N. V. Rybakova, spectroscopic evidence of TiF_4 complexes in alkali fluoride melts at 700-800ºC, 42nd IUPAC Congress, Glasgow, UK, August, 2009.
2. N. Rybakova, Y. Andriyko, J. Godinho, W. Artner, G. E. Nauer, Electrodeposition of TiB_2 out of FLINAK electrolytes: temperature and substrate effects, EUCHEM 2008, Conference on Molten Salts and Ionic Liquids, Copenhagen, Denmark, August, 2008.
3. N. Rybakova, O. Babushkina, W. Artner, G. E. Nauer, Electrochemical Co-deposition of TiB_2 and TaB_2 Layers out of FLiNaK Electrolyte, 61th Annual ISE Meeting, 26 Sep – 1 Oct 2010 Nice, France